Republic of Iraq
Ministry of Higher Education and Scientific Research
University of Kerbala
College of Engineering
Department of Electrical and Electronic Engineering

Controlling the Pneumatic Solar Tracker by Using Adaptive Neuro-Fuzzy Inference System

A Thesis Submitted to the Council of the College of Engineering/University of Kerbala in a Partial Fulfillment of the Requirements for the Degree of Master of Science (M.Sc.) in Electrical Engineering

Written By:

Hussain Musaab Khalaf

Supervised By:

Prof. Dr. Jamal Abdul-Kareem Mohammed

Prof. Dr. Ali Abdul Razzaq Abbas Altahir

April 2025 Shawwal 1446

بسم الله الرحمن الرحيم

يَرْفَعِ اللَّهُ الَّذِينَ آمَنُوا مِنكُمْ وَالَّذِينَ أُوتُوا الْعِلْمَ دَرَجَاتٍ وَاللَّهُ بِمَا تَعْمَلُونَ خَبِيرٌ

صدق الله العلي العظيم

(المجادلة: من الآية 11)

Dedicated to

My family

ACKNOWLEDGMENT

All thanks to Allah for giving me the strength to complete this study. I express my appreciation and gratitude to my supervisors, Prof. Dr. Jamal Abdul-Kareem Mohammed and Prof. Dr. Ali Abdul Razzaq Abbas Altahir, for their continuous encouragement and support during the whole stages of my study. Their advice and suggestions have contributed essentially to finishing this work. I am indebted to my colleagues and friends who have presented advice and pointed positive notes. Finally, I sincerely thank my wife and family for their continuous support and encouragement throughout my studies.

Supervisors Certification

We certify that this thesis entitled "Controlling the Pneumatic Solar Tracker by Using Adaptive Neuro-Fuzzy Inference System" which was prepared by " Hussain Musaab Khalaf," is under our supervision at the University of Kerbala in partial fulfillment of the requirements for the degree of Master of Science (M.Sc.) in Electrical Engineering.

Signature

Prof. Dr. Jamal Abdul-Kareem Mohammed

(First Supervisor)

Date: 30/4/2025

Signature

Prof. Dr. Ali Abdul Razzaq Abbas Altahir

(Second Supervisor)

Date: 30 / 4 /2025

Examination Committee Certification

We certify, as an examining committee, that we have read the thesis entitled "**Controlling the Pneumatic Solar Tracker by Using Adaptive Neuro-Fuzzy Inference System**" and examined the student "**Hussain Musaab Khalaf**" in its contents and what is related to, and found it meets the standards of a thesis for the degree of Master of Science (M.Sc.) in Electrical Engineering.

Signature:

Name: Prof. Dr. Ahmed Abdul-Hadi Ahmed

(Chairman)

Date: 5 / 5 / 2025

Signature:

Name: Asst. Prof. Dr. Wisam Essmat Abdul-Lateef

(Member)

Date: 30 / 4 / 2025

Signature:

Name: Lect. Dr. Ahmed Selman Hadi Altuma

(Member)

Date: 30 / 4 / 2025

Signature:

Name: Prof. Dr. Jamal Abdul-Kareem Mohammed

(Member)

Date: 30 / 4 / 2025

Signature:

Name: Prof. Dr. Ali Abdul Razzaq Altahir

(Member)

Date: 30 / 4 / 2025

Signature:

Name: Asst. Prof. Dr. Muayad Saleem Kod

(Head of the Department of Electrical Engineering)

Date: 26 / 5 / 2025

Signature:

Name: Prof. Dr. Haider Nadhom Aziz

(Dean of the Engineering)

Date: 26 / 5 / 2025

Abstract

The sun is one of the most important and indispensable sources of clean energy on our planet. Photovoltaic (PV) energy is nowadays the most viable and accepted solar energy. Solar photovoltaics involves the conversion of sun energy into electrical power. One way to boost the solar PV system's efficiency is to increase solar radiation time that directed to the solar panel, which means harnessing more sunlight onto the solar panels. This is achieved using sun trackers, which maintain solar PV panels always oriented to the sun's beams at the optimal angle.

This thesis aims to design and build a prototype of a dual-axis solar tracking system driven by two pneumatic actuators on a smaller scale, which can simulate real time system with an actual load because the pneumatic system has advantages over other actuators due to the simplicity of control, cost-effective, low maintenece and can operate on a wide range of harsh environmental locations. A group of tests were conducted on the tracking system on the day of September 16th 2024 in the city of Baghdad with latitude of (33.367°N) as this location the simulation and the experimental part were conducted.

Addtion to that, a comparison has been made between a fixed solar panel and one driven by pneumatic actuators to show how much power can be produced for a given local load. First, the components of the tracking system will be modeled, which mainly contains the PV panel, the pneumatic actuator system, and the control system. Three control methods has been simulated for the tracking system using Matlab/Simulink: Adaptive Neuro Fuzzy Inference System (ANFIS), Fuzzy Logic (FL), and the compare method to control the pneumatic actuators. The simulation showed that the ANFIS method increased the effeciency of the solar system by approximately 44.6% compared to the fixed panel system that because the ANFIS controller have adaptive features and can predicts the environmental changes due to data training and fuzzy reasoning, while FL method showed a 30.6% increase in solar energy harvest compared to the fixed panel system due to non adaptive properties. The comparison method is a simple process of comparing the readings of two identical optical sensors and has achieved 38.15% greater efficiency than fixe panel since this method took the data directly form the sensors. From the results above, the ANFIS is higher effeciency than FLC controller in about 10.7%.

Comparing the performance of the solar tracker setup in the experimental work under the ANFIS system with the corresponding simulated results, the experimental results showed a decrease of 6.51% over the simulation results. Also, the experimental

results of the system under the control of FL and the comparison method gave about 7.6% and 7.25% less than the results of the simulation results, respectively.

Contents

List of Tables

List of Figures

List of Abbreviations

AC	Alternating Current
AI	Artificial Intelligent
ANFIS	Adaptive Neural Fuzzy Inference System
ANNs	Artificial Neural Networks
ARM	Advanced RISC Machine
BJT	Bipolar Junction Transistor
CPU	Central Processing Unit
Dac	Double acting cylinder
DC	Direct Current
DSP	Digital Signal Processor
FL	Fuzzy Logic
FLC	Fuzzy Logic Control
FPGA	Field Programmable Gate Array
IEA	International Energy Agency
LDR	Light Dependent Resistor
MRI	Magnetic Resonance Imaging
NC	Normally Closed
NO	Normally Open
NREL	National Renewable Energy Laboratory
PID	Proportional – Integral – Derivative
PS	Pressure Source
PV	Photovoltaic
PVC	PolyVinyl Chloride
PWM	Pulse Width Modulation
UV	UltraViolet

List of Symbols

A	Piston Area
A_{panel}	Area of PV Panel
A_r	Cross Section Area of the Rod Piston
C_f	Non-Dimensional Coefficient of Discharge
C_v	Constant-Volume Specific
c_s	Coefficient of Frictional Viscous in Valves
I_{pv}	Photocurrent
F_f	Coulomb Frictional Force
F_L	External Load
G	Solar Irradiance
I	PV Current
I_d	Diode Current
i_{PV}	PV Panel Current
K	Boltzmann Factor
k	Heat Ratio
k_s	Spool Spring Constant
L	Initial Stroke of the Piston Rod
$\dot{m}$	Mass Flow Rate
M_L	Mass of the Load
M_p	Combined Mass of the Piston With Rod
M_s	Mass of the Spool and Coil
P	Air Pressure
$\dot{P}$	Rate of Change in Pressure
P_a	Absolute Atmospheric Pressure
P_{cr}	Critical Pressure
P_d	Downstream Pressure
P_{out}	Output Power

P_{PV}	Output Power of PV Panel
P_u	Upstream Pressure
$\acute{q}$	The Total Rate of Change in Internal Energy
q	Charge of an Electron
R^2	Coefficient of Correlation
R_s	PV Series Resistor
R_{sh}	PV Shunt Resistor
T	Air Temperature
T_{in}	Gas Temperature Entering the System
t_s	Solar Time
$\dot{U}$	The Rate of Change in Energy.
V	Chamber Volume
V	PV Voltage
v_{PV}	Voltage of PV Panel
$\dot{W}$	Work Rate
X	Rod Displacement
x_s	Spool Position
x_{so}	Compression of the Spring At Rest
A	Tilt Angle
B	Coefficient of the Frictional Viscous
γ	Azimuth Angle
Δ	Geographical Altitude Angle
η	Efficiency of the Panel
θ	Geographical Latitude Angle
μ	The factor of diode ideality
P	Air Density
ω	Hour Angle

Chapter One: Introduction

1.1 Overview

The sun is one of the significant elements on our planet. Humankind cannot live without it. These days, humans are suffering from global warming conditions and growing problems [1]. Meanwhile, people have to consider the bright side of these conditions. To manage the global warming problem, switch to more green and clean energy resources like sunlight, hydropower, and windmills and reduce oil-dependent energy use [2]. Researchers and big companies are developing machinery to invest in green energy and use it to gain more power. Big companies such as Q-Cells, BP Solar, Kyocera, Sanyo, and Sun Power have extensively utilized solar energy tracking projects. Due to its cost-free nature, many companies use solar or photovoltaic (PV) energy as a substitute power source. Since oil and gas prices are globally higher than ever, these companies are switching to green energy sources [3].

1.2 PV System

Several researchers dedicated their time to discover an alternative energy source as a substitute for gasoline. PV energy is one of the alternative energy resources available to the world [4]. PV energy is nowadays the most viable and accepted solar energy. Solar PVs involves the conversion of sun energy into power. Photons collide with silicon atoms, providing electron energy and allowing them to flow freely. The solar cell has an electric field, pushing unbound electrons in specific directions, and metal contacts transfer DC current. PV energy is currently the main application of solar energy globally, and it's described as sunlight, which consists of photons that give us energy with the help of PV properties. The photons are absorbed by a solar cell, which gives us electrical power due to its manufacturing techniques

[5]. The light stimulates the electrons present in the substance of the PV cell. Electrical power is produced by the flow of electrons down a pathway. Solar PV systems produce electric power to provide houses or other loads connected to them. The flow of electric power uses wires to transfer the electrons, directing them to the energy loads, which are batteries or the house's electrical system, where appliances and other electrical devices can be them. The battery system in solar systems helps store energy in case of excess power during average load or when using it at night when the sun is out and electric power is needed. Figure 1.1 shows a simple PV system which construct of PV panel, battery charger, battery, inverter to convert the DC power to AC power and the home load [6]. Maximizing the energy yield from PV systems in areas with reduced sunlight is difficult [7].

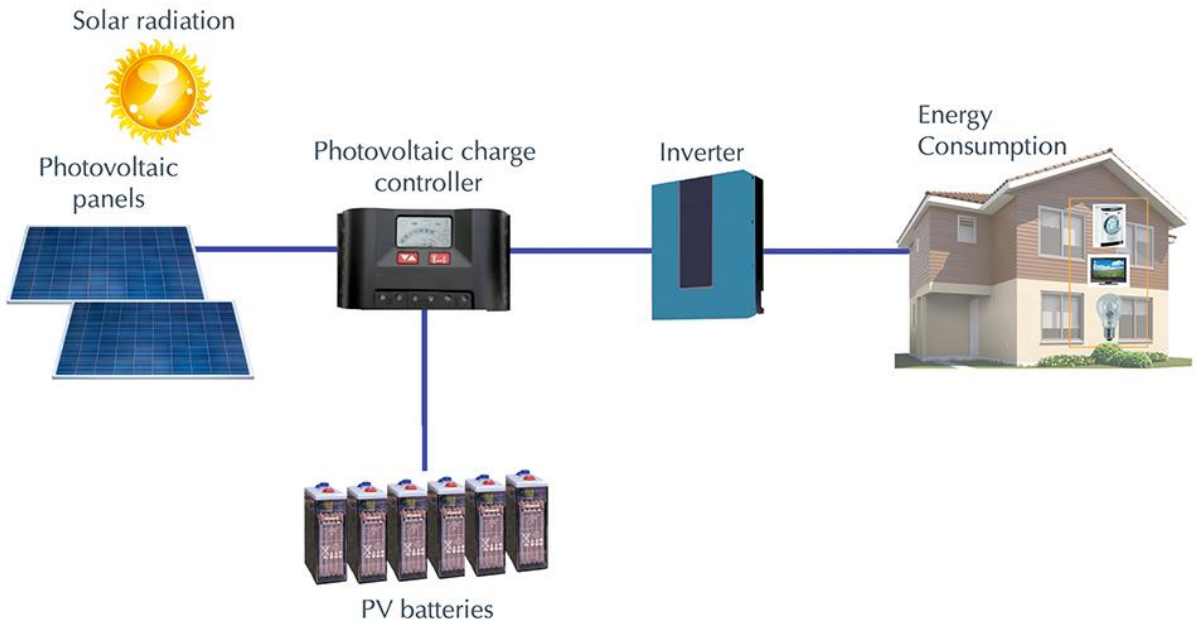

Figure 1. 1 PV system *image courtesy of bester energy*

Extensive research and developments are conducted to increase the efficiency of solar energy and minimize the overall cost of solar energy systems; the International Energy Agency (IEA) reports that while the annual growth rate of global

PV capacity is high, solar PV energy is not yet ready to completely replace conventional energy sources in the market, despite its benefits. While sophisticated techniques for PV material optimization remain challenging, advancements in system design and module building can significantly improve solar PV efficiency and reliability [8]. One way to boost the solar system's efficiency is to increase the time that solar radiation directed to the PV panel, which means more sunlight is applied to the solar panels. This is achieved using sun tracking devices, which keep the solar PV panels always oriented to the sun's rays at the optimum angle [9].

1.3 Solar tracking system

The solar tracking system has many techniques according to their components and drivers. They are classified into five main types: active which used an active actuator, passive which depends on thermal properties and specific metals for thermal expansion, semi-passive which have thermally expanded metals and active actuator to increase precision, manual which used manual gears to track the solar angles, and chronological tracking systems which depends on lookup table for the solar angles. The solar tracking system is classified into two types according to the tracking degree of freedom: single-axis and dual-axis tracking systems. The single-axis tracker will track only one solar angle either the tilt or azimuth angle while the dual-axis tracker will track both angles [10]. Figure 1.2 illustrates the types of solar tracking systems according to their degree of freedom.

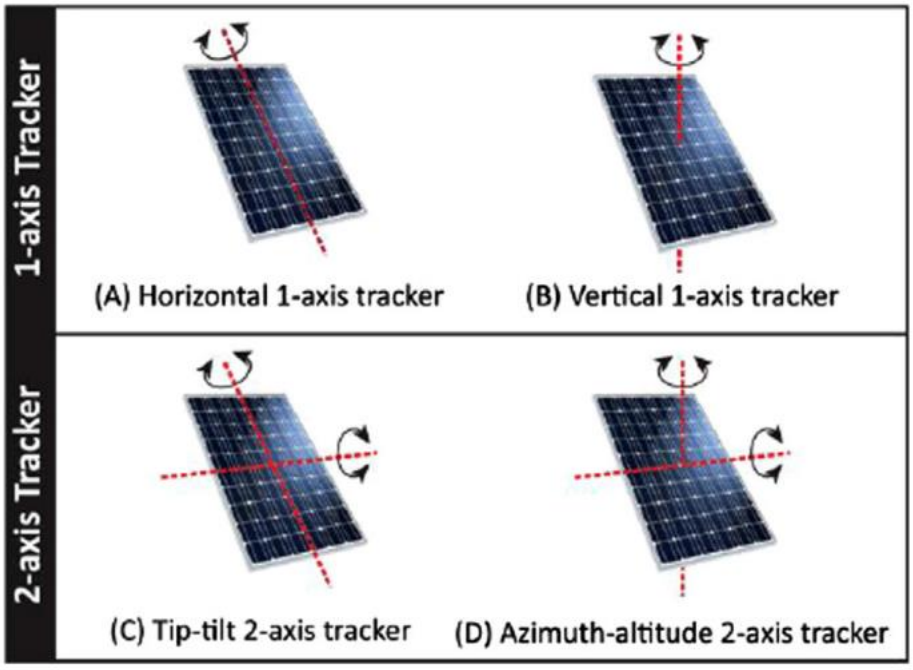

Figure 1. 2 single and dual axis tracking system [10]

This thesis aims to simulate and build a smaller-scale solar tracking system prototype, which can simulate a real-life system with an actual load. Also, a comparison between a fixed solar PV panel and a tracking one is made to show how much energy can be produced for a specific localized load [11]. To achieve the tracking mechanism, there must be precise actuators that constantly move the solar PV panels toward the sun.

1.4 Pneumatic actuator

Pneumatic systems in solar tracking systems are an innovative way to optimize the orientation of solar panels to maximize the collection of solar energy. Solar tracking systems are designed to improve the effectiveness of solar energy capture by maintaining the optimal orientation of solar panels toward the sun, increasing the amount of energy generated. While most tracking systems use electric motors, hydraulic systems, or mechanical gears, pneumatic systems offer an alternative based on air pressure. Pneumatic actuators have become a crucial driving component widely

employed in industrial robotics and autonomous systems [12]. Because of their unique properties, pneumatic actuators have become a significant alternative for actuators in automated material that needs handling operations. One challenging thing about pneumatic actuators is their system's nonlinearities, primarily attributed to air compressibility effects and frictional resistance in the actuators [13].

Many unknown parameters must be found and tuned to generate a dynamic response that resembles natural systems. Prof. J. L. Shearer established the theoretical basis for the dynamic management of pneumatic systems in late 1956. Shearer found the system's dynamics by formulating nonlinear differential equations, which the linear model subsequently followed. Shearer's methods for designing a prototype have been widely used in research. Many valves are used in his modeling to build the pneumatic actuator system [14]. The famous ones are on-off solenoid valves and proportional valves.

Strengths of on-off solenoid valve technology include a straightforward system design and a cost-effective solution, but also weaknesses such as a lack of adaptability, many challenges in accuracy placement, and difficulties in synchronizing timing accuracy. Meanwhile, the proportional valve is more complex and presents complicated terms in the control case. In the late 90's, a study was conducted to examine the use of pneumatic actuators in food packaging on a production line [15]. A pneumatic actuator was created for a construction robot in the year 2005 [16]. A construction robot was employed to place ceramic tiles. Pneumatic actuators have emerged in various applications such as building equipment, power drills, and many other applications for manufacturing purposes. In addition to their use in manufacturing applications, pneumatic actuators have also been applied in physical human interfaces for medical purposes. In the same year, researchers studied the use of an intelligent pneumatic cylinder to create a Global Physical Human

Interface Machine Interaction, which resulted in the invention of an Intelligent Chair Tool with many applications for disabled patients [17].

Pneumatic actuators were also used in a clinical robot helper in the early summer of 2010 [18]. Meanwhile, in specific medical applications and to improve the accuracy of needle positioning control, a pneumatic actuator system has been designed and applied in a Magnetic Resonance-examination Image-guided (MRI) prostate biopsy and radiation procedure application [19]. In addition to that, a pneumatic actuator systems have been used to produce an interactive-faced Polygon for a sensitive physical human interface. Pneumatic actuators deliver a considerable benefit over hydraulic actuators [20]. Pneumatic actuators use compressed air as their source. The advantage of using air compared to conventional actuators that use water or other fluids like certain kinds of viscous oil is that air is a cheap and accessible source. Hydraulic actuators depend on an external water or oil source to operate their system, but pneumatic actuators depend only on air to run their system which is clean and cheap source compare to oil and water. The application of these actuators will specify which one of these actuator more appropriate and which has advantage on their work environment. [21].

This will result in a more cost-effective option for pneumatic actuators than hydraulic actuators. Another handy and helpful feature of pneumatic actuators is their good power-to-weight ratio quality. The low air density compared to fluid resulted in a decrease in its weight-to-power ratio. In addition, pneumatic actuators have the potential to produce maximum forces over an extended duration, exceeding the capabilities of electrical actuators [22].

On the other hand, the use of electric actuators in the tracking mechanism can increase the temperature due to extended thermal expansion, resulting in a gradual decrease in performance accuracy. Pneumatic actuators are familiar for their straightforward construction, design, and high adaptability. It can be designed for various

applications, from small and portable household workspaces to large and big industrial machines [23].

Since the pneumatic actuators use air as their source, the system will offer a clean operating environment and ensure safety to the users compared to other actuators that use oil or electrical sources. Despite these advantages, the pneumatic device exhibits an important and noticeable output degree of nonlinearity resulting from the gas mass flow crossing the valve orifice and the friction forces inside the piston [24].

A precise dynamic representation is required to design a simple and cost-effective position control system for a pneumatic actuator system. Pneumatic actuator's properties are known for their simple design and ability to adjust quickly. It can be manipulated for too many spectrums of applications, from compact and portable domestic objects to sizable and robust industrial equipment.

The pneumatic valves regulate the air pressure within the cylindrical chambers, which will control the positioning process. Figure 1.3 shows the parts of the pneumatic double acting cylinder which contain two chambers and piston rod which: x is the rod displacement, A_1 and A_2 is the area of the chambers, $P_1$and P_2 is the pressure on the chambers, P_s is the pressure source, P_a is the ambient pressure, M is the external mass and A_r is the rod area [25].

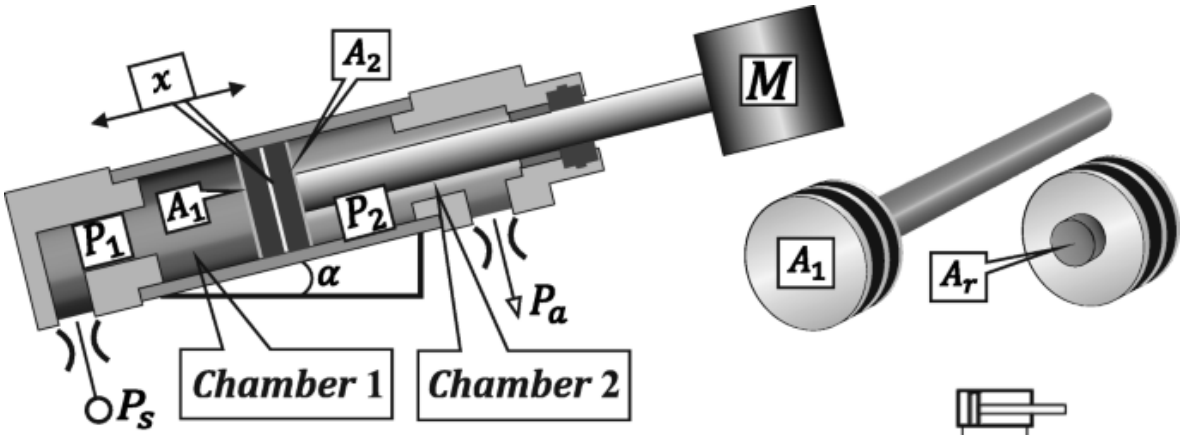

Figure 1. 3 pneumatic double acting cylinder [25]

1.5 Pneumatic valves

The control valve in an electro-pneumatic system, which regulate airflow into the actuator, can be categorized into two categories [26]. The first type is a proportional valve, which produces high control accuracy and linear behavior. Its functions act in the manner that the armature is located between the open and closed positions based on the input signal, making it favorable for a wide range of industrial automation applications. However, their high cost might affect the judgment of their unique qualities and complex arrangement. A proportional valve shown in Figure 1.5 is the costliest component in the system, with its price being comparable to the combined cost of all other elements. Because of this, its usage is limited to specific applications. On the other hand, on-off valves shown in Figure 1.4, which can be used in place of proportional valves, offer a cost-effective solution for building and developing electro-pneumatic systems due to their cost-effective property [27]. However, the operation of these valves is limited to either entirely open or wholly closed positions based on the electric input signal, which is unsuitable for the operational demands of the industrial automation area and its applications [28]. A Pulse Width Modulation (PWM) technique is used to address this issue.

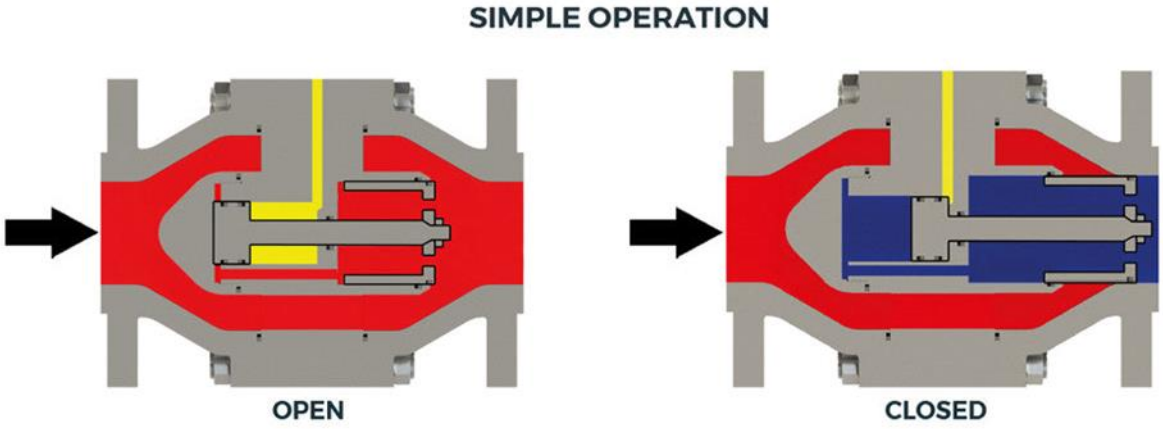

Figure 1. 4 principal of operation of on-off valve ***image courtesy of acad engineering***

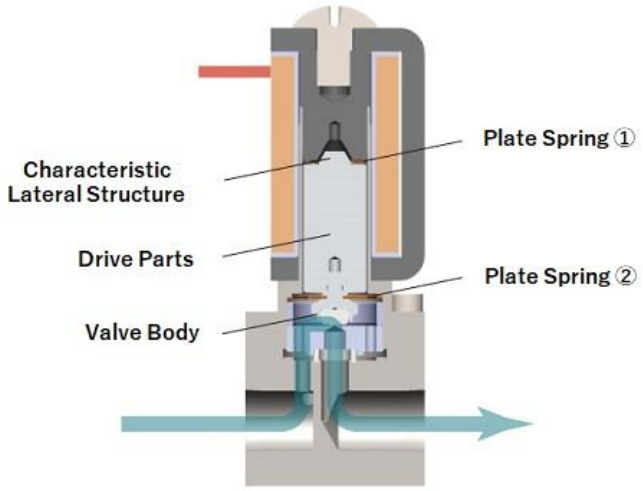

Figure 1. 5 The principle of operation of a proportional valve image is courtesy of Takano Co. Ltd.

The PWM technique allows systems that use solenoid valves to exhibit a behavior close to systems using proportional valves, and this technique will combine the low budget of solenoid valves and the properties of proportional valves [29]. The challenges in electro-pneumatic systems depend on using artificial intelligence (AI) techniques such as Fuzzy Logic (FL) and Artificial Neural Networks (ANNs), or any other field of artificial intelligence, which is used to automatically modify system parameters and boost the efficiency of system units [30].

1.6 Fuzzy logic control

Fuzzy logic (FL) is often employed in engineering applications due to its ability to address complex issues in a simple manner, particularly in areas like household appliances, automotive electronics, and industrial automation. This approach mimics human reasoning, allowing systems to handle uncertainty and imprecision more effectively [42]. Fuzzy logic controllers (FLCs) are well-suited for complex control systems [43].

1.7 Problem statement

Fixed solar panels suffer from a clear deficiency in generating electrical energy, so appropriate actuators must be used. Because hydraulic and electrical actuators cause an increase in the cost and size of the tracking system, in addition to the complexity of its control circuits when used as a tracking mechanism, it has been replaced with pneumatic actuators due to their advantage over other equivalent actuators. Increasing the size of the system may affect the motion response output of the solar tracker system.

Also, solar tracking devices usually suffer from problems in the accuracy of movement and smooth response to work, so it is necessary to use intelligent technologies to control the operation of the tracking system with satisfactory performance to some extent. Therefore, an Adaptive Neural Fuzzy Inference System (ANFIS) controlling the pneumatic solar tracker is employed to efficiently direct the solar PV panel toward the sun to achieve maximum energy absorption, thus maximizing electrical energy production as much as possible.

1.8 Motivation

1. To overcome the fixed panel diffeciency by using thedual axis solar tracking system.
2. To minimize the cost of the solar tracking system by using pneumatic actuators.
3. To boost the accuracy of the system by using AI method to control the solar tracker.

1.9 Thesis Objectives

This thesis aims to implement a closed-loop, Light Dependent Resistor (LDR)-based dual-axis solar tracking system driven by dual-acting pneumatic actuators and

controlled by AI techniques for maximum power harvested from the PV panel and minimize the cost of the actuator used in the system. Achieving this goal requires implementing the following objectives:

1- Modeling the components of the proposed tracking system.

2- Simulate the proposed system using MATLAB/Simulink.

3- Construct the tracking system and take the experimental results

4- Compare the experimental results and the simulation results on the three methods (ANFIS, FLC and compare method) used in controlling the tracking system.

5- discuss the results to show the power and weakness points of each method.

1.10 Thesis Organization

This thesis is organized into five chapters as follows:

- **Chapter One** includes an overview and introduction. This chapter provides a preliminary explanation and preliminary description of the proposed system.
- **Chapter Two** introduces the literature review. This chapter includes the literature survey of the solar tracking system. It also consists of the literature survey of pneumatic actuator, ANFIS and FLC system used in the tracking system.
- **Chapter Three** introduces the research methodology and mathematical models for parts of the proposed solar tracking system.
- **Chapter Four** includes tracking system simulation using ANFIS and FLC and comparing these methods with fixed-mounted panels and the experimental work and the comparison between the simulation and the experimental results.
- **Chapter Five** includes conclusions and future work that could add development to the tracking system.

Chapter Two: Literature Review

2.1 Introduction

This section provides an overview of existing studies in the literature related to the topic of solar tracking systems.

2.2 Related Works

People increasingly view solar tracking systems as a sustainable and cost-effective solution to maximize solar power absorption. The LDR sensors on the solar panels sense the solar azimuth and tilt angles, which harvest the solar illumination power. Examining the diverse and broad body of related work is necessary to understand solar tracking technology and identify potential future directions.

In the subsequent sections, the literature review will be conducted according to the following topics:

2.2.1 Solar tracking system

Solar tracking techniques are essential to optimize the use of solar panels. The first solar tracker was debuted in 1962, and it was entirely mechanical. Table 2.1 shows some researches and their techniques about solar tracking systems.

(Tudorache et at.,2012) [31] a single-axis solar tracking PV panel designed and executed by the University Politehnica of Bucharest in cooperation with Technosoft International SRL. The performance of the equipment was experimentally tested in comparison with a fixed PV panel. The solar tracking PV panel produced more energy than the fixed one by about 38%.

(Dhanabal el al., 2013) [32] the fixed photovoltaic (PV) panel and single axis solar tracking based on real-time clocking using an ARM CPU were compared for six days, both fixed and tracking systems were used in the experiment. The findings demonstrated that the solar tracking system boosted

energy received from the sun from 9:00 AM to 6:00 PM in the city of Tamil Nadu- India and increased efficiency by about 40**%.**

(Hammoumi et al., 2018) [33] when comparing the energy produced by the smart dual axis solar tracker with a fixed panel, trial results reveal that the smart dual axis solar tracker produces 36.26% more energy than the fixed panel. It is not necessary to have extensive understanding of electronic engineering and sun tracking technologies to execute the suggested active dual-axis solar tracker.

(Mohanapriya et al., 2021) [34] operating the machine requires a combination of firmware programming and hardware. In hardware manufacturing, four light-based resistors (LDRs) are utilized to catch the most incident light possible. Three stepper motors are utilized to move the solar panel based on the amount of incident light that the LDRs are detecting. The improvement in performance indicates that the efficiency is higher than that of a single solar tracker axis 6-7% than a fixed solar panel and the effeciency of the dual axis solar tracker is about 30–40%.

Table 2. 1 Related work on solar tracking system

Author (s)	Technique	Strength	Weakness	No. of citations
M. T. A. Khan & S. M. S. Tanzil, R. (2010) [35]	Solar tracking system used LDR sensors and ATMEGA controller	Information about control strategies	Single axis tracking system, and there is a hardware limitation	(163) researches
Tudorache, T., Oancea, C. D., & Kreindler, L. (2012) [31]	deals with the performance of a solar tracking PV panel of single axis type by means of a DC motor controlled by an intelligent drive unit	Used DSP technology based to control dc motor rotation	Embedded controller with no adaptive characteristics	(61) researches
Rengasamy, Dr. Dhanabal &	single axis solar tracking based on real-time clocking	High efficiency about 40%	Using single axis solar tracking technique	(163) researches

Mohanapriya, V., Manimegalai, V., Praveenkumar, V., & Sakthivel, P. (2021) [34]	Four LDR sensor with stepper motor to track the solar angles for single and dual axis solar tracking system	Results about single axis and dual axis comparing to a fixed panel	Using stepper motor with compare method between sensors	(22) researches
Shang, H., & Shen, W. (2023) [36]	Dual axis tracking system using photo sensor and stepper motor	A sound dual-axis tracking system with excellent tracking efficiency	Complex mechanical interface with the electric actuator	(106) researches
Bharathi, Venuturla & Ranjitha, R. & Ponni, A. & Deepthi, S. & Mageshkannan. (2013) [32]	using an ARM CPU	more than fixed panel		
El Hammoumi, Aboubakr & Motahhir, Saad & Abdelaziz, el ghzizal & Chalh, Abdelilah & Derouich, Aziz. (2018) [33]	simple active dual-axis solar tracker to track the sun's movement by using fewer components and low-cost as well	Simple and cost effective components with high efficiency	Using motors as an actuators with simple compare technique	(99) researches

2.2.2 ANFIS solar tracking systems

Solar tracking techniques are essential to optimize the use of solar panels. Table 2.2 shows number of studies concenring the ANFIS system.

(Toylan & Hüner, 2017) [37] in order to improve the efficiency of power collecting solar tracking systems should typically be linked with photovoltaic (PV) panels. This work presents a solar tracking system that incorporates the Adaptive Neuro-Fuzzy Inference System (ANFIS). Azimuth and zenith angles are controlled by two motors in the dual-axis solar tracking system. On the designated day, it was discovered that the solar tracking system used with ANFIS

in the Turkish city of Pinarhisar had a daily output power that was 47.76% greater than that of the fixed PV panel.

(Baisrum et al., 2021)[38] ANFIS used in solar tracking in the lab with the help of an ultraviolet (UV) sensor. The difference between the two sensor readings makes the controller receive this data, train the network, and then adjust the output for the pneumatic actuator to drive the solar panel to a position that makes the difference between the UV sensor readings almost zero. There are several complex notes about this system: training the data and tuning the parameters of the ANFIS controller. The current study will used a cost-effective sensor with real time data from the location.

(Sarr et al., 2023) [39] the field of heliostats has a significant impact on the performance and efficiency of solar tower power. To estimate heliostat error tracking quickly and correctly, prediction models based on the Artificial Neural Network (ANN) and Adaptive Neuro-Fuzzy Inference System (ANFIS) were used. According to a comparison of the results, intelligent approaches outperformed the traditional model based on geometric mistakes. In comparison to the ANN, the ANFIS model yields coefficients of correlation (R^2) of 0.97, 0.96, and 0.92 for the azimuth and altitude axes, respectively.

(Zulkornain et al. 2023) [40] because the ANFIS technique uses multiple processes—the Fuzzy layer, Fuzzy Rule layer, Normalization layer, and Output Membership layer—it exhibits excellent accuracy. MATLAB software is used to model the dual-axis solar tracker using the ANFIS technique, which enhances the solar system's performance. The outcome displays the average error obtained for both training and testing data, and the smallest error demonstrates how accurately the dual-axis solar tracker predicted the angle.

Table 2. 2 Related work on ANFIS system in solar tracking system

Author (s)	Technique	Strength	Weakness	No. of citations
Aldair, A. A., & Obed, A. A.(2016) [41]	A neuro-fuzzy controller, deployed on an FPGA board, regulates a dual-axis sun tracker utilizing optical sensors and linear actuators for PV panel orientation	Controlling the system using FLC and PID controller	Using FPGA controller and linear actuators	(20) researches
Toylan, H., & Hüner, E. (2017) [37]	The ANFIS model is combined modeling function of fuzzy inference with the learning ability of artificial neural network that has set of rules generated directly from the experimental data	Tracking system control depending on the solar angle which location and time of the panel depending on it	Sensorless control which will continue to work on the cloudy days	(15) researches
Baisrum, Baisrum & Setiadi, Budi & Sudrajat, Sudrajat & Wijayakusuma, Varian & Ulhaq, Hilmi & Hikmawati, Rina & Qamaruddin, Naufal & Hardiansyah, Sandi. (2021) [38]	Using UV light as a sensor, pneumtic actuator and ANFIS as control system technique	Train the data from the UV sensor using ANFIS control to drive the pneumatic actuator	Work done using UV lamp and UV sensors in the lab.	(10) researches

Sarr, M. P., Thiam, A., & Dieng, B. (2023) [39]	ANFIS and ANN models to predict heliostat tracking errors	Using AI technique in tracking system and discover which method give good results	Simulation results in lab with heliostat type of solar tracking system	(12) researches
Zulkornain, M. S. I., Noor, S. Z., Rahman, N. H., & Musa, S. (2023) [40]	The Analysis of Dual Axis Solar Tracking System Controllers Based on Adaptive Neural Fuzzy Inference System (ANFIS)	Using ANFIS properties to train part of given data to control the tracking system	Simulation based on how many membership function of the ANFIS system have	(6) researches

2.2.3 Fuzzy Logic Systems

FLC offer a robust and nonlinear approach, making them resilient to variations in load, supply voltage, and system parameters. Unlike traditional controllers, FL systems can handle imprecise and uncertain information, leading to more effective control performance.

(Abadi et al., 2014) [44] single-axis solar tracking system was designed by using an FLC system to optimize PV panel efficiency. The system employs a DC motor, intelligently controlled by a FLC that responds to input signals from LDR sensors. Experimental evaluation confirmed the system's effectiveness, achieving a 47% power gain over a fixed panel system.

(Kiyak and Gol, 2016) [45] a solar tracker system improves the efficiency of solar energy absorption, a crucial energy source for the future. This system incorporates both FLC and PID-based control systems to regulate its operation. The mechanical components, including the control mechanism, motor actuator, control circuit, and single-axis tracking system, have been designed and implemented. Experimental results demonstrate a significant 21.2% increase in energy output from the solar tracking system utilizing FL compared to systems without it. This highlights the potential for significantly boosting the performance

of solar energy systems through the integration of solar tracking technology. Furthermore, the FLC exhibits a comparable settling time to the PID controller, ensuring stability and responsiveness in the system's performance.

(**Yang and Xiao 2023) [46]** researchers conducted a comparative study between FLC and conventional sun-tracking systems. They developed two-axis sun-tracking systems based on comparing light intensity using the FLC method. Arduino microcontroller serves as the central control system, while LDRs measure light intensity at various angles. Two stepper motors drive the PV panel. The FLC assists the microcontroller in determining the optimal orientation of the PV panel. Experimental results indicated a significant 24.6% increase in output power efficiency for the FLC-based system compared to conventional tracking systems

2.2.4 **Pneumatic Actuators**

(Aliyari-Shoorehdeli and Najafi, 2013) [47] a closed pneumatic solar tracking system was proposed to optimize energy acquisition and minimize associated losses. The suggested method enables a timed rotation determined by the microcontroller, ensures minimal consumption through the closed pneumatic system, and facilitates enhanced motion control via the rotational position sensor of the pneumatic cylinders. Increased precision in rotation and tilt inclination optimizes overall energy storage while reducing heat loss within the specified closed pneumatic system. The research outlines the system components and their interactions aimed at minimizing energy usage. A draft cost analysis was also provided.

(Alboteanu et al., 2015) [48] the tracking system for PV panels exhibited elements of pseudo-equatorial tracking system utilizing a pneumatic drive was explicitly discussed. The simulation of the automatic drive system was conducted using specialized software called FluidSim. The simulation results demonstrated the progression of the standard parameters of the pneumatic drive

The accuracy and responsiveness of a single-axis sun tracking system was studied using a pneumatic drive system with a UV sensor. The system used a mechanical mechanism controlled by digital and proportional valves. Data processing was managed by an ANFIS architecture. The performance of the system was evaluated using a UV lamp. Under idle conditions, the average error was 1.6 degrees, while under load conditions, the average error was 2.5 degrees. The dynamic response overshoot was 2.08% and the steady-state error was 1.25% [38]

Chapter Three:
Mathematical Modeling for the Pneumatic Tracking System

3.1 Introduction

In this chapter, the mathematical modeling of the proposed tracking system, which is divided into several subsystems, will be modeled. Each subsystem will be addressed separately, starting with the PV panel and the equations for modeling the solar panel system. After that, the components of the pneumatic actuating system will be discussed. This actuator mainly consists of a double-acting cylinder that can be modeled as a piston rod position, a left and right chamber, and a pneumatic valve. This can help us understand the parameters affecting these components and how to tune them to simulate the pneumatic actuator in Matlab/Simulink for the solar tracking system. After that, the control system model represented by the ANFIS and FLC system, its rules, and layers will be presented. These controllers rely on the input signals, which can be mapped using the tilt and azimuth angles of the latitude and day on which the proposed system operates. These parameters are essential to maximize the accuracy of the proposed solar tracking system.

3.2 Modeling of PV panel

Modules are stacked in a series-parallel configuration for the PV power plant to deliver the required voltage and current levels [49]. A PV cell's output current is:

$$I = I_{pv} - I_d - \frac{V+R_S I}{R_{sh}} \quad (3.1)$$

where I_{pv} is the photocurrent, V is PV voltage, the current I_d can be represented more elaborately by the Shockley diode and by the following formula:

$$I = I_{pv} - I_0 \left[exp\left(\frac{q(V+R_sI)}{\mu KT}\right) - 1 \right] - \frac{V+R_sI}{R_{sh}} \quad (3.2)$$

where I_0 is the saturation current for the diode

q is the electron charge

μ is the factor of diode ideality

K is Boltzmann constant which equal to 1.380649×10^{-23} J/K

T is the absolute temperature for the p-n junction.

The thermal voltage v_t is defined in the following formula:

$$v_t = \frac{kT}{q} \quad (3.3)$$

PV panels are typically made up of several PV cells connected in series and parallel. Cells connected in series enhance the panel's terminal voltage, whereas parallel cells increase the output current under the same irradiance. PV panels employ roughly the same one-diode model the popular PV simulation model, provides a realistic representation of solar cell performance, is easy to implement, universally recognized, and facilitates collaboration and comparison of results, taking into account the number of cells in Shockley's equation and substituting the formula (3.3) in (3.2), as follows:

$$I = I_{pv} - I_0 \left[exp\left(\frac{V+R_sI}{\mu N_s V_t}\right) - 1 \right] - \frac{V+R_sI}{R_{sh}} \quad (3.4)$$

where N_s is the number of series cells

R_s is the series resistor

R_{sh} is the shunt resistor

Figure 3.1 shows the electrical equivalent circuit of the PV cells

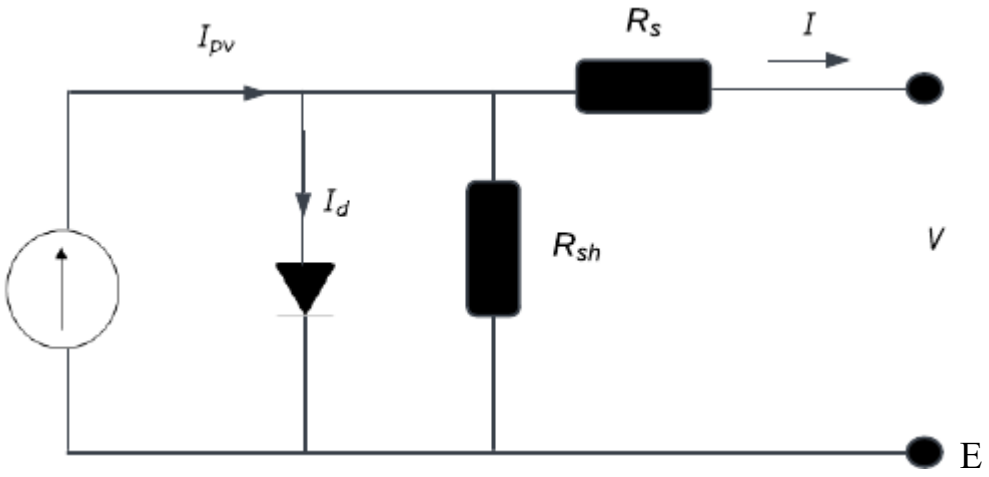

Figure 3. 1 Equivalent circuit for PV panel

Table 3.1 summarizes the technical requirements for PV panels employed in the proposed design. The PV power can be computed as follows:

$$P_{PV} = v_{PV}\, i_{PV} \tag{3.5}$$

The dynamic efficiency of the PV can be calculated from the formula (3.6) as follows:

$$\eta(100\%) = \frac{P_{out}}{G * A_{panel}} \tag{3.6}$$

where ŋ is the efficiency of the PV panel

P_{out} is the output power collected from the PV panel.

G is the solar irradiance measured in W/m^2.

and A_{panel} is the area of the PV panel and equal to 0.18725 m^2 (0.535*0.35) as shown in Table 3.1.

Table 3. 1 PV Panel Technical Specifications

Item	Symbol	Specification
Model	DG-P25W Poly Ethylene	25 W PV 144 cell
Dimensions	Height x Width x Thickness	535×350×18 mm
Maximum DC voltage	V_{mp}	18V
Maximum DC current	I_{mp}	1.39A
Maximum power	P_{max}	25W
Open circuit voltge	V_{oc}	21.24V
Short circuit current	I_{sc}	1.53A

3.3 Modeling of pneumatic actuator

Pneumatic system actuator models are derived from theoretical analysis or system properties techniques. Although various modeling approaches have been proposed, most researchers in this field have depended on mathematical analysis.

The time-varying nature of the load, along with the volume, pressure, and temperature of the gas within the cylinder, and the mass flow rate passing through the valve, are crucial considerations for pneumatic actuator systems [25]. Friction forces present within the system can complicate control efforts. To enhance the accuracy of controller performance, several researchers have focused on modeling friction force to develop effective compensation strategies. This review will initially explore theoretical mathematical models, followed by linear and system identification methods. Next, models of friction force and pneumatic actuators involving physical or mechanical modifications will be delved into.

Figure 3.2 provides an illustrative block diagram of a double-acting operating system. The load dynamics are derived from the piston load dynamics.

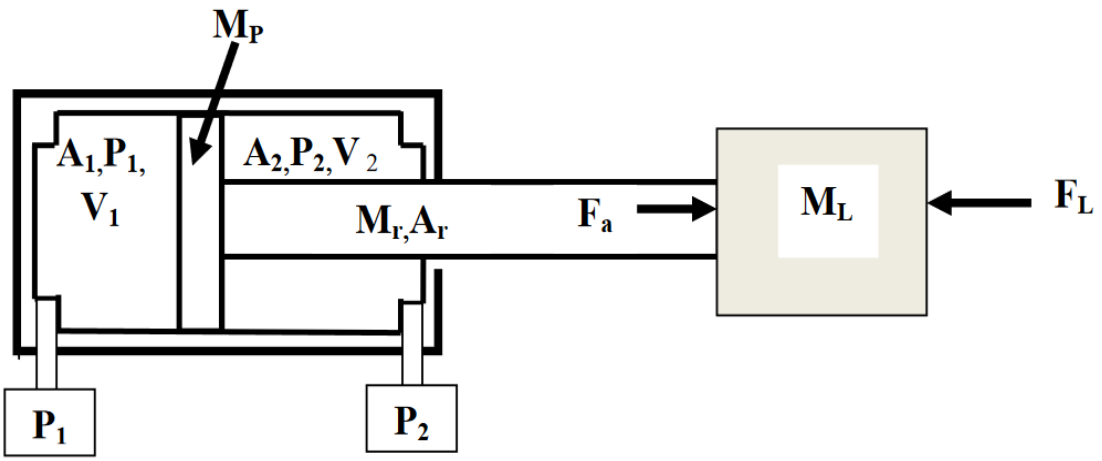

Figure 3. 2 Block diagram of pneumatic cylinder

3.4 Modeling of piston rod load

The formula of the motion for the combined piston rod load can be illustrated as [50],

$$(M_L + M_p)\ddot{x} + \beta\dot{x} + F_f + F_L = P_1A_1 - P_2A_2 - P_aA_r \quad (3.7)$$

where:

M_L is the mass of the load.

M_p is the combined mass of the piston with rod.

x is the rod displacement.

β is the coefficient of the frictional viscous.

P_1 and P_2 are the pressure values in cylinders' chambers.

F_f is the coulomb frictional force.

F_L is the external load.

P_a is the absolute atmospheric pressure.

A_1 and A_2 are the piston areas of the chambers.

A_r is the cross section area of the rod piston.

M_r is the mass of the rod.

V_1 and V_2 are the volume of the chambers.

F_a is the ambient force of the rod.

The expression on the right-hand side of the formula (3.7) represents the active force of the pneumatic actuator arising from the net pressure force acting on the piston. To control the power output of the actuator, the pressure level in the cylinder chamber must be fine-tuned using a control element (a pneumatic valve). This requires a detailed model of the pressure dynamics in the two chambers of the actuator and the valve dynamics.

3.5 Modeling of pneumatic chambers

In this part, the mathematical model is formulated that is necessary for each pneumatic cylinder chamber to link the pressure with the mass flow rate and piston linear velocity. In literatures, the authors derived the equations under the assumption of no heat transfer during the charging and discharging processes. In this section, the pressure dynamics equation has been derived to explain the varying thermal properties of the cylinder during the charging and discharging processes of the pneumatic chambers.

The general model of a gas volume consists of three formulas: the state equation (the law of perfect gas), the equation for mass conservation (the continuity formula), and the formula of energy [51]. These formulas can be put for each chamber putting in the assumption that the gas used in the system is perfect, the temperature and pressure in the pneumatic chamber are uniform, and the potential and kinetic energy terms are neglected. Considering the mass m, pressure P, temperature T, control volume V, density ρ then the law of ideal gas can be written as follows [52],

$$P = \rho\, R\, T \tag{3.8}$$

Applying the principle of mass conservation and using the perfect gas constant R, the rate of the mass flow can be expressed as,

$$\dot{m} = \frac{d}{dt}(\rho\, V) \tag{3.9}$$

which can be written in another form as,

$$\dot{m}_{in} - \dot{m}_{out} = \dot{\rho}V + \rho\dot{V} \tag{3.10}$$

Here, $\dot{m}_{in}$ and $\dot{m}_{out}$ represent the inlet and outlet mass flow rates of the chamber, respectively. The energy formula, which states that the rate of energy change within the system is equal to the net rate of energy transfer into the system, can be expressed as:

$$\acute{q}_{in} - \acute{q}_{out} + kC_v(\dot{m}_{in}T_{in} - \dot{m}_{out}T) - \dot{W} = \dot{U} \tag{3.11}$$

In this equation, k represents the heat ratio, C_v is the constant-volume specific heat capacity, T_{in} is the gas temperature entering the system, $\dot{W}$ is the rate at which.work is being done, and $\dot{U}$ is the rate of change in energy. The total rate of change in internal energy, which is the sum of the changes in internal energy of all the particles in the system, is given by:

$$\dot{U} = \frac{d}{dt}(C_v mT) = \frac{1}{k-1}\frac{d}{dt}(PV) = \frac{1}{k-1}\left(V\dot{P} + P\dot{V}\right) \tag{3.12}$$

Here, the gas in ideal situation, $C_v = \frac{k}{k-1}$ can be applied . Substituting this relation with $\dot{W} = P\dot{V}$ and (3.11), into (3.12), it yields:

$$\acute{q}_{in} - \acute{q}_{out} + \frac{k}{k-1}\frac{P}{\rho T}(\dot{m}_{in}T_{in} - \dot{m}_{out}T) - \frac{k}{k-1}\,P\dot{V} = \frac{1}{k-1}\,V\dot{P} \tag{3.13}$$

Assuming thermal equilibrium between the incoming flow and the gas within the chamber, the energy balance equation reduces to,

$$\frac{k-1}{k}(\acute{q}_{in} - \acute{q}_{out}) + \frac{1}{\rho}(\dot{m}_{in} - \dot{m}_{out}) - \dot{V} = \frac{V}{kP}\dot{P} \tag{3.14}$$

If the process is assumed to be adiabatic, meaning there is no heat transfer into or out of the system ($\acute{q}_{in} = \acute{q}_{out}$), the rate at which the chamber pressure changes with respect to time can be determined from equation (3.14) as,

$$\dot{P} = k\frac{P}{\rho V}(\dot{m}_{in} - \dot{m}_{out}) - k\frac{P}{V}\dot{V} \tag{3.15}$$

Or, substituting ρ from (3.8) into (3.15) yields,

$$\dot{P} = k\frac{RT}{V}(\dot{m}_{in} - \dot{m}_{out}) - k\frac{P}{V}\dot{V} \tag{3.16}$$

Assuming an isothermal process, where the temperature remains constant, the change in internal energy is negligible,

$$\dot{U} = C_v \dot{m} T \tag{3.17}$$

Equation (3.14) can be written as follows,

$$\acute{q}_{in} - \acute{q}_{out} = P\dot{V} - \frac{P}{\rho}(\dot{m}_{in} - \dot{m}_{out}) \tag{3.18}$$

Consequently, the time rate of change of pressure will be given by,

$$\dot{P} = \frac{RT}{V}(\dot{m}_{in} - \dot{m}_{out}) - \frac{P}{V}\dot{V} \tag{3.19}$$

When comparing equations (3.16) and (3.19), a careful examination reveals that the sole distinction between them is the heat ratio term k. Therefore, both of the formulas can be rewritten in the following form,

$$\dot{P} = \frac{RT}{V}(\alpha_{in}\dot{m}_{in} - \alpha_{out}\dot{m}_{out}) - \alpha\frac{P}{V}\dot{V} \tag{3.20}$$

The coefficients α, α_{in}, and α_{out}, which range from 1 to k, reflect the specific heat transfer occurring during the process. Equation (3.20) enables estimation of these coefficients without requiring detailed knowledge of heat transfer characteristics. The bounded uncertainty of the estimation, limited to k -1, is significant for control system design. To model the charging process accurately, the parameter α_{in} should be chosen close to the specific heat ratio k. For the

discharge phase, the parameter α_{out} must be chosen closer to unity. When considering the thermal effects of piston movement during compress and expand process, using a value of α = 1.2 provides a more accurate description.

Considering the piston displacement origin to be the stroke midpoint, the following formula can be used to calculate chamber volumes [53]:

$$V_i = V_{0i} + A_i(\frac{1}{2}L \pm x) \tag{3.21}$$

Here, i = 1, 2 denote .cylinder's chamber index. V_{0i} represents the in-active volume, which includes end-stroke volume and the volume in the admission ports that is not directly involved in the compression or expansion process, A_i is the area of the piston chamber, L is the initial stroke of the piston rod and x is the rod displacement, noted that the negative sign in the rod retraction process and the positive sign represent the rod displacement during compression. The difference between A_1 and A_2, the piston's chambers areas, is because of the piston rod area. Substituting (3.21) into (3.20) yields the temporal derivative of the pressure in the cylinder chambers:

$$\dot{P}_i = \frac{RT}{A_i\left(\frac{1}{2}L \pm x\right)}(\alpha_{in}\dot{m}_{in} - \alpha_{out}\dot{m}_{out}) - \alpha\frac{PA_i}{V_{0i}+A_i(\frac{1}{2}L \pm x)}\dot{x} \tag{3.22}$$

The new pressure equation is a more comprehensive model that considers several factors: Thermal behavior during charging and discharging, the compression or expansion process of the air caused by the movement of the piston, the difference in the effective area of the piston on its two sides, the volume of the chamber that is not swept by the piston (inactive volume), and the effect of air flowing in or out of the chamber. The first term in the formula represents the impact of the airflow on the chamber pressure, while the second term accounts for the influence of the piston's movement.

The cylinder chamber can be supplied with flow from two different sources; from the pressurized reservoir tank through the valve and tube connecting to it, and the

nearby chamber, provided that its pressure exceeds that of the target chamber and the piston seals are not fully intact. Potential air leakage paths from the cylinder chamber include the valve, piston seals, and the nearby chamber. While pneumatic cylinders with rubber seals typically have minimal leakage between chambers, low-frictional cylinders with Teflon or graphite seals can experience significant leakage. The next section will derive mathematical expressions to quantify the inlet and outlet flows in these systems, taking into account the potential for leakage.

3.6 Modeling of the air valve

Pneumatic valves play a critical role in actuator systems, enabling precise and rapid control of airflow into and out of the actuator chambers. A wide range of valve designs are available, varying in orifice geometry, flow regulation element, number of paths and ports, and actuation mechanism [54]. The study concentrates on proportional valves that are actuated by electric coils. These valves offer many advantages over traditional valves, including nearly linear flow characteristics, rapid response times, low leakage, the competence to control the pressure in both chambers with a single signal form controller, minimal hysteresis, and low internal friction.

A commercially available Position x, four-way, proportional valve from Numatics. Incorporated. was utilized. The valve is designed to balance the forces acting on it due to pressure differences, meaning that the forces acting on it from both sides are equal when the valve is closed. To keep the spool in its closed position, two coil springs are used to provide a restoring force.

Accurate flow control is made possible by this design, which enables quick and exact modifications of the valve orifice area. The air that is compressed will flow inward ($\dot{m}_{in} > 0$, $\dot{m}_{out} \approx 0$) if the spool is moved in a positive way, connecting chamber 1 to the tank via the supply channel. The exhaust path will

connect chamber 2 to the environment, causing the air to flow outward ($\dot{m}_{in} \approx 0$ and f$\dot{m}_{out} > 0$). Now, it can present a developed model for the position x valve. Although this analysis is based on a specific model of a pneumatic proportional spool valve, the methodology and equations can be easily modified to accurately represent the behavior of any other commercially available valve of this type.

To accurately model the behavior of the valve, two key components needed to be considered: the dynamics of the spool, which is the moving part that controls the flow, and the mass flow rate of the fluid through the variable orifice, which is the opening in the valve that changes size to regulate the flow.

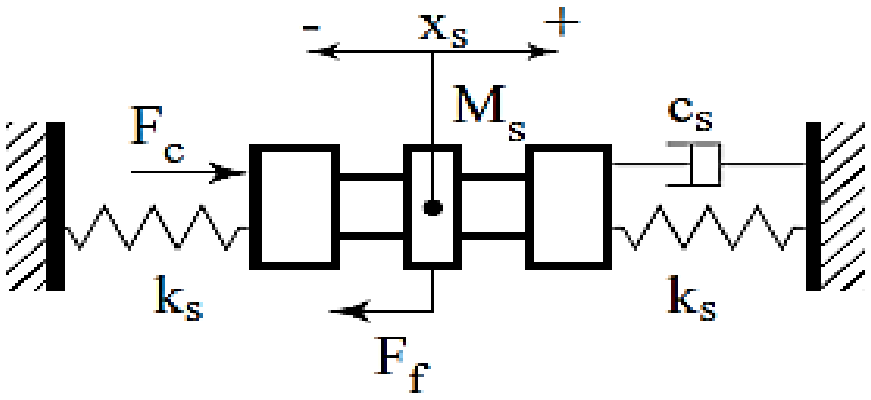

Figure 3. 3 Equilibrium of Valve Spool Dynamic [54]

The dynamic behavior of the valve spool can be described by the following equation of motion [54]:

$$M_s\ddot{x}_s = -c_s\dot{x}_s - F_f + k_s(x_{so} - x_s) - k_s(x_{so} + x_s) + F_c \tag{3.23}$$

where x_s represents the spool position, x_{so} denotes spring compression at rest, M_s is the combined mass of the coil and spool, c_s is the coefficient of frictional viscous, F_f is the coulomb frictional force, F_c is the force resulted by the coil and k_s is the spool spring constant,. By reducing the formulas describing the force exerted by springs to simpler terms, the following expressions can be arrived at:

$$M_s\ddot{x}_s + c_s\dot{x}_s + F_f + 2k_sx_s = F_c \tag{3.24}$$

The coulomb friction force, F_f is neglected due to the application of a noise signal to the coil. Using the equation that relates the force generated by the coil to the current flowing through it, and ignoring F_f, the equation becomes:

$$M_s\ddot{x}_s + c_s\dot{x}_s + 2k_s x_s = K_{fc} i_c \tag{3.25}$$

In the above equation, K_{fc} represents the force constant of the coil, and i_c denotes the current coil. The pressure loss incurred across the valve orifice is often important to consider, demanding the simulation of compressible, turbulent flow conditions. If the ratio of the pressure upstream of the orifice to the pressure downstream exceeds a specific value P_{cr}, the flow attains sonic speed (choked flow state) and becomes linear dependent on the upstream pressure. The choked flow mode of operation is considered simple and fast operation [50]. Conversely, for pressure ratios below P_{cr}, the mass flow exhibits nonlinear dependence on both upstream and downstream pressures where the proportional mode of operation is considered complex but exhibit high accuracy. The equation that is commonly used to calculate the mass flow rate through an orifice with a cross-sectional area A_v is:

$$\dot{m}_v = \begin{cases} C_f A_v C_1 \frac{P_u}{\sqrt{T}} & if \quad \frac{P_d}{P_u} \le P_{cr} \\ C_f A_v C_2 \frac{P_u}{\sqrt{T}} \left(\frac{P_d}{P_u}\right)^{\frac{1}{k}} \sqrt{1 - \left(\frac{P_d}{P_u}\right)^{\frac{k-1}{k}}} & if \ \frac{P_d}{P_u} > P_{cr} \end{cases} \tag{3.26}$$

$$\text{And } A_v = \frac{\pi}{4} d^2 \tag{3.27}$$

where $\dot{m}_v$ is the mass flow rate across the valve orifice, C_f is a non-dimensional coefficient of discharge, and P_u is up.stream pressure and P_d is downstream pressure and d is the diameter of the solenoid valve..

$$C_1 = \sqrt{\frac{k}{R}\left(\frac{2}{k+1}\right)^{\frac{k+1}{k-1}}} \quad ; \quad C_2 = \sqrt{\frac{2k}{R(k-1)}} \quad ; \quad P_{cr} = \left(\frac{2}{k+1}\right)^{\frac{k}{k-1}} \tag{3.28}$$

The constants C_1, C_2, and P_{cr}, specific to a given fluid, are important parameters in equation (3.28). For air gas ($k = 1.4$), these values are $C_1 = 0.04042$ and $C_2 = 0.15618$, while $P_{cr} = 0.528$. The interpretation of upstream and downstream pressures in equation (3.26) depends on the process either retract or compress. During charging, the supply tank pressure is upstream, and the cylinder's chamber pressure is downstream. For discharging, the roles are reversed. The same thing can be applied to model the flow of leakage between chambers, with appropriate adjustments to the area of the valve and pressure definitions.

3.7 Adaptive Neuro-Fuzzy Inference System

Figure 3.4 illustrates a typical ANFIS architecture. In this architecture, Sugeno fuzzy models [55] are commonly used. These models are preferred due to their ability to be easily understood, their efficient computation, and their built-in methods for optimization and adaptation. For simplicity, it is considered two inputs *x* and *y*, and one output, *z*.

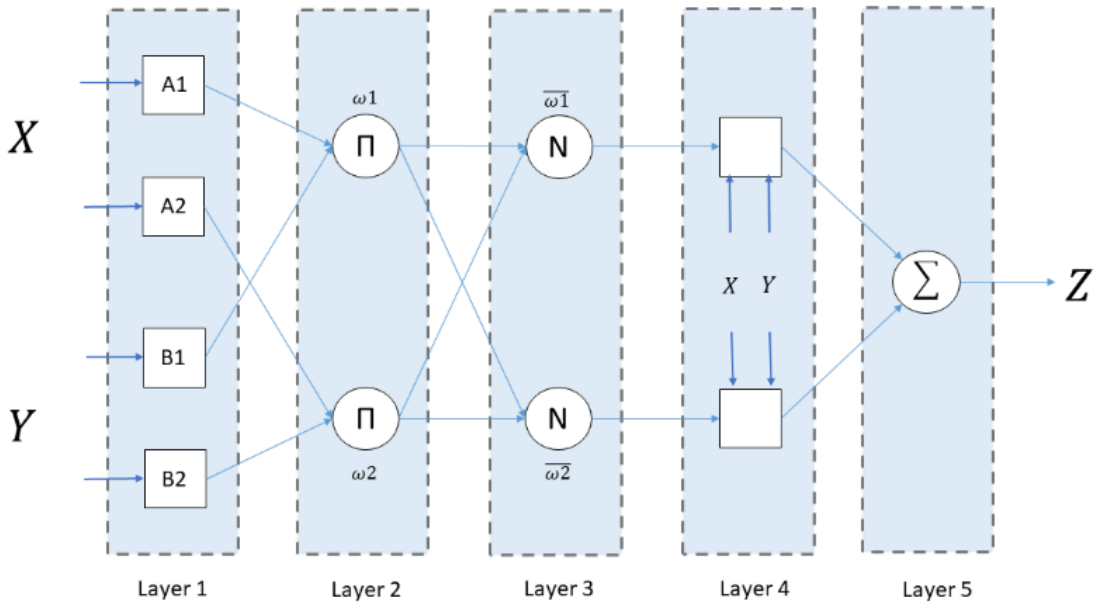

Figure 3. 4 ANFIS Structure

For a first-order Sugeno fuzzy model, a common approach involves using a set of rules with two fuzzy if-then rules. The rule set can be stated as follows:

Rule 1: if x is A_1 and y is B_1; then $Z_1 = P_1X + Q_1Y + R_1$

Rule 2: if x is A_2 and y is B_2; then $Z_2 = P_2X + Q_2Y + R_2$

While A_i and B_i are the fuzzy.groups used in the.antecedent, the P_i, Q_i, and R_i are design variables derived from the process of training. As in Figure 3.4, the ANFIS consists of the following five layers:

Layer 1: Every node i in the first layer's nodes is calculated using the following function:

$$\begin{cases} O_i^1 = \mu_{A_1}(x) \ \ where \quad i = 1,2 \\ O_i^1 = \mu_{B_{i=2}}(y) \ \ where \quad i = 3,4 \end{cases} \tag{3.28}$$

Any fuzzy membership function can be used by μ_{A_i} and $\mu_{B_{i=2}}$.

Layer 2: Each node within this layer determines the degree to which a particular rule is activated by multiplying the membership values of the input variables:

$$O_i^2 = \omega_i = \mu_{A_i}(x)\,\mu_{B_i}(y) \ , \qquad i = 1,2 \tag{3.29}$$

Layer 3: The i-th node situated in this layer evaluates the proportion of the i-th rule's activation relative to the total activation of all rules by dividing the i-th rule's firing strength by the sum of the firing strengths of all rules:

$$O_i^3 = \bar{\omega}_i = \frac{\omega_i}{\sum_{j=1}^{n} \omega_j} \tag{3.30}$$

Layer 4: The i-th adaptive node within this layer determines the extent to which the i-th rule contributes to the final output value. This is calculated using the following node function:

$$O_i^4 = \bar{\omega}_i z_i = \bar{\omega}_i(p_i e + q_i de + r_i) \tag{3.31}$$

where p_i, $q_i and\ r_i$ are the training parameters and e and de represent error and change of rate of error between two inputs.

Layer 5: The final node in this layer which is fixed combines the individual contributions from each rule to determine the overall output value by adding them together and divided them on the sum of all weights:

$$O_i^5 = \sum_{i=1}^{2} \overline{\omega_i} z_i = \frac{\omega_1 z_1 + \omega_2 z_2}{\omega_1 + \omega_2} \quad (3.32)$$

If the ANFIS system is modeled as shown in Figure 3.5, the ANFIS system structure contains two inputs in the first layer represented by the readings of sensors LDR1 and LDR2 from the microcontroller. The second layer shows how to divide the input into three membership functions with values (small, meduim, and big), and the membership used, and the simulation was the membership of the triangle. The third layer follows this to fuzzify the second layer by the fuzzy rules, then the fourth layer of the ANFIS system where the normalization operation to the data output from the third layer, and finally to the summation process to the all the nodes to give the output signal which is defined as the voltage level for the pneumatic system to drive the solar panel.

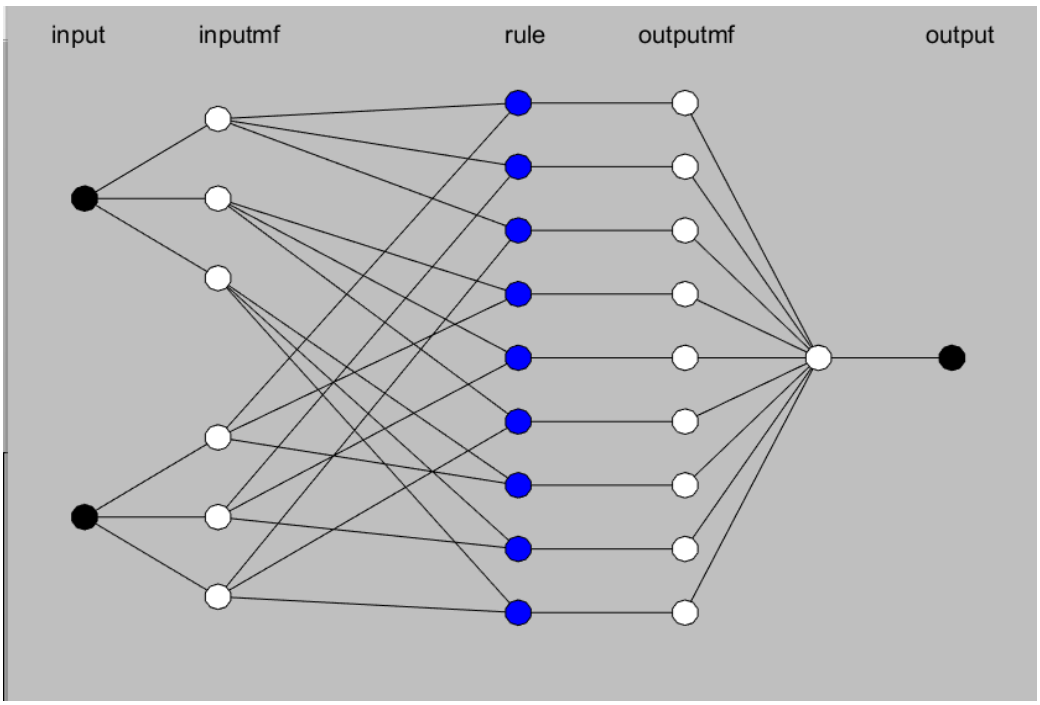

Figure 3. 5 ANFIS Structure for the Proposed System

All the possible data from the two LDR sensors are put in the training, and the corresponding output, as shown in Figure 3.6, is the process of the ANFIS network to train the data, predict any data read by the sensors, and give an output that maps the input signal. The training used 100 epochs and three triangle memberships for each input signal. The error was significantly low, as shown in Figure 3.7, and about 6.7×10^{-8} is considered a good training process.

Each data input from the sensor is bounded between (0-1023) since the microcontroller has an analog-to-digital converter with a 10-bit quantization level; dividing these levels into 11 segments makes it 121 possible outputs. The output will range [-5, 5V] for the ANFIS training process. The data source from workshop that have the input and output data, the optimization method used hybrid method where the training method used forward and backpropagation with 100 epochs. The input for the system is three membership function with one output which is voltage level for the pneumatic valve.

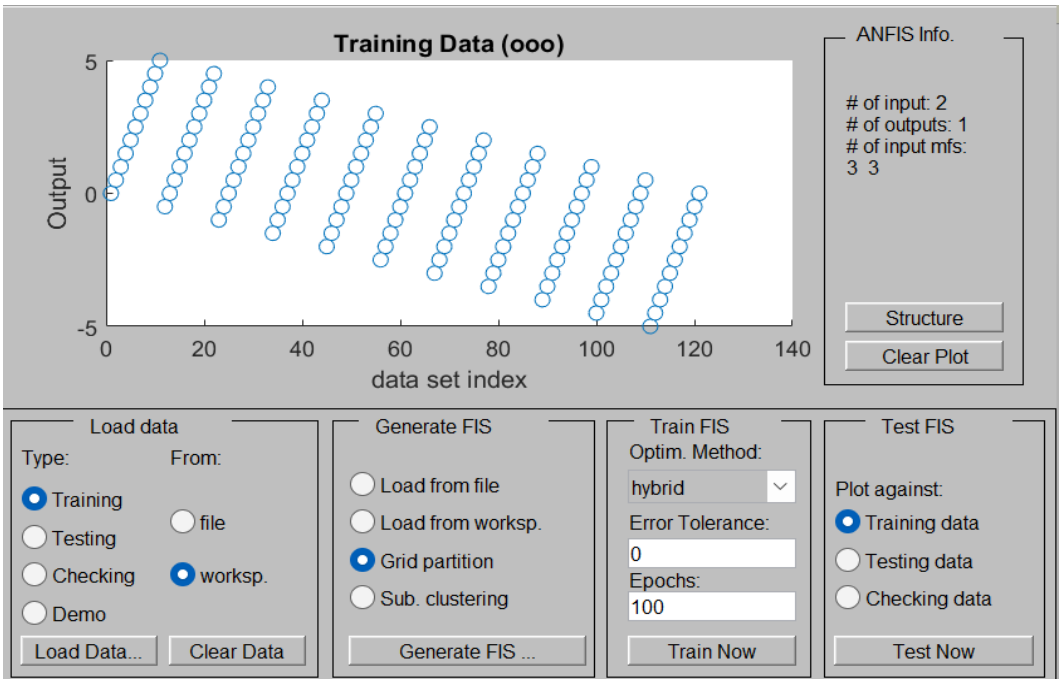

Figure 3. 6 ANFIS Training.

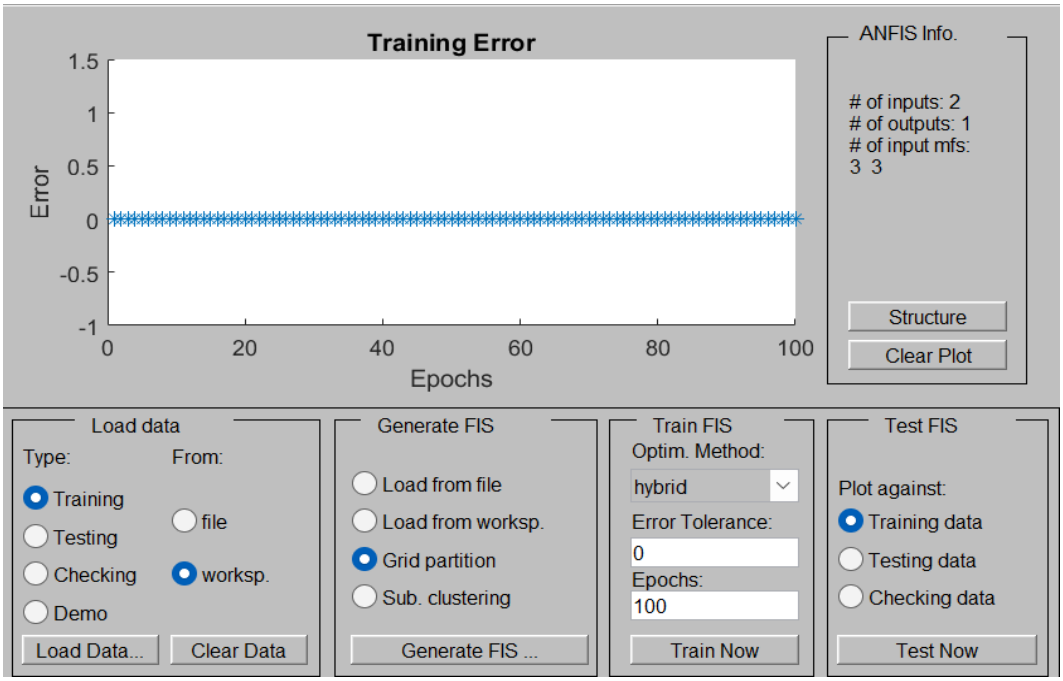

Figure 3. 7 Complete Training and Estimated Error

3.8 Modeling of fuzzy logic controller

FL is a form of many-valued logic in which any actual number between 0 and 1 might denote the truth values of its variables. This technique addresses partial truth, which may possess either an exact or erroneous truth value [56]. In contrast, Boolean logic permits variables to possess only truth values of 1 or 0. FL was conceived to address the reality that decisions are often based on ambiguous and non-numerical information. These models can recognize, illustrate, alter, interpret, and utilize ambiguous and inaccurate information and data.

The FL is implemented because of the system's adaptability and applicability in online and offline contexts [57]. The FLC provides solutions to intricate issues. Utilizing exact functions, the FL can analyze several inputs and render judgments. The FLC necessitates reduced spatial requirements. The FL system emulates human cognitive processes, facilitating the management of challenging situations. Regulate the sensor’s signals via fuzzy logic.

Figure 3.8 and Figure 3.9 illustrates the utilization of a two-input signal and a single-output signal. The first input is the error between two sensors' readings for specific angles; e.g., the error between LDR_{north} and LDR_{south} will enter the FLC system to control the direction of the tilt angle. Meanwhile, the difference between the LDR_{west} and LDR_{east} will control the azimuth angle via the FLC system. The derivative of the error would be the second input for the FLC system, which impacts the FLC output signal through a set of rules as shown in Figure 3.10. The parameters for the FLC was set was AND as minimum, OR as maximum and defuzzification is centroid which considered a default parameter for FLC system in Matlab/Simulink.

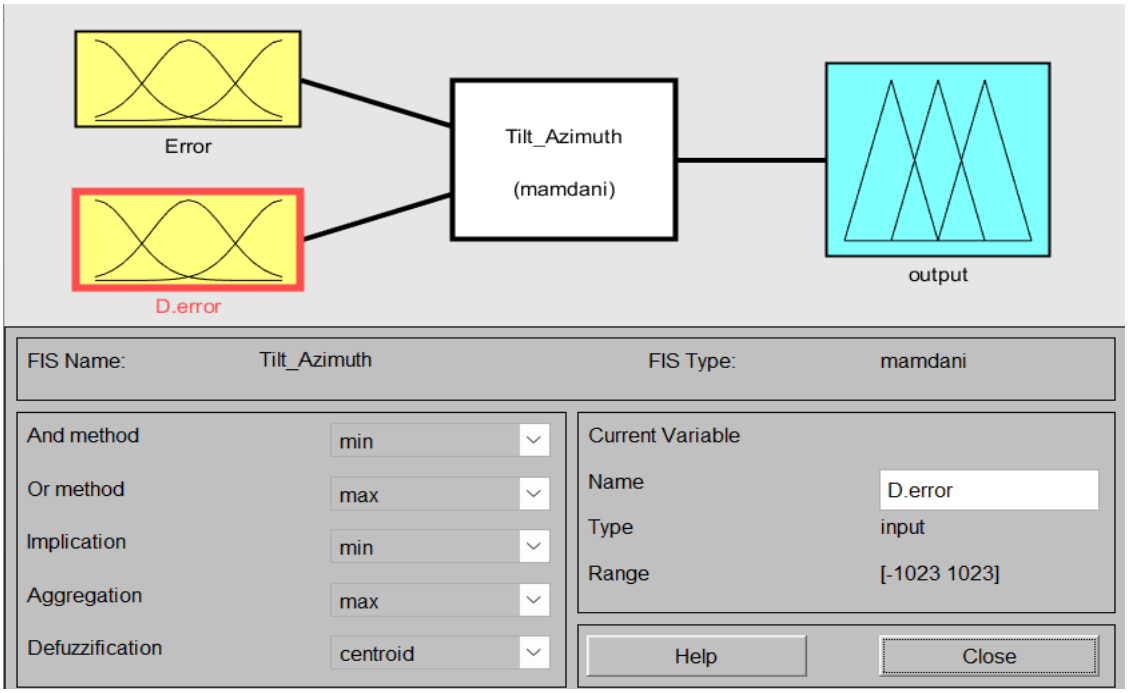

Figure 3. 8 Inputs and Output of the FLC System

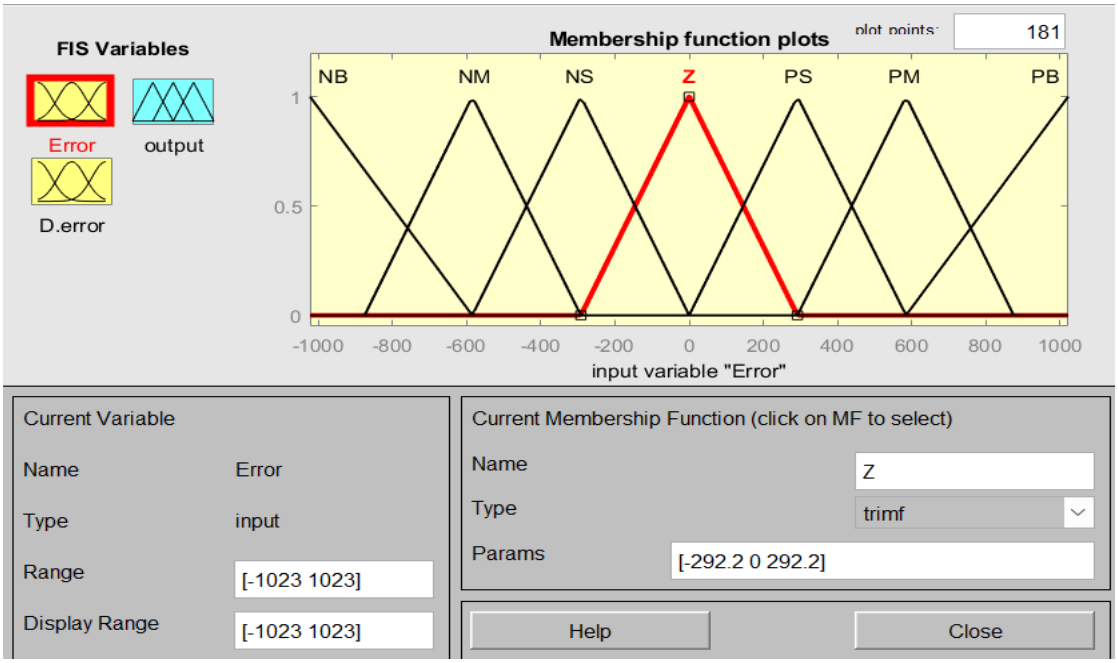

Figure 3. 9 Membership Functions of the Input

Every input has been divided into seven membership functions, as shown in Figure 3.9 (zero Z, positive big PB, negative big NB, positive medium PM, negative medium NM, positive small PS, and negative small NS). Figure 3.10 shows the membership function between the two inputs and the corresponding output for the FL system. The range of the input was maximum and minimum error of the controller's reading, which is (-1023 to 1023).

The output of the FLC also contains a seven-membership function with the same type of function, which is a triangle membership function, as shown in Figure 3.11. The triangle membership function has the advantage of simplicity, which specified with 3 points only and does not require any complex mathematical models so it is easy to be programmed. Still, the range will differ from the input signal to (-5 to 5) to match the upcoming joint system that needs this range to drive the actuators where -5 represents fully retract, zero standstill and 5 corresponds fully compress.

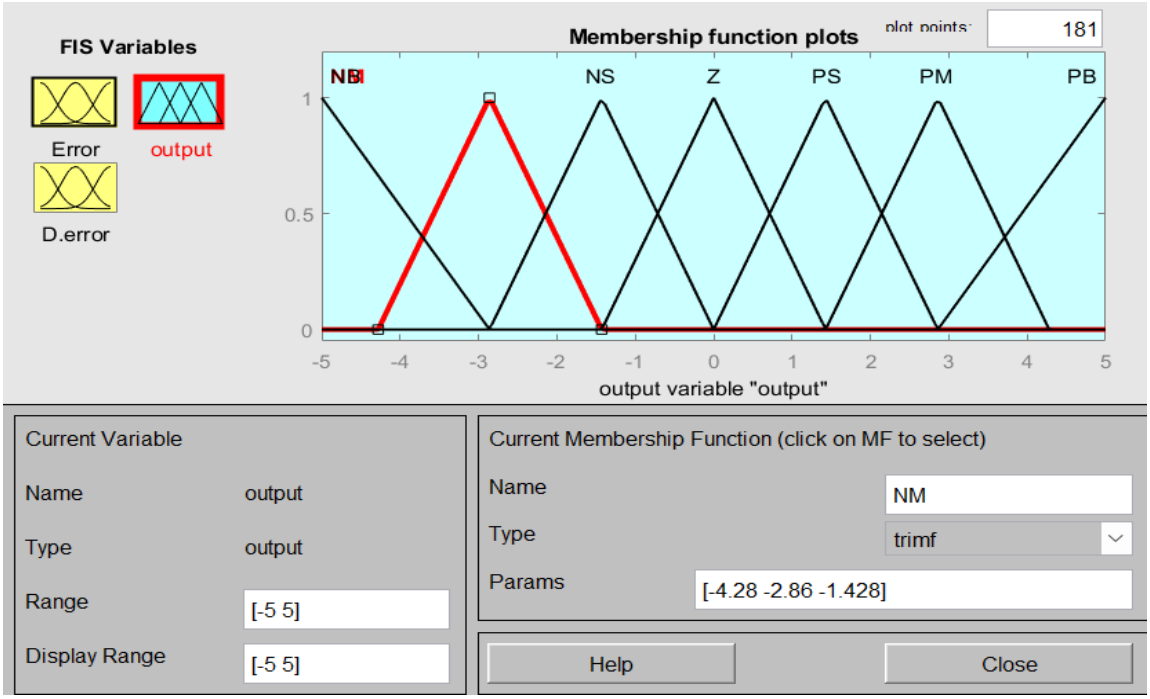

Figure 3. 10 Output Membership Function and its Range

Error/ D.Error	NB	NM	NS	Z	PS	PM	PB
NB	**NB**	**NB**	**NB**	**NB**	**NB**	**NB**	**NB**
NM	**NB**	**NB**	**NB**	**NM**	**NM**	**NM**	**NS**
NS	**NB**	**NM**	**NS**	**NS**	**Z**	**NS**	**PS**
Z	**NB**	**NM**	**NS**	**Z**	**PS**	**PM**	**PB**
PS	**NS**	**PS**	**Z**	**PS**	**PS**	**PM**	**PB**
PM	**Z**	**PS**	**PM**	**PM**	**PB**	**PB**	**PB**
PB	**PB**	**PB**	**PB**	**PB**	**PB**	**PB**	**PB**

Figure 3. 11 The Rule Base of the FLC System

3.9 Modeling of Compare Method Control

Compare method is considered as a direct method of controlling the tracking system. Comparing the readings between to specific sensors to give an output for the pneumatic actuator is the main process of this method. This is done by programming the controller with specific code to compare the readings between LDRnorth and LDRsouth for tilt angle, and LDRwest and LDReast for azimuth angle. Appendix 2 showed the code for the compare method where the input is the sensor readings and the output is the rod position. Keeping in mind a threshohold value is set between to readings and this represent the accuracy factor for this method. Figure 3.12 shows the computer flowchart for the this method, it begins with the input readings and this leads to move the double acting cylinder for the desired solar angles.

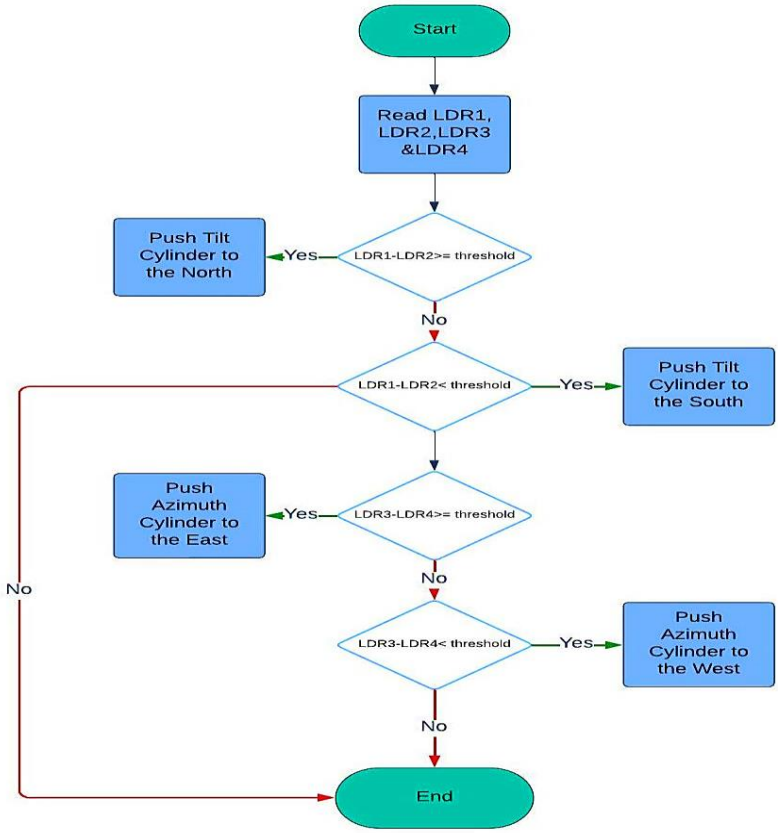

Figure 3. 12 Flow chart of the compare method

3.10 Modeling of solar angles

Understanding solar angles, used to describe the particular angles at which the sun appears in the sky is essential to understanding the sun tracking system. Figure 3.13 illustrates two important angles: the azimuth angle (γ) and the tilt angle (α). The angle created by the sun's rays and the horizontal plane is known as the tilt angle, while the angle made by the north axis and the vertical line extending from the sun is called the azimuth angle.

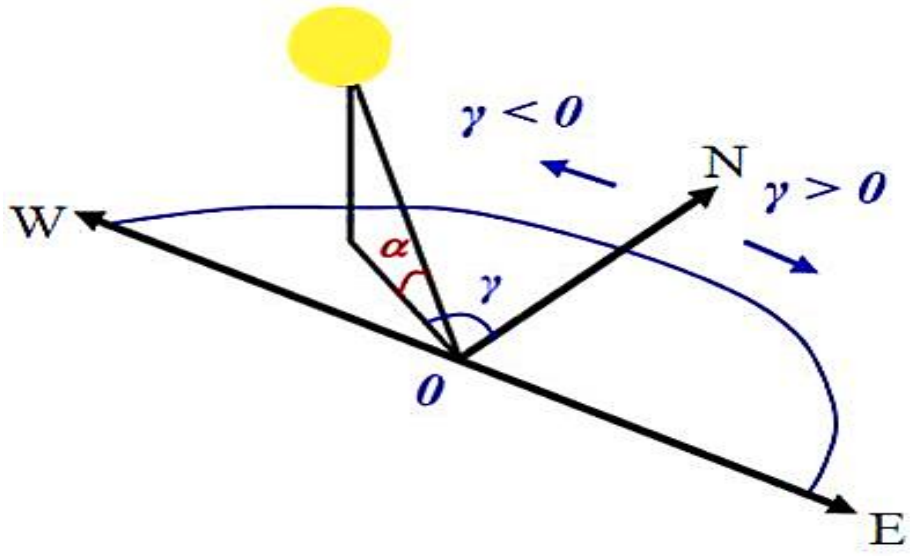

Figure 3. 13 The Sun Tilt and Azimuth Angles [58]

These angles can be computed as follows [58]:

$$\alpha = sin^{-1}(sin\,\delta\,sin\,\theta + cos\,\delta\,cos\,\omega\,cos\,\theta) \tag{3.33}$$

where α, θ, and δ are the tilt, latitude, and altitude angles, respectively. δ may be expressed as follows:

$$\delta = 23.45 \sin\left[\frac{360(n+284)}{365}\right] \tag{3.34}$$

where n represents the day count, for example the 1st of January, n = 1 and the 23rd of August $n = 31 + 29 + 31 + 30 + 31 + 30 + 31 + 23 = 236$, etc. Moreover, ω is the hour angle and is found by:

$$\omega = 15(t_s - 12) \tag{3.35}$$

where t_s is the solar time; in addition, the azimuth angle (γ) is calculated as follows:

$$\gamma' = \sin^{-1}\left(\frac{-\cos\delta \times \sin\omega}{\cos\alpha}\right) \tag{3.36}$$

In a particular case, if $\cos\omega \geq \frac{\tan\delta}{\tan\emptyset}$ then, $\gamma = 180 - \gamma'$, else $\gamma = 360 + \gamma'$

Chapter Four: Simulation and Experimental Work of the Solar Tracking System and Discussion

4.1 Introduction

This chapter deals with modeling, simulation, and analysis of the performance results of the proposed pneumatic solar tracking system. Figure (4.1) shows the schematic diagram of the system starting with the structure of the PV panel which has two degrees of freedom to achieve the tilt and azimuth angle movement, that structure is built to set the PV panel on it. The LDR sensors are set in the PV panel with four locations. The pneumatic system contains: a double-acting cylinder connected to the PV structure, on-off valves that are electrically connected to the microcontroller, and mechanically connected to the double-acting cylinder and pressure valve via PVC tubes. The control pressure valve regulates the pressure source which is a tank full of air. The control system contains mainly from microcontroller and the supporting circuit to ensure the operating condition and protection of the microcontroller. The sensors that are set on the PV panel are connected to the microcontroller which will process the signal and give an output signal to the pneumatic valves. Simulation of the proposed system model will be implemented using MATLAB/SIMULINK R2023a. In this thesis, three methods were used to control the position of the solar PV panel to obtain the highest power from the panel: comparison control, FL control, and ANFIS control. The simulation and the experimental work are done in Baghdad with a latitude of (33.367°N) on the days of 16-22 September 2024 with all these days being sunny days.

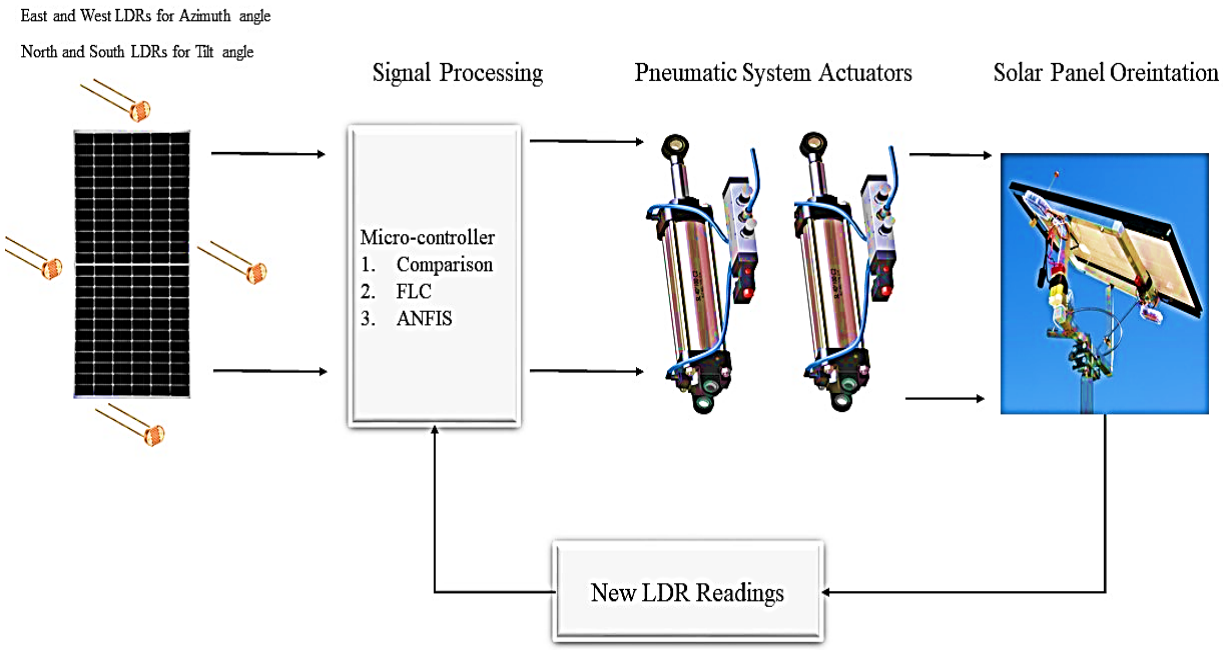

Figure 4. 1 Block Diagram of the Proposed Tracking System.

4.2 Solar Panel Characteristics

The power generated by solar PV cells fluctuates continuously due to changes in temperature and radiation intensity where the power harvested from PV panel is decreased by the increased temperature. It acts as a profile that depicts fluctuating radiation and temperature. Figure 4.2 illustrates a solar panel's I -V and P-V curves at various irradiation levels. The I-V curve demonstrates the correlation between the voltage and current output of the solar panel. The current rises with the voltage until it reaches a maximum, after which it declines.

The P-V charts illustrate the correlation between the voltage and power output of the solar panel across varying irradiance levels. Solar irradiance refers to the quantity of solar radiation incidents on a surface per unit area. The P-V curves are denoted in kW/m², indicating the irradiance level in kilowatts per square meter. As the irradiance level rises, the P-V curve ascends. This suggests that PV panels possess distinct specifications detailed in Table 4.1, which lists the parameters of the PV panels. The temperature effect in hot areas can by managed

by using low temperature coefficient panel or by using cooling techniques for the panel in these areas.

Table 4. 1 Technical Specification Used in the Design of PV Panels

Parameters under standard conditions (i.e., 1000 W/m^2 and 25 ^{o}C)	**Specification**
DG-P25W Poly Ethylene	25 W PV 144 cell
Dimensions	535×350×18 mm
Nominal PV Panel	25 W
Open Circuit Voltage	21.24 V
Short Circuit Current	1.53 A
Maximum Voltage	18 V
Maximum Current	1.39 A

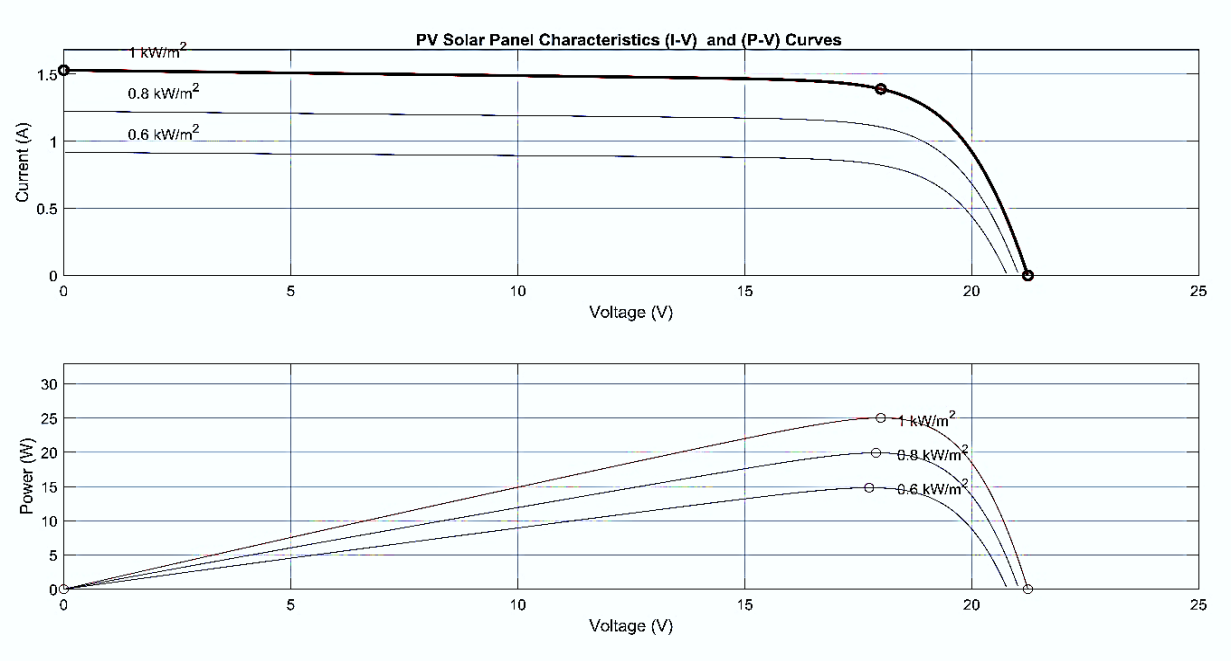

Figure 4. 2 PV Solar Panel Characteristics (I-V) and (P-V) Curves

4.3. Solar Angles Simulation

Solar angles are simulated by MATLAB/Simulink using the modeling in chapter 3, which demonstrated the azimuth and tilt angles. These two angles are significant for the solar tracking process.

The information needed for the simulation is the latitude angle and day count, choosing the location of Baghdad, whose latitude is (33.367°) and choosing the day of September 16 to conduct the tests, which counts (n = 255).

The solar equations are modeled using Matlab/Simulink as shown in Figure 4.3 to extract the optimal tilt and azimuth angle for that specific day, as shown in Figures 4.4 and 4.5. where the maximum angle for azimuth was at 5:45 PM and the tilt angle is restarted at the 5:49 PM for the location and day count mentioned.

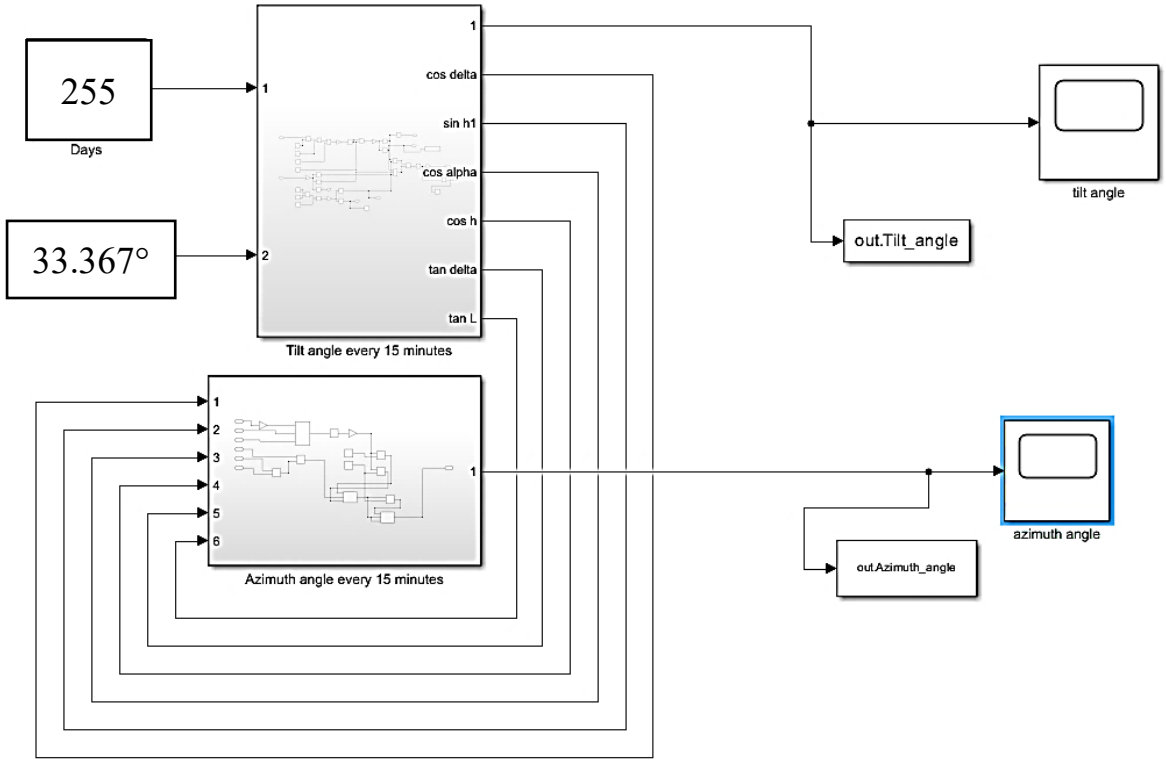

Figure 4. 3 Simulation Circuit Diagram for Solar Angles Modeling

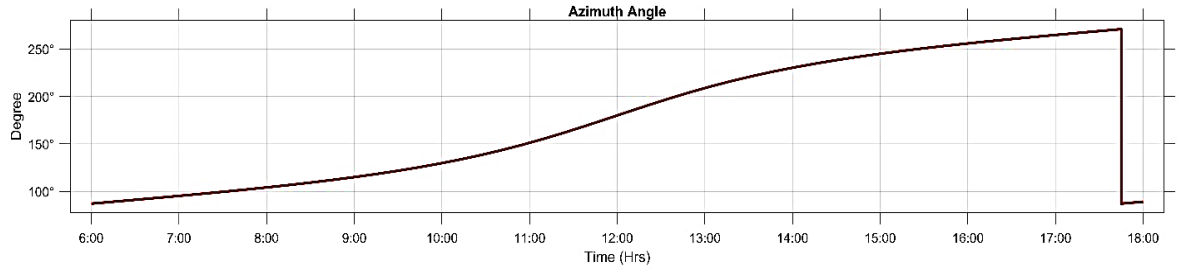

Figure 4. 4 Hourly distribution of azimuth angle.

Figure 4.4 shows the change in the azimuth angle, measured in degrees, of the sun's horizontal angle across daylight hours from 6:00 AM to 6:00 PM. The sun appears to move from east to west across the sky. The sun's azimuth angle increases throughout the day, starting from a low value in the morning and reaching a maximum value at the end of the day. The exact shape of the line and the maximum azimuth angle reached will depend on the latitude and longitude of the location where the solar panel is installed. The sun's azimuth angle changes throughout the year, with different maximum values at various times.

Solar tracking systems adjust their orientation to follow the sun's path throughout the day, maximizing solar energy capture.

The solar panel's tilt angle, as shown in Figure 4.5, changes throughout the day to optimize energy capture. It starts at a low angle in the morning, increases to a maximum around midday, and then decreases towards evening. The line forms a parabolic curve, with the maximum tilt angle around midday. This is because the sun's position in the sky changes throughout the day, and the panel's tilt angle needs to be adjusted accordingly to maximize sunlight exposure.

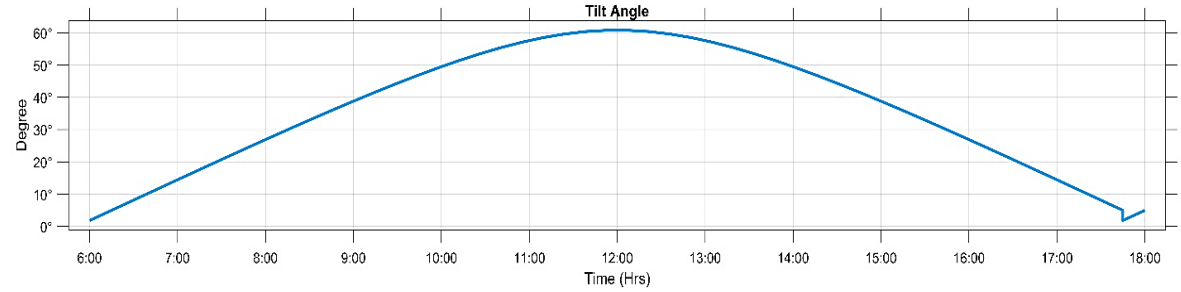

Figure 4. 5 Hourly distribution of tilt angle.

From Figures 4.4 and 4.5, the azimuth and tilt angles for the given day and location were azimuth angle from 87° to 268.85°, and the tilt angle began from 1.85° to 60.8° at 12:00 P.M and back at 5:50 P.M.

This simulation is essential for the next step; by mapping these data as an input sensor for the given angle, the sensors produced from mapping the solar angle will be input signals to the control system that drives the pneumatic actuators.

4.3 Pneumatic System Siumlation

The pneumatic system proposed in the tracking system contains a double-acting cylinder, 2/2 solenoid valve, pressure control valve, and pressure supply. Figure 4.6 and Table 4.2 shows the parameters of the pneumatic cylinder. The difference in area and volume between left and right chamber because of the area accupied by the rod piston.

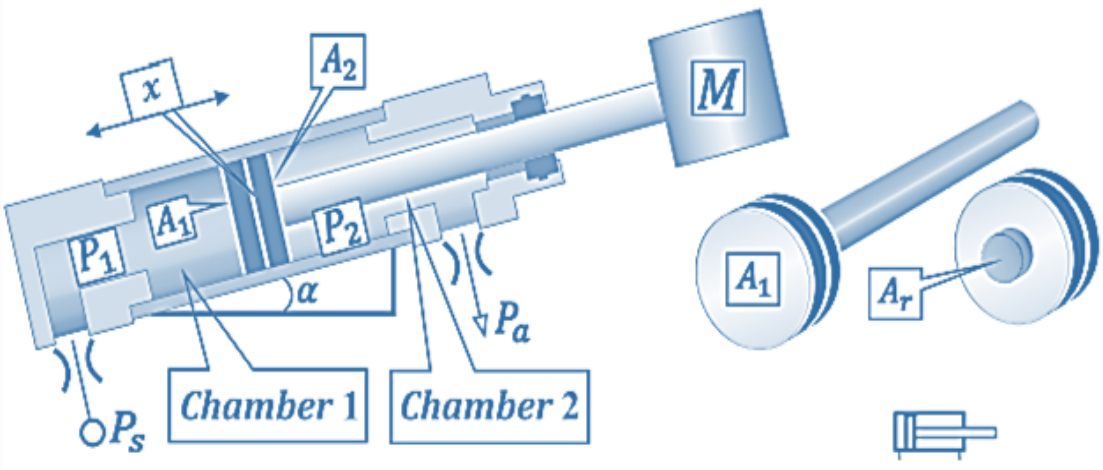

Figure 4. 6 Double-acting cylinder parameters [40]

Table 4. 2 Parameters for the pneumatic actuator system

Parameters	Specification
Rod Maximum stroke (L)	200 mm
Area of left chamber (A_1)	1.5×10^{-3} m^2
Area of right chamber (A_2)	1×10^{-3} m^2
Volume of left chamber (V_1)	1.64×10^{-5} m^3
Volume of right chamber (V_2)	1.03×10^{-5} m^3
Working Temperature (T)	300 K
Gas constant (R)	8.314 J/mol.K
Solenoid valve diameter (D)	8×10^{-3} m
Absolute ambient pressure (Pa)	0.003 Bar
Rod effective area (Ar)	0.314×10^{-3} m^2
Mass of the rod (ML)	0.1 kg
Friction force (F_F)	4 N

4.3.1 Scenario 1: Rod Position versus External Force

The parameters that affect the rod position displacement are the external force (FL), the external mass (Ms), and the input pressure of the pressure supply (Ps). In the first scenario, the effect of the external force against the rod position of the double-acting cylinder is shown in Figure 4.7. In this case, a constant input pressure of 4 bar and an external mass of 5 kg are applied. It is inversely proportional to this force. Figure 4.7 demonstrates how the rod position changes over time in response to different applied external forces. As the external force increases, the rod position will reach its maximum stroke faster. This suggests a direct relationship between the two variables.

The lines show that the rod position increases gradually, indicating a dynamic response to the applied force. Many lines facilitate a comparison of the impacts of

various external influences. The higher slope of a line correlates with a more rapid increase in rod position over time for that specific force. This information can be used to develop control strategies for mechanical components.

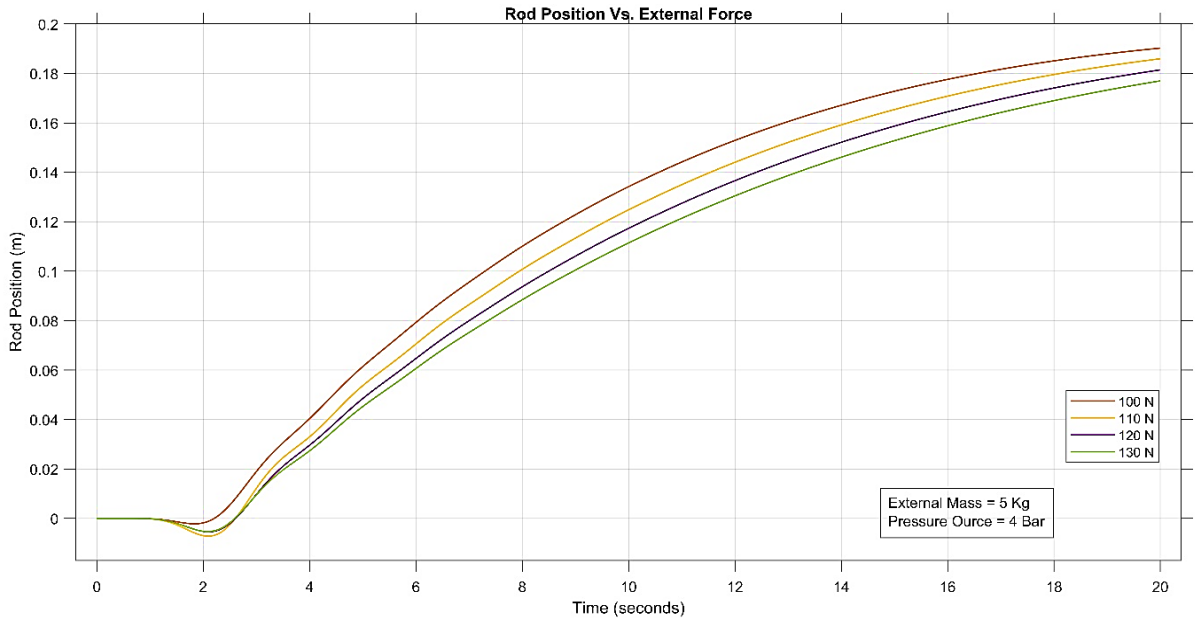

Figure 4. 7 Rod Position for different readings of External Force.

4.3.2 Scenario 2: Rod position versus masses

The second scenario is the effect of external mass on the rod displacement, where an input pressure of 4 bar and an external force of 100 N were simulated, resulting from the application of different masses (5, 15, 25, and 35) kg. It is noted that there are no significant changes between these results, and therefore this parameter does not affect the rod displacement compared to other parameters as shown in Figure 4.8.

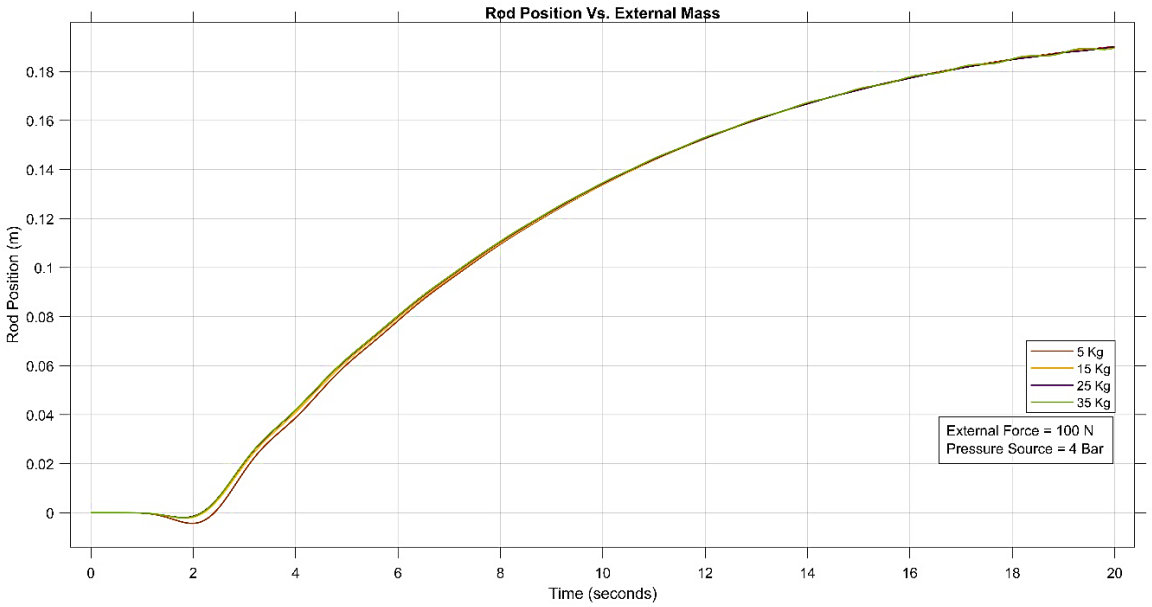

Figure 4. 8 Rod position for different readings of external mass

4.3.3 Scenario 3: Rod position versus input pressure

The third scenario analyzes the effect of the input pressure of the pneumatic supply system on the rod position. At the same time, the other parameters will be fixed: the external force at 100 N and the external mass at 5 kg. As shown in Figure 4.9, the input pressure will directly affect the rod position. By applying different pressures (4, 6, 8, and 10 bar), increasing the input pressure of the supply will decrease the time the rod needs to reach its maximum stroke. The lines show that the rod position rises gradually, indicating a dynamic response to the applied pressure.

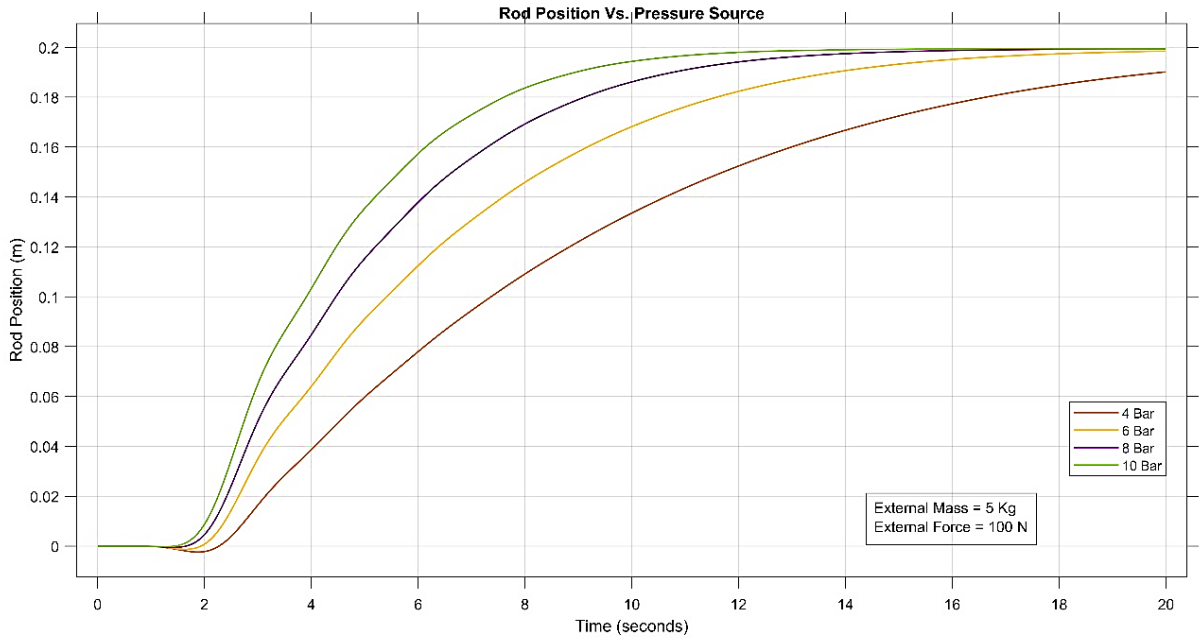

Figure 4. 9 Rod position for different readings of pressure source

4.3.4 Scenario 4: : Rod position versus external force and input pressure

Here the effect of external mass on the displacement of the rod was neglected. A relationship can be established between the external force FL and the pressure source Ps to give the same rod position curves in the simulation and continuous adjustment of the above parameters. Then the relationship between the external force and the input pressure is completed. The result is a fourth-degree polynomial describing the relationship between these two parameters and give a good response in the case of rod displacement as shown in Figure 4.10.

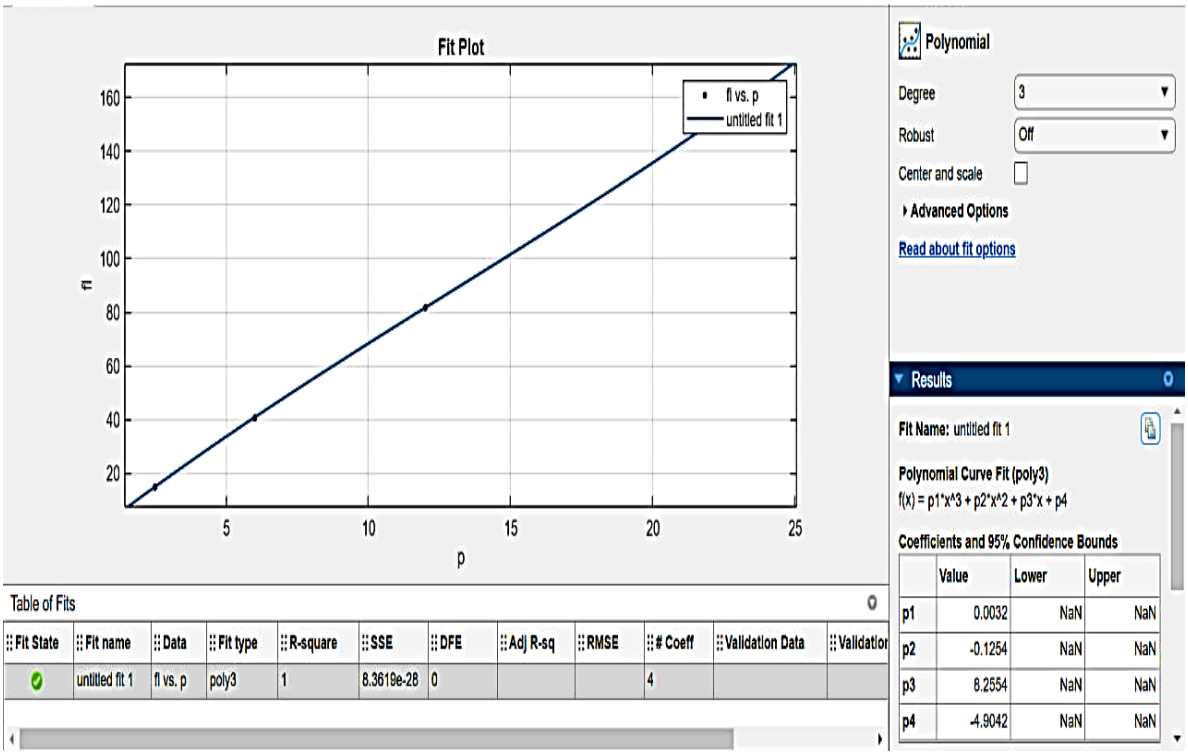

Figure 4. 10 External force Vs. Pressure source

The interpolated result using Matlab function of linear interpolation for the relationship between the external force and the input pressure with the coefficient of polynomial shown in figure 4.10 is:

$$FL = 0.0032 * Ps^3 - 0.1254 * Ps^2 + 8.2554 * Ps - 4.9042$$

The cubic polynomial coeffiecient p_1 to p_4 reprenet the n^{th} parameters for the polynomial.

4.4 Pneumatic system simulation using Simscape

Simscape, a part of MATLAB's Simulink, is a powerful tool for modeling and simulating physical systems, including pneumatic systems. Simscape has a powerful library for pneumatic system components, which helps design, construct, simulate, and produce results for specific systems. Figure 4.11 shows the simulation of the pneumatic system using the library of Simscape where port A and B is inout and output port for the solenoid valve, block Atm represent the

heat tranfer properties for the pneumatic actuator, L is the control signal port and R is the mechanical port for the rod piston. The design contains a double-acting cylinder, a 2/2 solenoid valve, a pressure source, and a reservoir. Each component has parameters that can be tuned to achieve the desired output.

1. Double-acting cylinder: It has been chosen to have a maximum stroke of 15 cm with a piston area of 2 cmm^2 with standard thermodynamic parameters.

2. 2/2 Solenoid valve: It has a two-port, input, output, and control signal. The controller provides the control signal in the proposed system. Its parameters are an orifice diameter equal to 1mm and a discharge coefficient of 0.3. It is noted that with constant pressure, the orifice diameter is directly proportional to the rod speed, the same as the discharge coefficient parameter.

3. Pressure source: 4 bar pressure was selected for the simulation. The pressure source is directly proportional to the rod speed.

4. Reservoir: This block is needed to complete the pneumatic system. The atmospheric pressure is selected for the block, and the reservoir block is imagined as a tank where the pressure source takes the gas from it, and the exhaust valve releases the gas to it.

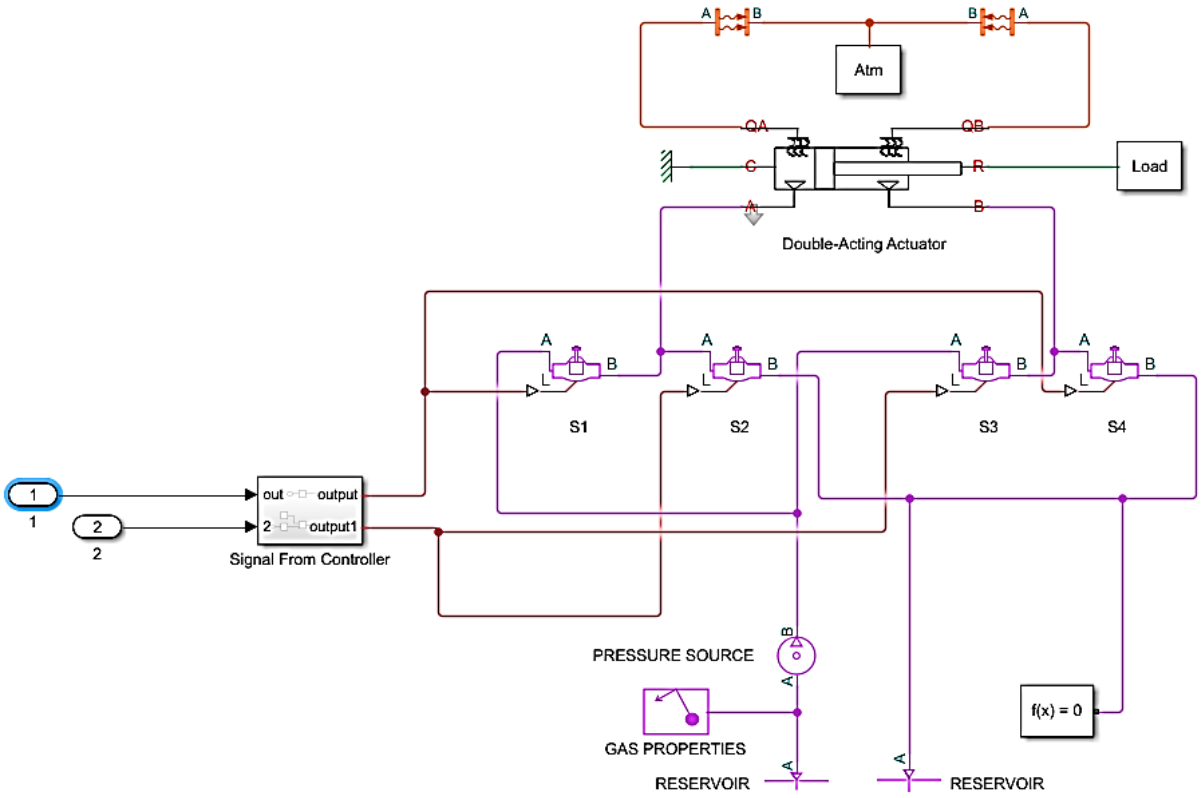

Figure 4. 11 Simulation of pneumatic system circuit diagram

The double-acting cylinder is constructed of two chambers and a cylindrical rod. Controlling the airflow from the solenoid valve can drive the rod position to the desired location. The 1st two solenoid (S1 and S2) valves control the left chamber, and the other two valves (S3 and S4) control the right chamber's airflow. Table 4.3 illustrates the rod's movement according to the input signal to the solenoid valves.

From the connection between the valves shown in Figure 4.11, the 1st valve works as a compressed valve to the left chamber, and the 2nd valve works as an exhaust valve to the left chamber. The same thing happened to the 3rd and 4th valves working as compress and exhaust, respectively, to the right chamber. The four valves control the double-acting cylinder for extension and retraction of the cylindrical rod.

Table 4. 3 Rod displacement via solenoid valve's signal

Status	S1	S2	S3	S4	Rod direction	Rod status
1	On	Off	Off	On	Left to Right	extend
2	Off	On	On	Off	Right to Left	retract
3	Off	Off	Off	Off	Stop	Stop

4.5 Simulation of fuzzy logic system

The solar equations were beneficial to derive the optimum azimuth and tilt angles for a specific location and day. This data is set as an input signal and serves as the default LDR sensor readings for the FLC system. The FLC system for the proposed system needs two inputs, which are the error reading between two sensors for one solar angle and the error rate of change so that the output data from the solar angle simulation is set to obtain a reading for the LDR sensors. The FLC system will process this reading to get an output signal that drives the pneumatic actuator.

As shown in Figure 4.12, the input to the FLC system will be the error and the rate of change of the error. This input will have seven trigonometric membership functions for greater accuracy of the system. The output from the FLC system will drive the pneumatic actuator for optimum solar angle.

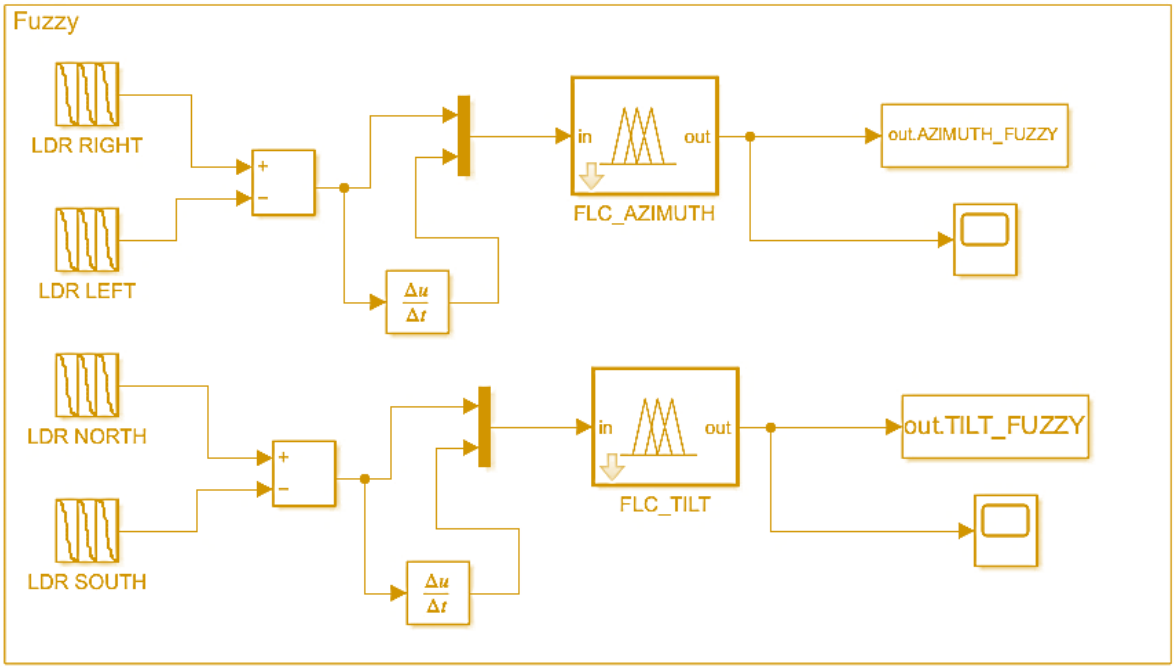

Figure 4. 12 Simulation of FLC system

Figure 4.13 demonstrates the rod position of the pneumatic actuator that drives the solar panel. The double-acting cylinder will extend until it reaches 9 cm at noon, then begin to retract to its initial position, simulating the tilt angle position. This displacement occurs according to the output signal from the FL control system, which processes the input signal of two virtual LDR sensors placed on the north and south of the solar panel to regulate the tilt angle over time, as shown in Figure 4.14. Meanwhile, Figure 4.15 depicts the movement of the rod cylinder to the azimuth angle position driven by the FLC system. The rod of the double-acting cylinder will continue to move until it reaches a stroke of 13.5 cm at 6 P.M. This movement is generated according to the input signal to the corresponding valves taken from the output signal from the FL system as shown in Figure 4.16. The FLC system takes the data from the east and west LDR placed on the solar panel and regulates the azimuth angle during the day.

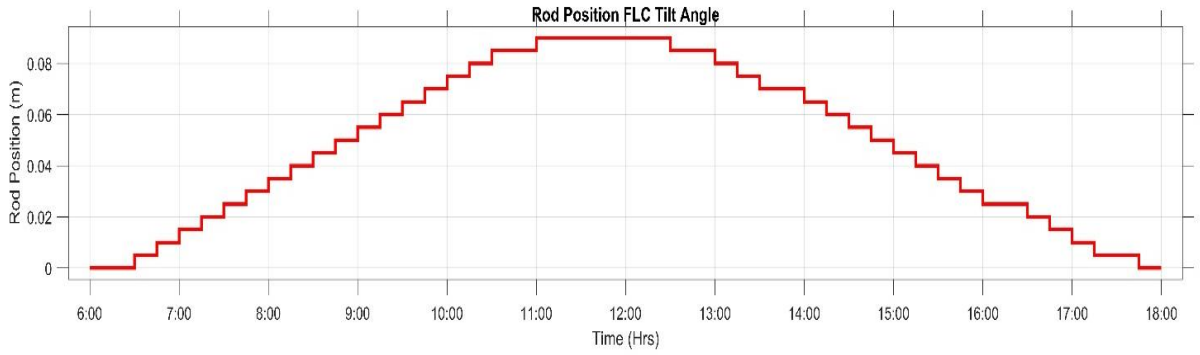

Figure 4. 13 Rod position from FLC for tilt angle

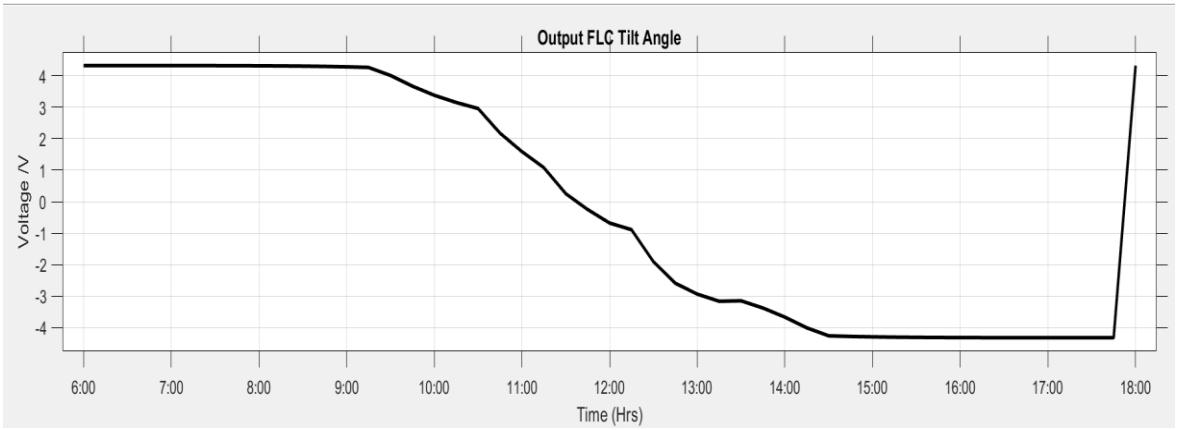

Figure 4. 14 Output data from FLC for tilt angle

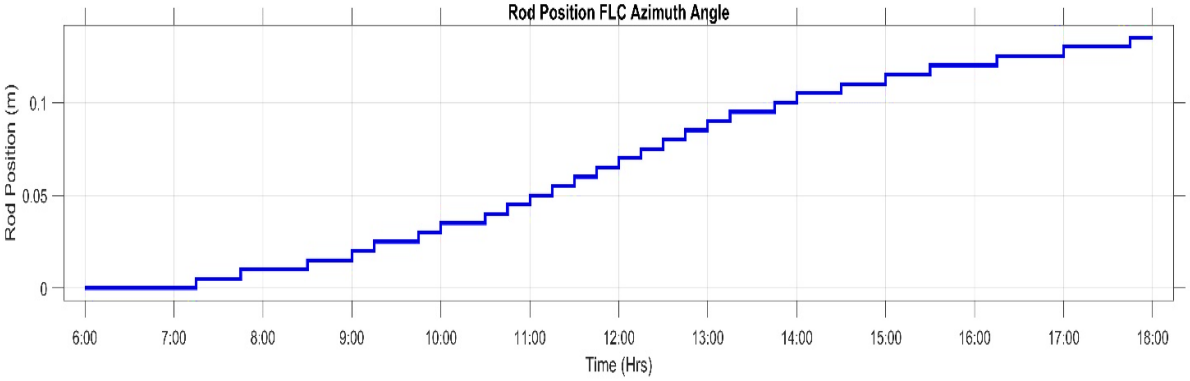

Figure 4. 15 Rod position under FLC for azimuth movement

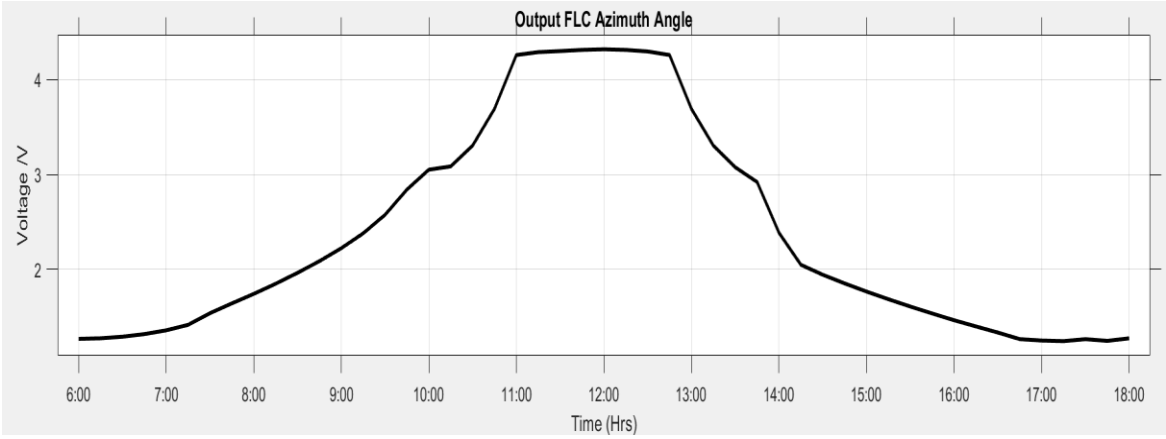

Figure 4. 16 Output data from FLC for azimuth movement

4.6 ANFIS Simulation

ANFIS is a hybrid intelligence system that combines the learning capabilities of NNs with the FL reasoning of a fuzzy inference system. In MATLAB, ANFIS can be implemented using the Fuzzy Logic Toolbox. Figure 4.17 shows the simulation block diagram of ANFIS by Matlab for azimuth and tilt movements.

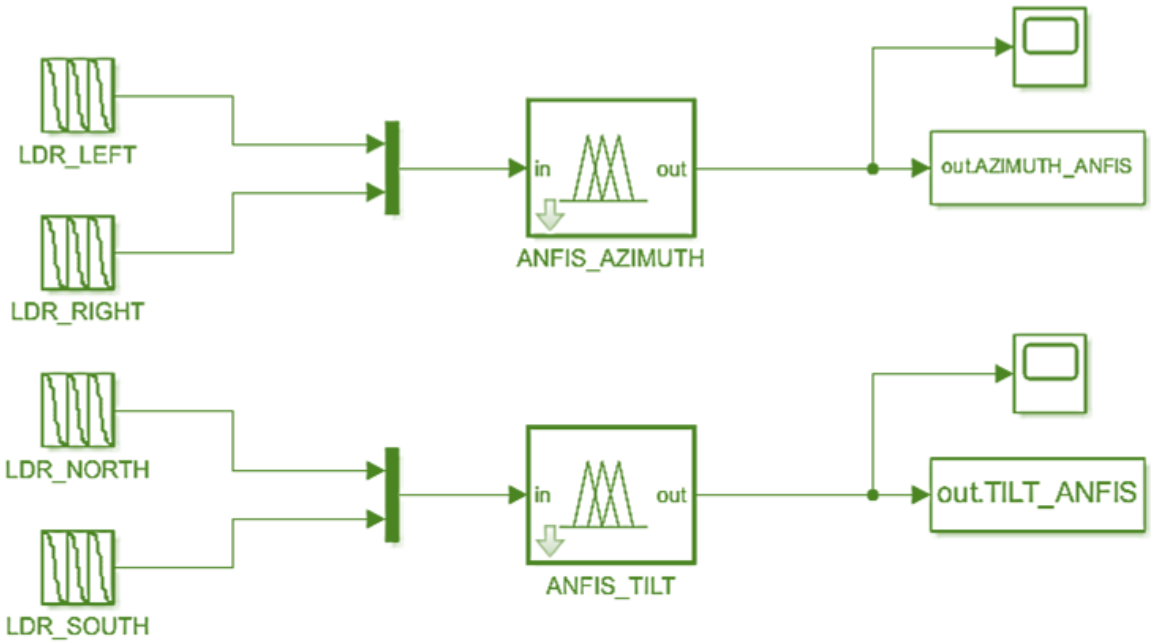

Figure 4. 17 Block Diagram for ANFIS System Simulation

The simulation of the ANFIS system will have the same FLC simulation, two inputs representing mapped sensor readings for specific solar angles, a block for ANFIS system trained data, and one output representing the input signal to the pneumatic actuator to drive the solar panel as shown in Figure 4.18.

Figures 4.19 and 4.20 demonstrate the ANFIS controller's output signal with two input-mapped signals from the simulation of the optimum tilt and azimuth angles for a specific location and day. These signals represent the four LDR sensors, north and south for the tilt angle and east and west for the azimuth angle, which are inputted to the ANFIS controller. The neural network in the ANFIS system is trained to input typical tilt, azimuth mapped to LDR readings, and expected output data to drive the cylinder rod to a specific location. The source of the data to train the ANFIS controller is a workspace that have LDR readings' and the output is the rod position. The input signal range is (0-1023) since the suggested controller has an ADC with a 10-bit quantization level. It gives us a division of 1024 levels of data, while the output data ranges from (-5 to 5) to simulate the output voltage from the controller to drive the pneumatic valves.

In the case of tilt angle, the rod will move during the day starting from 6 A.M and reach 10 cm at noon, then retract its position gradually to the origin around 6 P.M as shown in Figure 4.19, while in azimuth angle, the rod displacement will change from 0 cm to 13.5 cm at 6 P.M. as shown in Figure 4.20.

As shown in Figures 4.13, 4.15, 4.18, and 4.20, the rod position in the FLC controller and ANFIS controller are almost compatible with the rod displacement and the velocity. The two systems will be compared in the case of harvested solar power to ensure their compatibility with the driving pneumatic actuator.

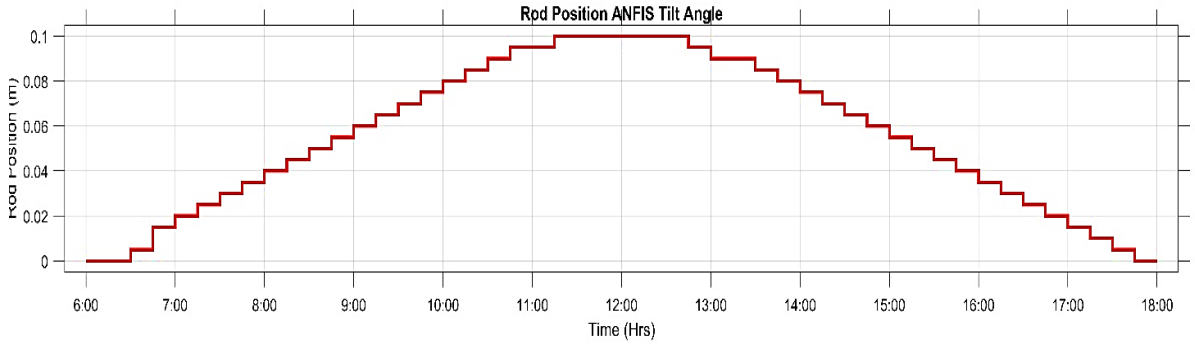

Figure 4. 18 Rod Position from ANFIS for Tilt Angle.

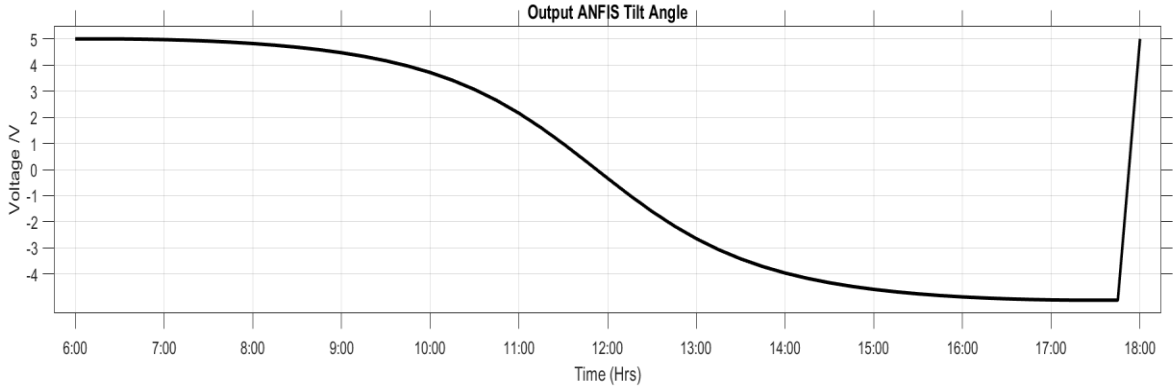

Figure 4. 19 Output Data from ANFIS for Tilt Angle.

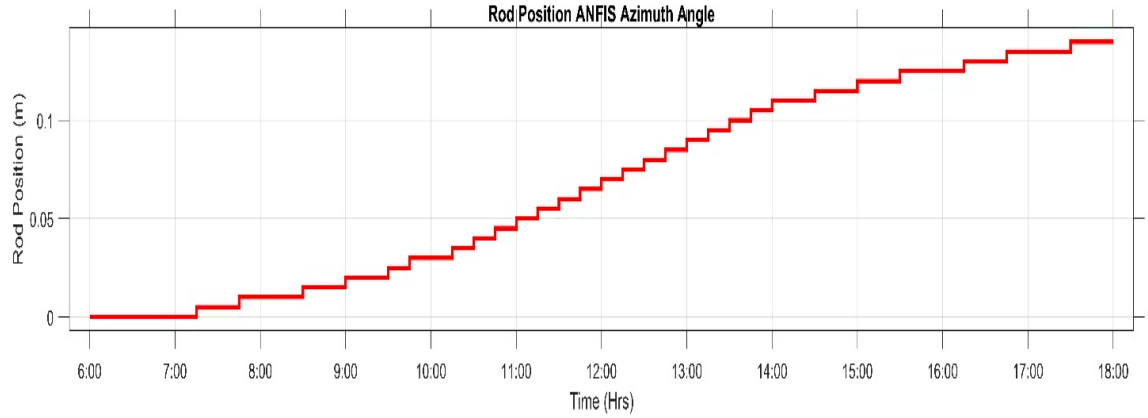

Figure 4. 20 Rod Position and ANFIS Output for Azimuth Angle.

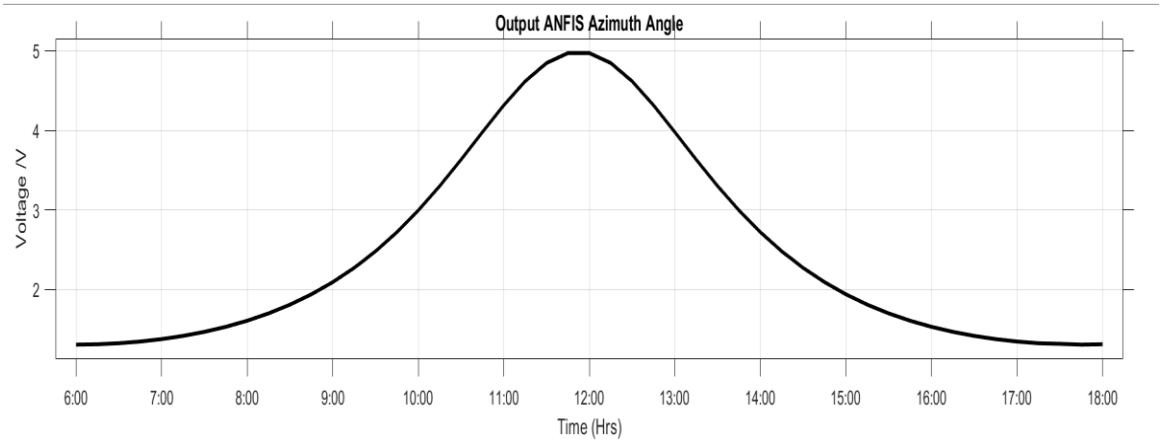

Figure 4. 21 Output Data from ANFIS for azimuth Angle

4.7 Compare method simulation

The comparison method directly compares output readings from the LDR sensors to move the pneumatic actuators to the corresponding angles. It takes the difference between LDRnorth and LDRsouth and gives an output signal for the valves to direct the solar panel to the optimum tilt angle. As for the azimuth angle, the difference between LDReast and LDRwest readings indicates the presence of a set of valves to adjust the solar panel's position to the optimum azimuth angle. Table 4.4 lists the solar panel's movement and the LDRs' reading.

Table 4. 4 LDRs reading vs. double-acting cylinder movement

LDRs readings	Corresponding angle	Double acting cylinder
LDR_{north}-$LDR_{south} \geq$ threshold	Tilt angle	Tilt double acting cylinder – retract
LDR_{south}-$LDR_{north} \geq$ threshold	Tilt angle	Tilt double acting cylinder - extend
LDR_{east}-$LDR_{west} \geq$ threshold	Azimuth angle	Azimuth double acting cylinder – extend
LDR_{west}-$LDR_{east} \geq$ threshold	Azimuth angle	Azimuth double acting cylinder - retract

Since the location of this sensor is relatively close, a threshold value between the readings is needed for more accuracy. Putting the sensors inside a tube will achieve this threshold. From the experiments, an inversely proportional relationship between the tube length and the threshold value is observed. Putting a light source 1 meter away from the LDR sensors on the solar panel used and without using a tube for these LDRs, requires a threshold value of 1% of the maximum sensor reading value. Inserting the tube of 2.5 cm gives us a 10% maximum value; using a 4 cm tube gives an acceptable threshold value of 17%, a good percentage for stable movement of the double-acting cylinder. Note that the more distance between the sensors, the lower the threshold value needed for an accurate tracking system.

Depending on the input signals coming from four LDR sensors and taking the difference between those signals for tilt and azimuth angle into account the threshold value, the position of the rod can be seen during the day. Figure 4.22 shows the rod position for tilt angle. The rod position starts from 6 A.M and increases gradually till 12 P.M. of 13 cm and then gradually retracts back to its original position. Figure 4.23 shows the rod movement during the day for azimuth angle, where the rod begins to move at 7 A.M. and gradually extends until it reaches the maximum stroke of 15 cm near 4 P.M and holds that position until 6 P.M.

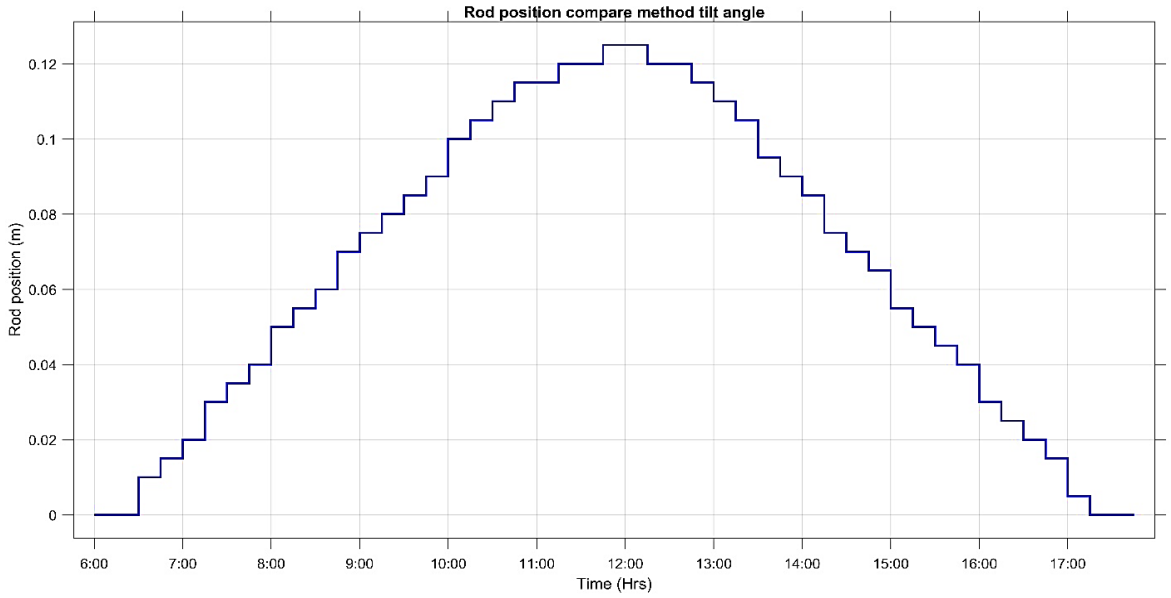

Figure 4. 22 Position of the rod using the tilt angle compare method.

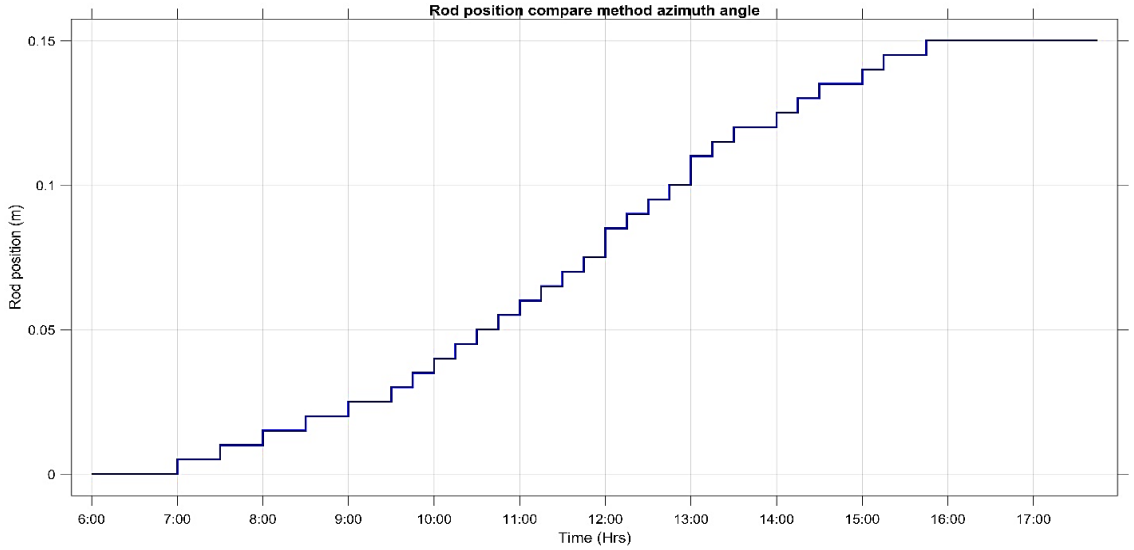

Figure 4. 23 Position of the rod using the azimuth angle compare method.

Using the comparison method, solar irradiance during the day and the total power harvested from these displacements can be obtained from the tilt and azimuth angles using the solar panel model. Figure 4.24 demonstrates the solar irradiance for 12 hours using the data from tilt and azimuth angles obtained from the comparison method under the simulation process.

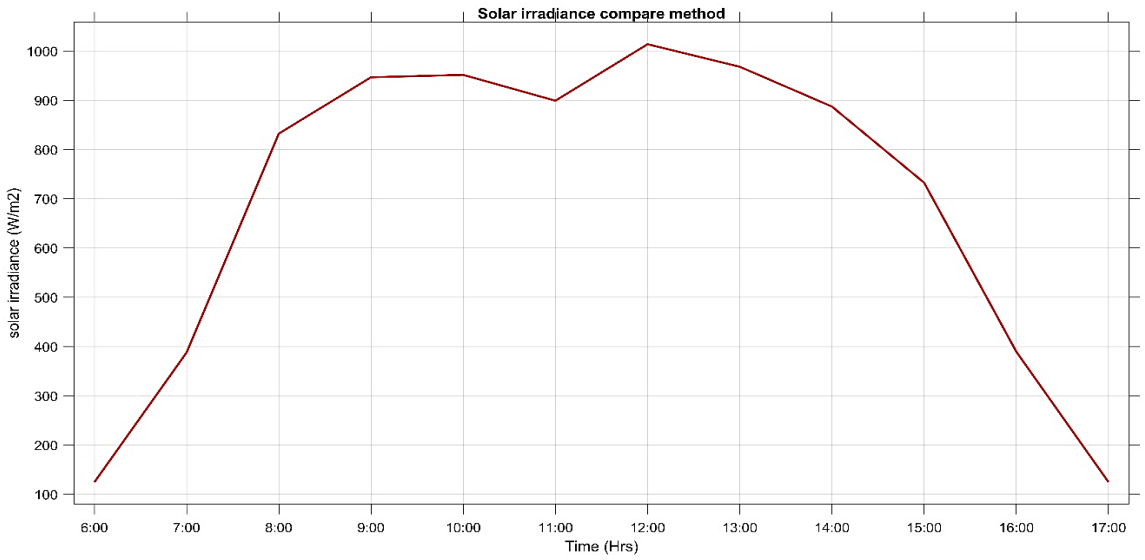

Figure 4. 24 Solar irradiance using the comparison method

4.8 Overall system simulation

After designing and simulating the pneumatic system, controllers, and solar PV panel individually, the overall system can be simulated to see the best control system to maximize the harvested solar energy.

First, solar irradiance data is needed for the specific location and time of the day. The National Renewable Energy Laboratory (NREL) shown in Appendix 1 has massive data on solar energy worldwide, as shown in the Appendix 1. It will help gather more information about the site where a solar panel works and can simulate the system using this data.

By entering the necessary information into their database, it is possible to obtain the solar radiation of the site in which they work, which is the location in Baghdad.

The website can deliver solar irradiance data for dual-, and single-axis tracking systems and fixed roof or wall-mounted hourly each day of the year.

These data will be processed in the simulation program to see the efficiency of the dual-axis tracking system based on the pneumatic actuator data collected from the earlier simulation.

By selecting the same data collected in the solar angle simulation in Figure 4.3, the PV panel in Table 4.1, the pneumatic system in Figure 4.11, and the solar radiation collected for the fixed panel and the 2-axis tracker from the NREL database shown in Appendix 1, the efficiency of the pneumatic tracking device can be calculated using FLC, ANFIS, and comparison of control system methods. In the simulation of the overall system, solar power can be collected from the solar panel, the PV panel efficiency under FLC, ANFIS, and comparison method can be compared, and the method of dual-axis tracker with fixed panel system can be compared as follows:

1. Solar angle subsystem: simulates the tilt and azimuth angles with input parameters of latitude of the location where the solar panel is installed and the day of the year. This modeling is according to the solar equations shown in Figure 4.3.
2. Fuzzy subsystem: simulates the mapped input sensors using an FLC system with seven triangular membership functions. If the input signal (LDRnorth and LDRsouth), the output is the input signal to the pneumatic system for tilt angle, and if the input signal (LDRwest and LDReast) the output is the input signal to the pneumatic system for azimuth angle as shown in Figure 4.12.
3. ANFIS subsystem: simulates the mapped input sensors using the ANFIS system with three triangular membership functions. If the input signal (LDRnorth and LDRsouth), the output is the input signal to the pneumatic system for tilt angle, and if the input signal (LDRwest and LDReast), the

output is the input signal to the pneumatic system for azimuth angles as shown in Figure 4.17.

4. Pneumatic actuator subsystem: simulates the rod position for tilt and azimuth angle with input signals from the FLC, ANFIS, or compare method subsystems as shown in Figures 4.13, 4.15, 4.18, 4.20, 4.22, and 4.23.
5. Rod position versus solar irradiance subsystem: takes solar irradiance data from the NREL database and simulates the rod position controlled by FLC, ANFIS, and comparison methods. Figure 4.25 shows the tracking controller with the solar irradiance output during the day. This block's output is displayed in Figure 4.26, which shows the tracking system in use along with the associated solar irradiation for that system throughout the day. Next step, the solar irradiance data will be input into the solar panel model to investigate the output power harvested from each tracking system.

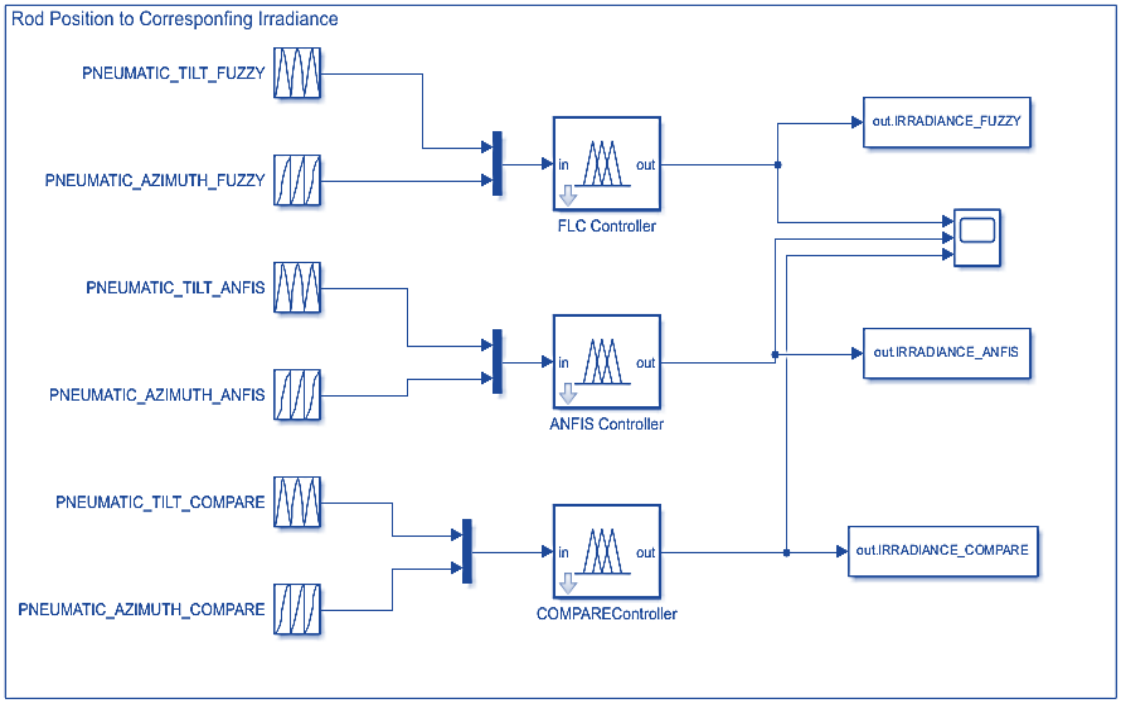

Figure 4. 25 Rod position for the specific controller and the corresponding solar irradiance

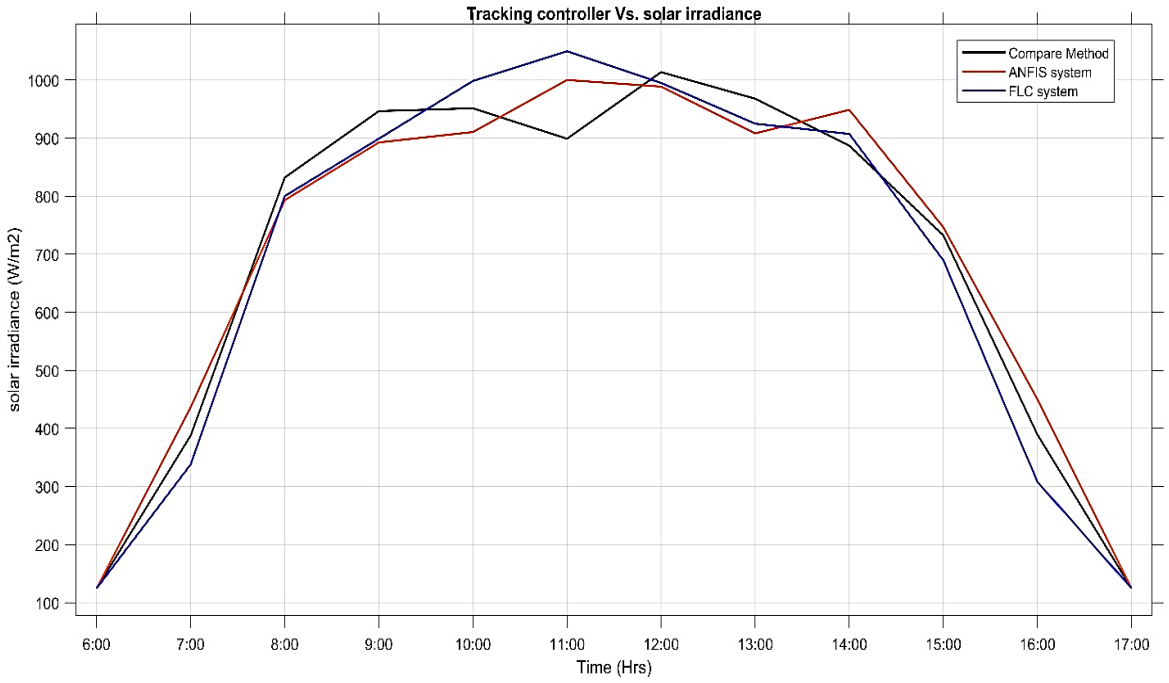

Figure 4. 26 Hourly distribution of solar irradiance under various tracking controllers

6. Solar panel subsystem: simulates the PV panel with input parameters of solar irradiance and temperature as shown in Figure 4.27. The temperature parameter for all simulated controllers will be fixed at 35° for simplicity, and the readings of the output current and voltage from the PV panel with specifications shown in Table 4.1. The output current and voltage will be multiplied to get the output power of the solar panel.
7. Solar irradiance subsystem: simulates the solar irradiance output from the previous subsystem with a solar panel model with specific parameters giving an output power. The system is driven by ANFIS, and FLC, and compares method with dual-axis tracking and fixed panel as shown in Figure 4.28.

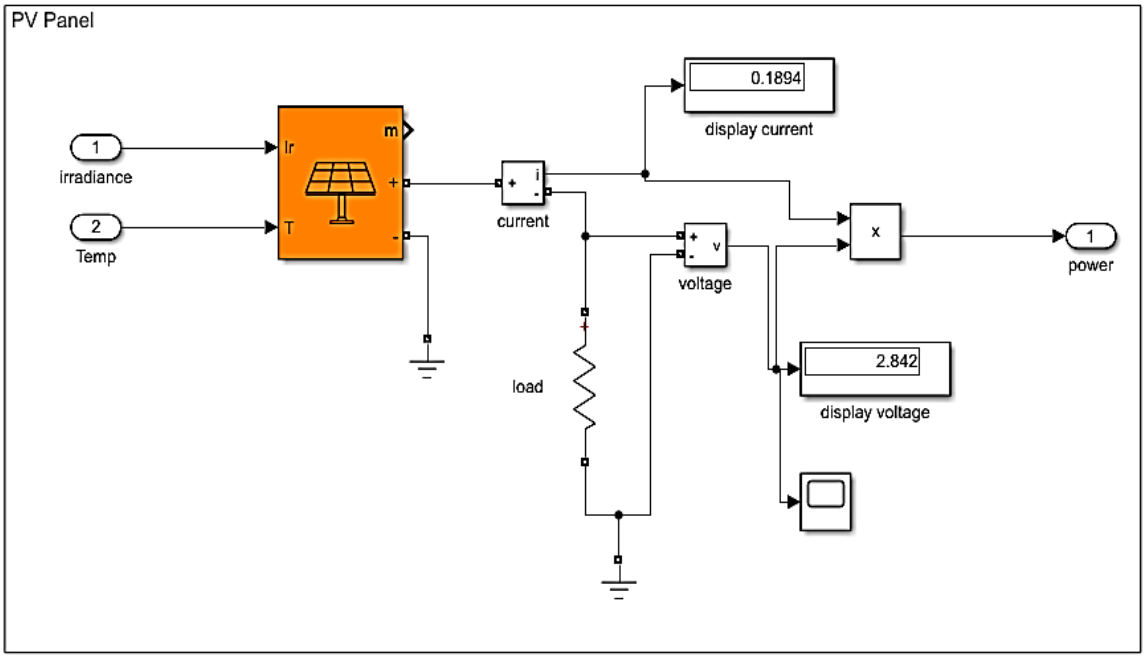

Figure 4. 27 Block diagram of pv panel simulation

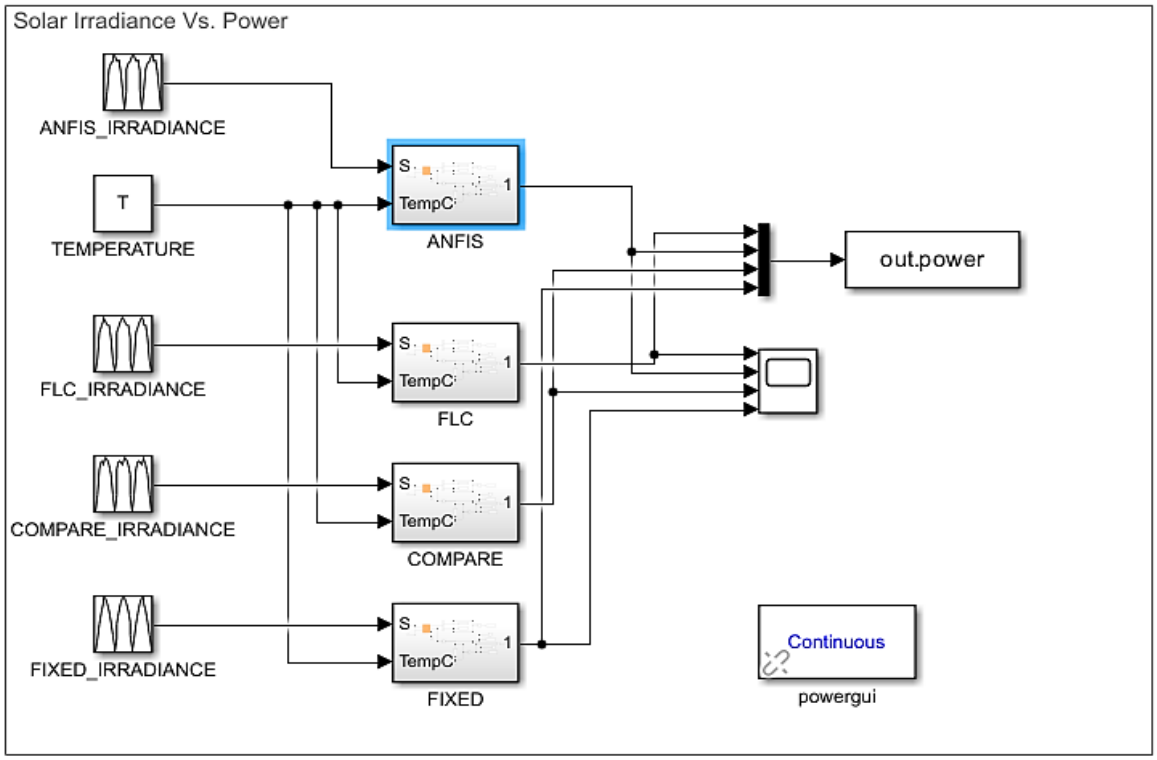

Figure 4. 28 Output power simulation for FLC, ANFIS, compare method and fixed panel

The blocks above calculate the output power of the three cases of dual-tracking systems and fixed-mounted panels.

Figure 4.29 shows the output power during the day for the dual-axis tracking system under FLC, ANFIS, comparison method, and with a fixed PV panel.

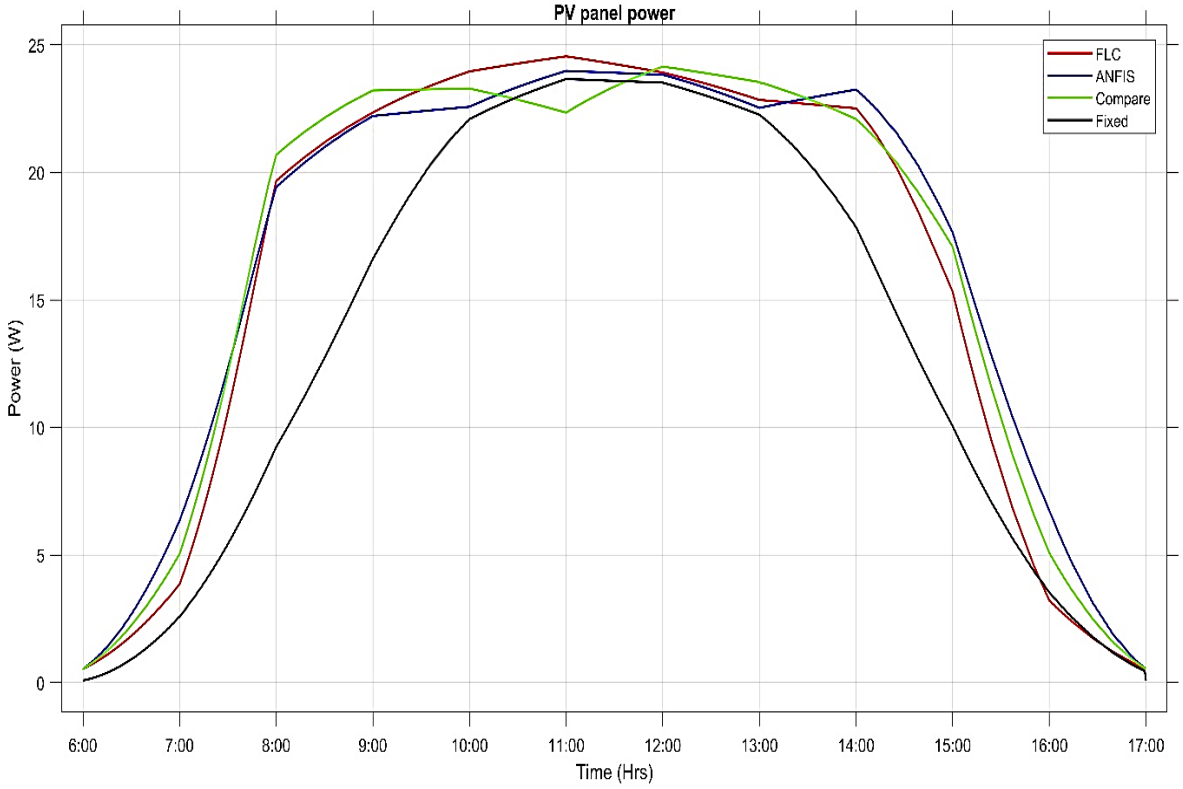

Figure 4. 29 Solar Power using Dual Axis FLC, ANFIS, Compare and Fixed Panel

4.9 Comparison between FLC, ANFIS, and Fixed Panel

From Figure 4.29, the power during the day can be calculated by calculating the area under the curve of each of these systems.

The results of the average power of the moving PV panel in the case of the FLC system were equal to 1791 W during the day, while in the ANFIS system, the power was measured at 1982 W, and its value using the comparison method was 1894 W, while the power obtained in the case of the fixed panel was 1371 W.

From these results, the following conclusions are drawn:

1. The highest power that could be obtained from the solar panels was from the ANFIS controller, followed by the comparator method and then the FLC system. In contrast, the fixed plate had the least power.
2. By comparing the effect of different control techniques for the tracking system on the output power with a fixed PV system, the improvement of the ANFIS system was 44.6%, and the improvement percentage of the comparative method was equal to 38.15%, while, the FLC was about 30.6%.

4.10 Experimental Work

This section deals with the practical side of the thesis and includes the construction of the dual-axis pneumatic solar tracking system, including all components, execution of tests, collection of experimental data, and comparison between real-time experimental performance data and results obtained from simulation.

4.10.1 System components

The solar tracking system proposed is constructed addition to the PV panel and its structure frame from three main components: the control system, pneumatic actuator, and input sensors. These components will help drive the solar panel toward the required sun angles for maximum energy harvested during the day.

1. Solar panel

A 25W Polycrystalline and 21.24 V solar PV panel was used in the experimental system setup. The technical specification of the panel was previously mentioned in Table 4.1. These specifications were close to the simulation results. The solar panel was simulated at a constant temperature of 25°. Since the experimental result was taken at the same location and closed days

of the year, it is expected that the results will be close to the simulation results, especially in the early and late hours, because the temperature in those periods was close to 25 oC, while the results differ somewhat at noon, because of the high temperatures at that time.

2. Control system

The control system used in the proposed system was built in several stages, each stage having a special character for controlling the operating system. The control system mainly consists of:

A. Aduino Uno mirco-controller

Arduino UNO as shown in Figure 4.30 is a low-cost, flexible, and easy-to-use programmable open-source microcontroller board that can be integrated into a variety of electronic projects. This board was programmed by Arduino IDE program with C++ code and that code was designed to read the input analog signal and write with output digital signal from predefined pins. The output signal will drive the following stage which is the relays that drive the actuator. The specification of this micro-controller as follows:

1. IC: Microchip ATmega328P (8-bit AVR core)
2. Clock Speed: 16 MHz on Uno board, though IC is capable of 20 MHz maximum at 5 Volts
3. Flash memory: 32 KB, of which 0.5 KB used by the bootloader
4. SRAM: 2 KB
5. EEPROM: 1 KB
6. Operating Voltage: 5 Volts
7. Digital I/O Pins: 14
8. Pulse Width Modulation (PWM) Pins: 6 (Pin # 3, 5, 6, 9, 10 and 11)
9. Analog Input Pins: 6
10. DC Current per I/O Pin: 20 mA

11. DC Current for 3.3V Pin: 50 mA
12. Size: 68.6 mm x 53.4 mm
13. Weight: 25 g

Figure 4. 30 Arduino Uno micro-controller

B. 8-Channel relay

Since the actuating system works on 24V D.C and the output signal from the Arduino gives only 5V D.C, the relay system is needed to give a D.C level voltage to drive the pneumatic actuator. Figure 4.31 shows the pin diagram of the 8-channel 5V relay module. The module is very important for the control circuit to protect the microcontroller and to feed the actuator system the voltage it needs. The relay has the following features:

1. Power Supply Voltage: 5V DC
2. Current: Greater than 100mA
3. Load: 250V 10A AC or 30V 10A DC
4. Size: 134.6 × 53.6 × 19.5mm
5. Equipped with mounting holes around, hole diameter 3.1 mm.
6. When input is at low level, the relay is off, and the indicator light is on.

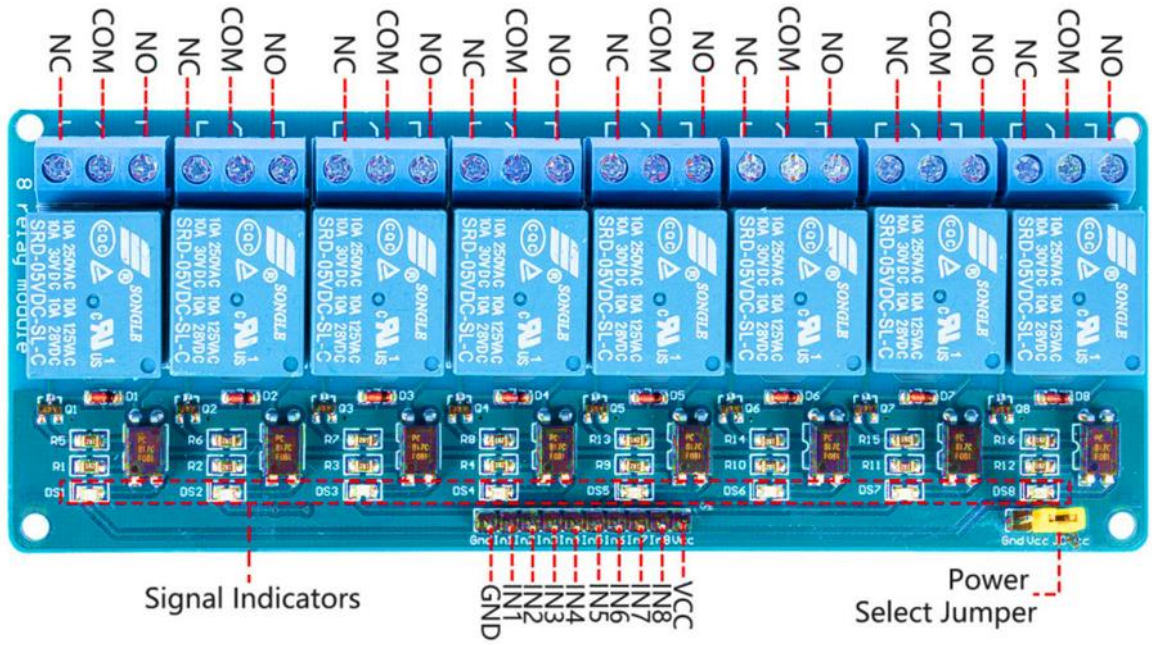

Figure 4. 31 Pin Diagram of 8 Channel 5V Relay Module

The pin configuration for this module is as follows:

1. **VCC:** This is the positive power supply input from the main control.
2. **GND:** Ground connection.
3. **IN1~IN8:** The signal input pins for the relays. When a low-level signal is input, the Normally Open (NO) contact of the relay connects with the Common (COM) terminal.
4. **NO (Normally Open):** This is the load connection when the relay is active (ON). In the off-state, NO is not connected to the COM (Common) terminal.
5. **COM (Common):** This terminal serves as the common connection for both NO and NC (Normally Closed) pins.
6. **NC (Normally Closed):** This is the default load connection, which is connected to the COM terminal when the relay is OFF or in its default state.

C. Buffer circuit

By connecting the relay module directly to the microcontroller, it appears to be a load problem which causes the relay to hang.

To override this problem a buffer circuit is needed with high output power to drive the relay module, that because the 8-channel relay drains high current that the microcontroller cannot provide

Introducing the TIP41C transistor as a buffer circuit between the relay module and the Arduino Uno microcontroller will resolve the hanging issues.

The TIP41C can be used for any general purpose of switching and amplification application. It can be used as a switch to drive many loads at the same time, though the sum of all loads should not increase from 6A. It can drive DC motors, high-power LEDs, high-power relays, bulbs, devices, etc.

TIP41C has the following features:

1. Type: NPN Bipolar Junction Transistor (BJT)
2. Collector-Emitter Voltage (VCEO): 100V
3. Collector-Base Voltage (VCBO): 100V
4. Emitter-Base Voltage (VEBO): 5V
5. Collector Current (IC): 6A continuous (maximum)
6. DC Current Gain (hFE): Typically around 15 to 75
7. Transition Frequency (ft): Around 3 MHz.
8. A built-in heatsink for maximum heat dissipation when operating at full throttle.

Figure 4.32 shows the pin configuration of the buffer transistor TIP41C.

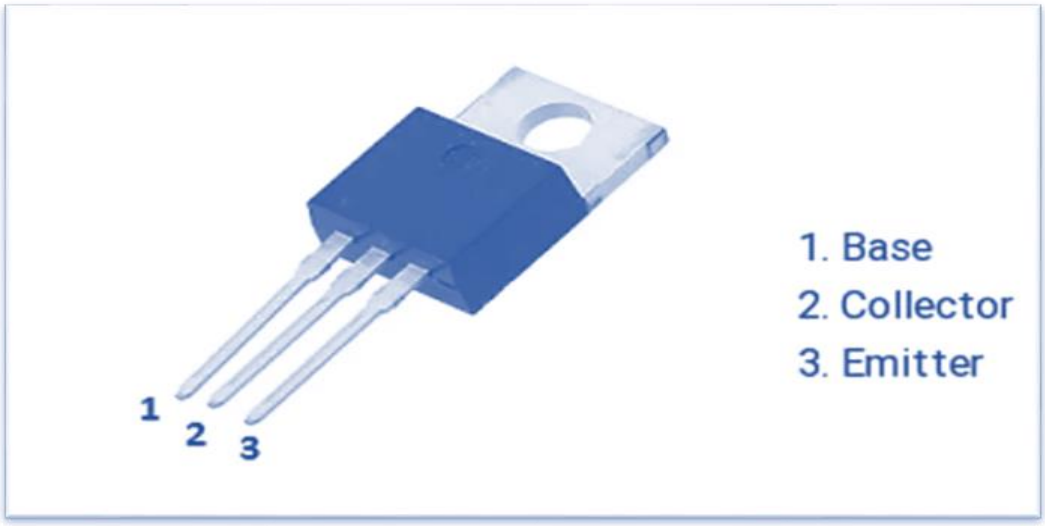

Figure 4. 32 Pin Configuration of TIP41C

The base pin will be connected to the output pin of the Arduino Uno. The emitter pin will be connected to the ground and the collector pin will be the output pin that is connected to the relay module through a resistor. TIP41C will operate as a switching device with high power through a small base current due to its specification of low impedance.

D. PV Load

The load system used in the proposed tracking system was a pure resistive load of 100W 15 Ohm power resistance. On its branch the voltage and the current output from the PV panel was measured to calculate the output power. Figure 4.33 shows the resistor used in the proposed system.

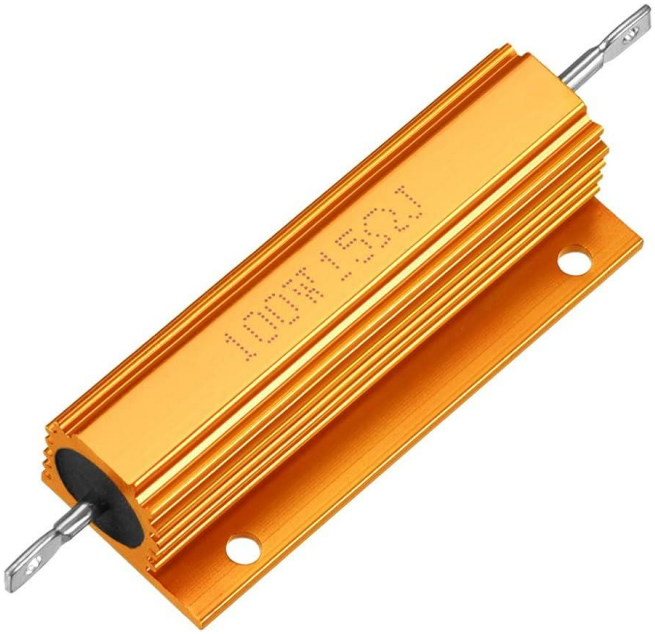

Figure 4. 33 Power resistor 100W 15 Ohm

3. Pneumatic actuating system

The proposed solar tracking system has a pneumatic actuator that drives the solar panel to the desired solar angles to maximize energy absorption. This system is built from: a double-acting cylinder, solenoid valves, a pressure control valve and the pressure source or a reservoir. All these components are connected through a PVC pipe.

A. Double-acting cylinder

A double-acting cylinder is a pneumatic device that has two chambers and a rod piston. The left and right chambers are controlled via pneumatic valves to drive the rod piston to the right and left positions. The rod piston is mechanically connected to the solar panel's structure and that is responsible for guiding the PV panel to the desired solar angle.

Previously, in Figure 3.1 in the third chapter, the schematic diagram of the double-acting cylinder used in the proposed tracking system was demonstrated, and the mathematical modeling of the cylinder, its movement, and the parameters

that affect the rod's displacement and speed were explained. Figure 4.34 shows the double-acting cylinder used in the experimental work. The cylinder has the following specifications:

1. Model: Expflex 25x150
2. Diameter of the cylinder: 25 mm
3. Maximum stroke: 150 mm
4. Fluid: Air
5. Motion pattern: double action
6. Maximum pressure: 10 bar
7. Pipe size: 1/8"

Figure 4. 34 Double-acting pneumatic cylinder Expflex25×150 mm

B. On-Off Solenoid Valve

2V025-08 Solenoid valve was used to control the airflow into the double-acting cylinder. This valve is an on-off valve, which means that the valve opens and closes completely depending on the electrical signal coming from the controller. The control signal will actuate the coil inside the valve to open the

orifice between the inlet and outlet side and permit the air to flow. Figure 4.35 shows the on-off solenoid valve that is in the proposed solar tracking system.

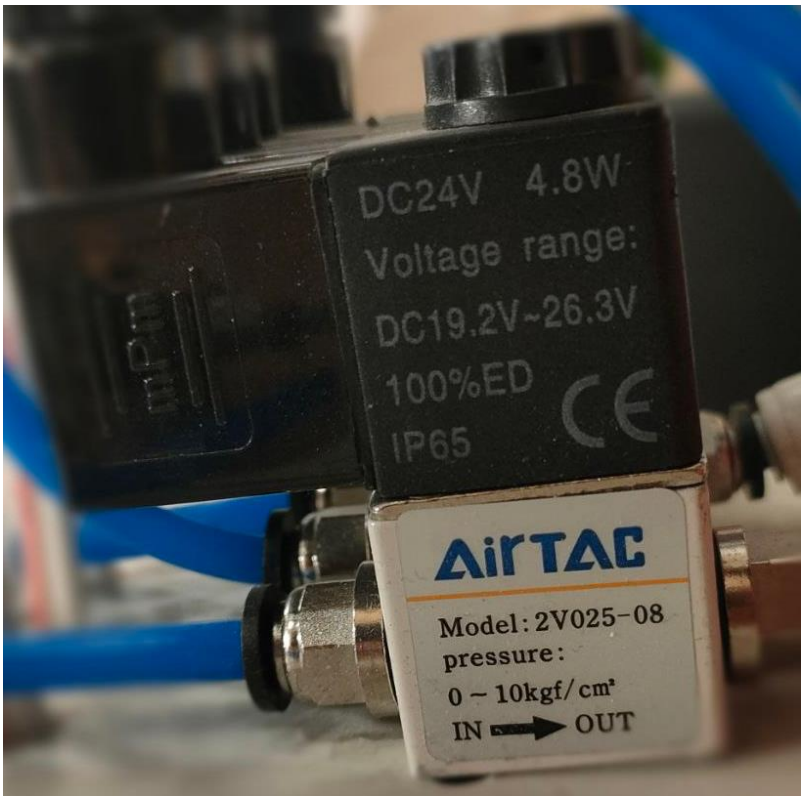

Figure 4. 35 2-Way ON-OFF Solenoid Valve

Table 4.5 shows the specification of the solenoid valve, where the fluid is air gas, the action of the valve is direct act normally closed depending on the signal that enters the valve coil, the port size is 1/8" and the maximum working pressure of the valve is 10 bar. The valve coil is working on 24V DC and the power dissipation for opening the orifice between the inlet and the outlet is 4.8W.

Table 4. 5 The Specification of the Solenoid Valve

Parameter	specification
Model	2V025-08
Fluid	Air
Acting	Direct acting
Orifice size	2.5 mm
Port size	1/8 inch
Pressure range	0-10 bar
Material body	Brass with nickel plated

C. Pressure control

Since the tank reservoir is filled with air at 40 bar pressure and the pneumatic valve operates at a maximum pressure of 10 bar, a pressure control regulator was included in the pneumatic system to control the input pressure to the system and this in turn controls the rod displacement in the double acting cylinder.

Figure 4.36 shows the pneumatic pressure control which is established by one inlet, one outlet, a regulator switch to control the pressure, and a pressure gauge to read the output pressure from the device. To adjust the output pressure from the control, it is needed to pull up the regulator switch and turn it to the desired pressure reading and then pull down again to lock the pressure control to that desired reading.

Table 4.6 demonstrates the specification of the pressure control. The model used in the experimental work was AR2000. The fluid used was air gas, maximum pressure was 10 bar, adjustable pressure control from 0.5-9 bar, and a working temperature from -20° to 70°.

Figure 4. 36 Pressure Control Valve

Table 4. 6 The Specification of the Pressure Control

Parameter	Specification
Model	AITAC AR-2000
Fluid	Air
Temperature range	-20-70°C
Port size	1/4 inch
Pressure range	0.5-9 bar
Maximum pressure	10 bar
Weight	200g

4.10.2 Steps to build the system

The proposed solar tracking system shown in Figure 4.37 and 4.38 was built according to the following steps:

1. The solar panel was connected to the steel structure that moves in two directions according to the solar angles. The sensors were also installed on a tube mounted on the steel structure and at four locations (north, south, east, and west) of the solar panel as shown in Figure 4.38 (b). the output connection from the PV panel is connected to the resistor via measuring equipments to calculate the output power.
2. All components of the pneumatic system are installed in their designated places The pneumatic components are connected to each other by special pipes that can withstand the air pressure used (the highest pressure is 10 bar for the air system) as shown in Figure 4.38 (a). The interconnection starts from the reservoir tank to the pressure regulator and then to the solenoid valves (four valves for each air cylinder). The air cylinder moves the solar panel either at a tilt angle or at azimuth angle to match the required solar angle as shown in Figure 4.37(a).
3. Connecting each two solenoid valves for each chamber belonging to the pneumatic cylinder, where one of the valves works to compress the air inside the cylinder chamber and the other works to empty the chamber of compressed air.
4. The solenoid valves were fed by a power supply. This supply is a rechargeable electric battery with a voltage corresponding to the valve operating voltage of 24 V, via a relay system.
5. The relay system was connected to the microprocessor via a buffer circuit to protect the microprocessor from the high current drawn from the relay as shown in Figure 4.37(b).

6. The microprocessor was equipped with the buffer circuit. The buffer plays a major role in amplifying the current as well as providing necessary protection to the microprocessor.

7. The signals that enter the microprocessor are comming from the LDR sensors. Thes signals are processed by programming the microprocessor with one of the various control methods such as artificial intelligence; FLC, ANFIS. The ANFIS is a powerful processing method and has the ability to predict emergency weather variables, compare the method, and then analyze the results of these three methods.

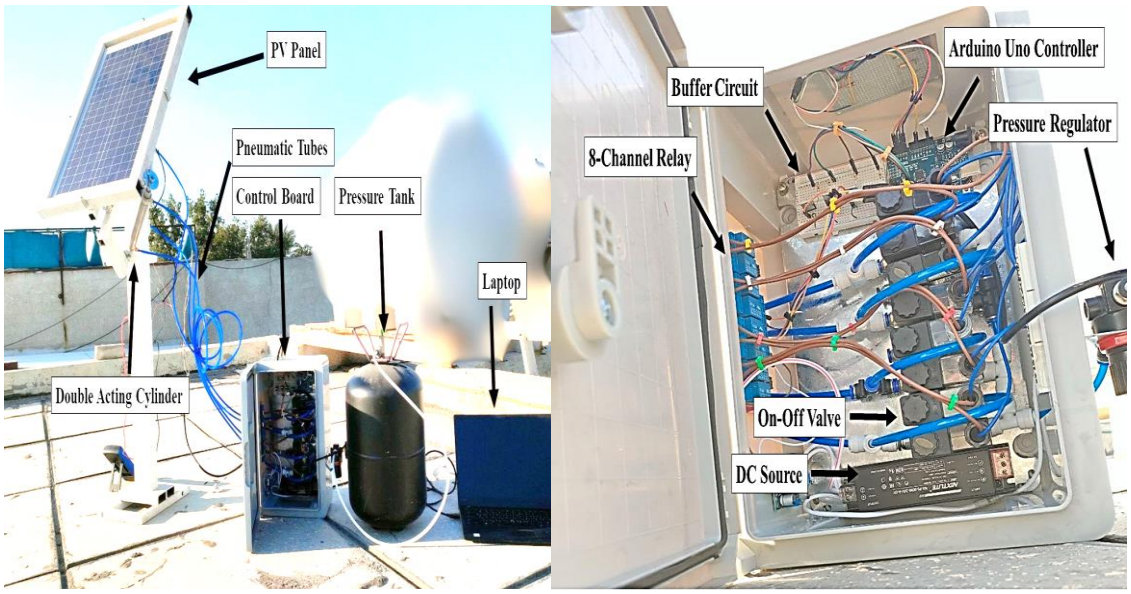

(a) (b)

Figure 4. 37 the proposed system (a) the overall system compenets (b) the control board

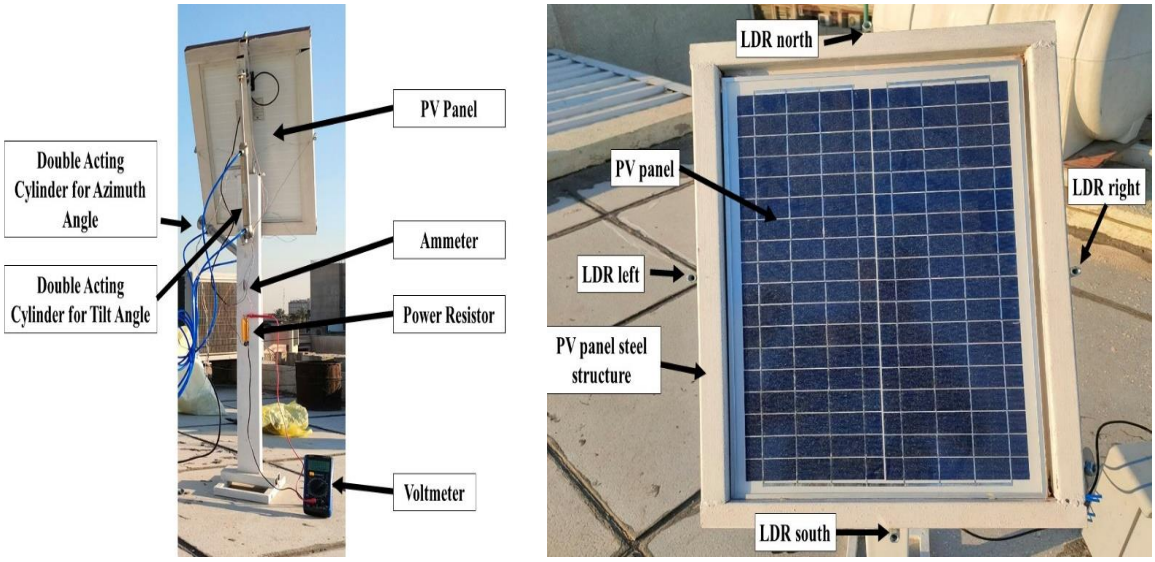

Figure 4. 38 the proposed system (a) double acting cylinder for azimuth and tilt angle (b) LDR distribution on PV steel structure

4.11 Exprimental results

Figure 4.39 shows the power harvested from the PV panel during the day when applying the ANFIS method to control the pneumatic tracking system in the simulation and experimental cases. From the results of the performance comparison between the simulation model and the experimental system, it was found that the power obtained experimentally from the solar panels is 38.1% more than the fixed panel and about 6.51% lower compared to the simulation.

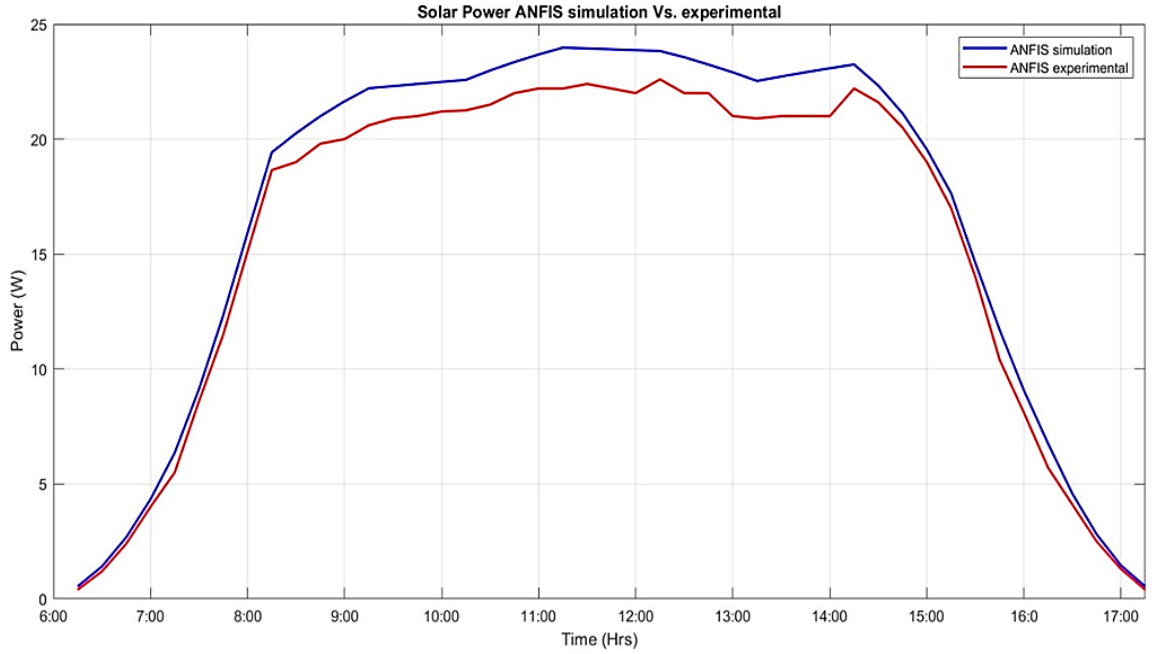

Figure 4. 39 PV power under ANFIS control for simulation and experimental systems

Also, it was found that when using the FLC controller in the solar tracking system, the power obtained from the PV panel experimentally is about 23%, which decreases by approximately 7.6% compared to the simulation results, as shown in Figure 4.40.

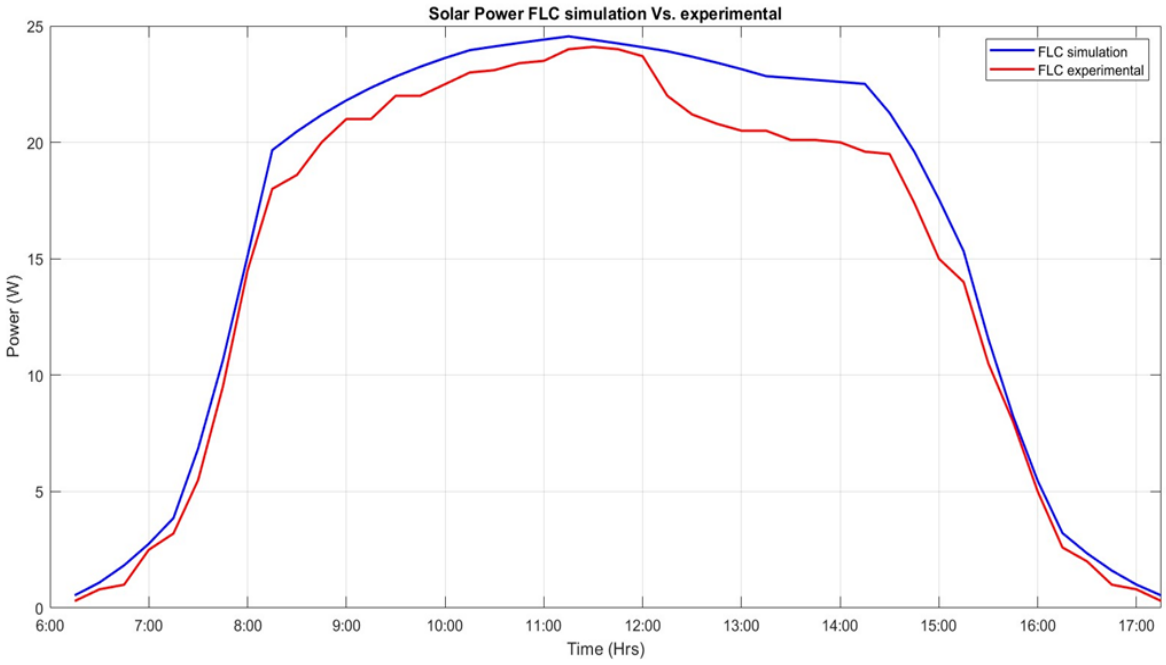

Figure 4. 40 PV power under FLC control for simulation and experimental systems

When applying the comparison method to control the tracking system, it was found that the performance was better than the FLC system. It was found that the improvement was 30.9% more than the fixed panel system, the practical system decreased from the simulation results by 7.25%, as is clear from the PV power curves in Figure 4.41.

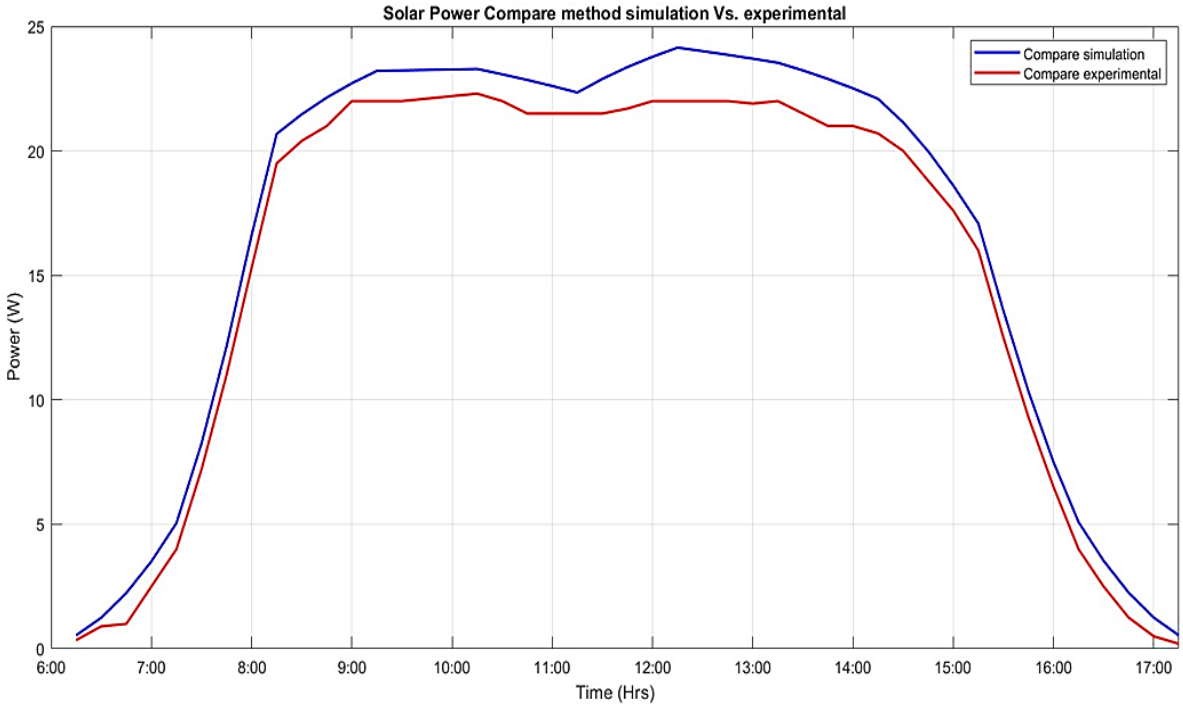

Figure 4. 41 PV power under compare method control method for simulation and experimental

4.12 Average efficiency

From the data collected from the three methods for controlling the solar tracking system: ANFIS, FL, and comparison method, the efficiency during the day for the solar panel can be calculated given the data in figures 4.39, 4.40, and 4.41.

The average efficiency can be calculated to show which method will improve the PV panel efficiency during the day, this can be achieved by simply taking the average of these readings.

The calculation revealed that the ANFIS controller gave an average boost to the average efficiency of the PV panel by 10.4%, followed by the compare method by 10.23%. meanwhile, the FL controller gives the solar panel an average efficiency of 9.93%. figure 4.42 shows the average dynamic efficiency for the three methods controlling the dual-axis tracking system.

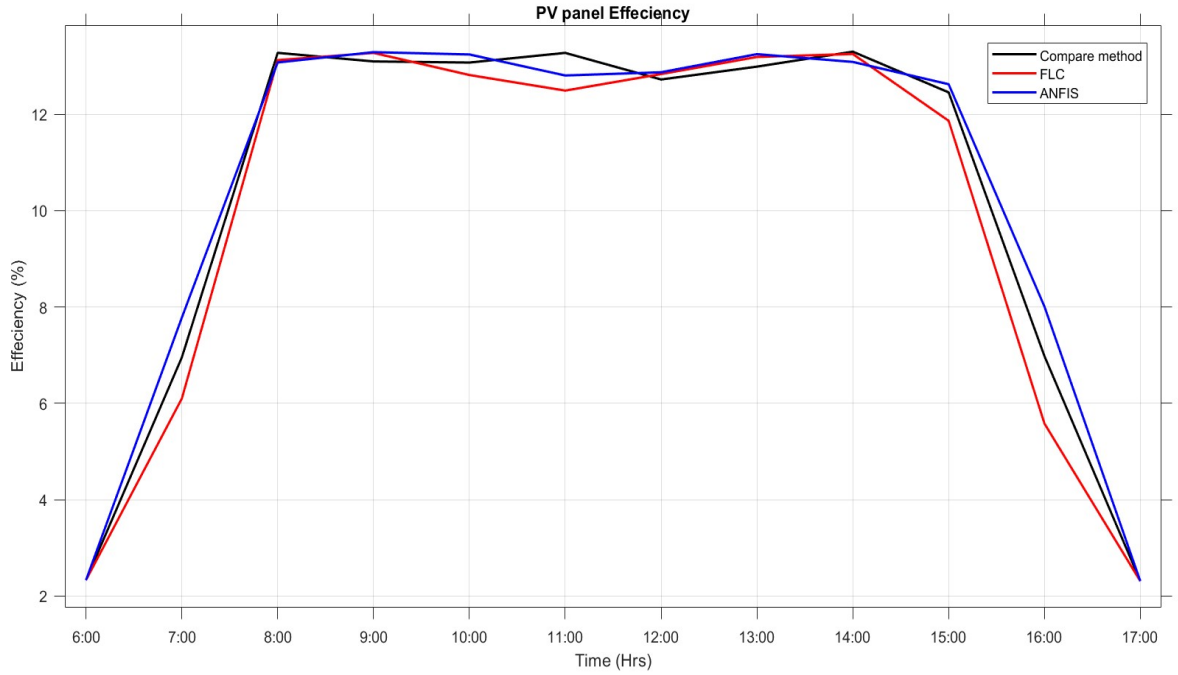

Figure 4. 42 The efficiency of PV panel

4.13 Results Discussion

From the above comparison results, it is concluded that the ANFIS control system for the pneumatic actuator used for the solar tracking system is the most efficient system for both the simulated and experimental system cases in terms of the amount of power obtained from the PV panel due to its characteristics in adapting to the input signal readings supported by a powerful neural network built on trained data from the environment.

This is followed by a comparison method of control, and because of the real-time factor represented in reading the sensor signals and sending them to the actuating system to act accordingly, taking into account the threshold value that has a

relationship value to the distance between the sensors and the tube that covers the sensor to obtain more accurate readings.

Although the FLC system has an improvement rate of 30.6% compared to the fixed panel system, the efficiency of this FL control system will have the lowest values between the ANFIS system and the comparison method system. The FLC system deals with input data with no adaptive process. It can be seen in Figures 4.14 and 4.16 that the output data from the FLC system is not as smooth as in the ANFIS system shown in Figures 4.19 and 4.21 when dealing with tilt and azimuth angle, respectively as shown in Figure 4.43.

The experimental results showed that the ANFIS system in the solar tracking system using the pneumatic actuator system is less different from the simulation results among the three control methods. The experimental work of the ANFIS system differed from the simulation by about 6.51% due to the real readings of solar data and the difference between the simulation results that were calculated at 25^{o}C and the experimental results in which the temperature ranged between 25-41^{o}C. The solar data readings also differ from the simulation presented on Dec. 16, 2024, and the results were taken on Dec. 20, 2024. Also, the ANFIS system increased the average efficeincy of the PV panel 10.4%.

The performance results for harvesting power from solar panels under FLC during the experimental work decreased from the simulation results by about 7.6% for the same reasons mentioned above, which are the temperature and the date the simulation took place on Dec. 16, 2024, and the experiment was on Dec.18, 2024. The difference between the experimental results and the simulation results was in a comparative manner. About 7.25% and this difference is due to the same reasons mentioned above, temperature and the day the data was taken, for the simulation was Dec. 16, 2024, and for the experimental work Dec. 19, 2024. The calculation considering the average efficiency during the day, the FLC

system increases the efficiency of the PV panel by about 9.93%, meanwhile, the compare method increases more efficiency of the PV panel by about 10.23%. From the above, it can be concluded that the ANFIS system used in the solar tracking system driven by pneumatic actuators is superior to the rest of the proposed control systems, the FLC, and the comparison method in both simulated and experimental results. Several conclusions and future works will be presented in Chapter Five.

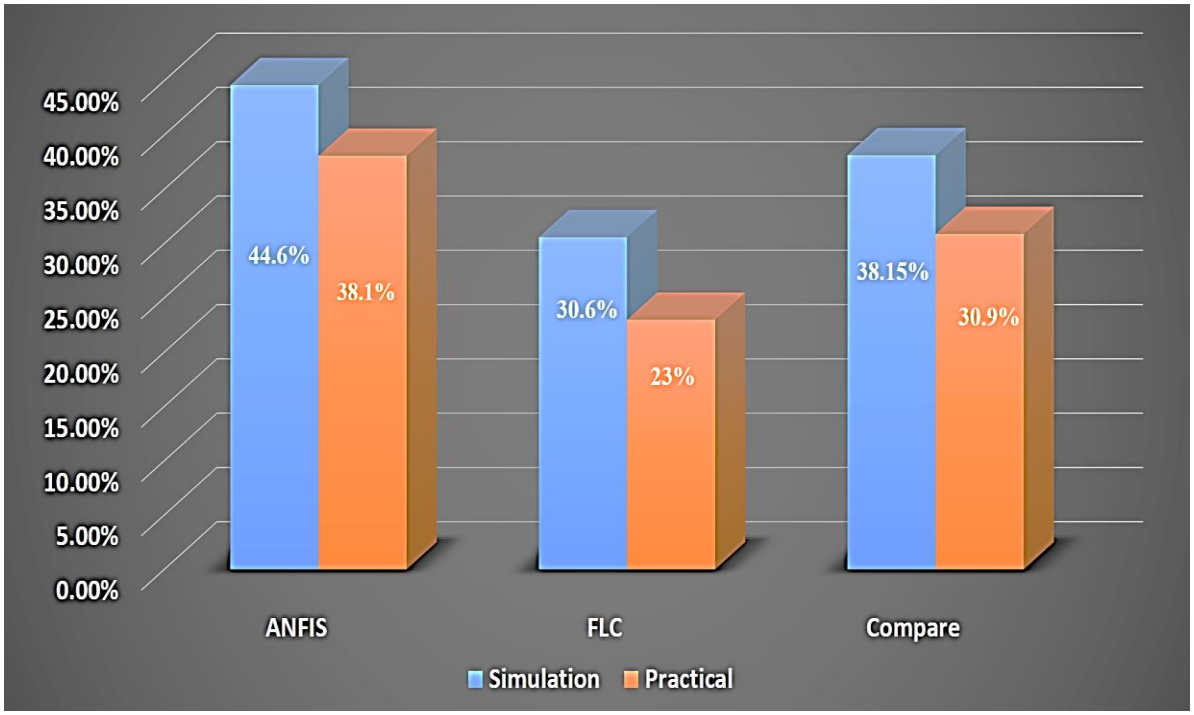

Figure 4. 43 Percentage power efficiency improvement

Chapter Five: Conclusion and Future Work

5.1 Conclusion

In this thesis, the use of artificial intelligence techniques to regulate the moving of a dual-axis solar tracking system driven by pneumatic actuators is examined. Utilizing such techniques has the benefit of increasing system efficiency, which allows for greater power harvesting from the solar panel. Several conclusions were drawn after testing the proposed system in a simulation environment using Matlab/Simulink and real-time experimental work, and collecting data:

1. Using the three proposed control methods (ANFIS, FLC, and comparison method) to control the position of the pneumatic actuator in the simulation shows an increase in solar PV panel efficiency of 44.6%, 30.6%, and 38.15%, respectively compared to the fixed panel system.
2. From the experimental results, the solar energy harvest was 38.1% for the ANFIS controller compared to the fixed panel, the improvement for the FLC control system was 23% while the comparison method was 30.9% compared with the fixed mounted panel system.
3. In the experimental work, the solar tracking system's solar energy harvest was 6.51% lower than the simulation model for ANFIS, around 7.6% lower for FLC, and 7.25% lower utilizing the comparison method.
4. The average efficiency of the PV panel has been improved through the three methods: ANFIS, FLC, and compare the method with the percentage of 10.4%, 9.93%, and 10.23% respectively, these closed results give the impression the efficiency of the PV panel is independent of the controller used in dual axis tracking system.

5. The difference between the simulation and experimental part due to many factors including the temperature used in simulation part was 25°C meanwhile in the experimental part was changing during the day from 25 to 41°C. Addition to that the environmental factor like humidity, dust and solar radiation. Also the simulation occurs in 16 September 2024, however, the experimental part was conducted through 18-22 September 2024 and this will give us a slight difference in the azimuth and tilt angle. These differences can by minimized by taking the results the same day and add a disturbance factor in the simulation part to emulate the weather conditions.

5.2 Future work

This thesis developed a fundamental aspect of a dual-axis tracking system using a pneumatic actuator system. However, the quest for a more sustainable and efficient future demands further exploration. Here are some exciting avenues for future work, based on the findings of this study:

1. **Using a proportional valve in a pneumatic system**

However, the cost of the propotional valve is more than the conventional on-off valve, but its linearity characteristics can be considered an advantage if controlled by a cost-effective controller.

2. **Using a 3/2 on-off valve in a pneumatic system**

The 2/2 on off valve is easy to control with a simple cotroller, however using an 3/3 on off valve will reduce the components the peumatic actuator system but will complicate the control system, consierding the control of this type of valve and the way that effect, the dual-axis tracking system can give a different results and shorten the penuamtic actuator system.

3. Using a Hybrid actuator system

Using a hybrid system that includes both pneumatic actuators and electric actuators for driving the solar tracking system and controlling it through a cost-effective controller may have a different result in some locations regardless of the environment in which the solar system will operate.

4. Applying adaptive sensorless control based observer design for pneumatic system in solar tracker.

References

[1] Maka, A. O., & Alabid, J. M. (2022). Solar energy technology and its roles in sustainable development. Clean Energy, 6(3), 476-483. https://doi.org/10.1093/ce/zkac023

[2] Abbass, K., Qasim, M.Z., Song, H. et al. A review of the global climate change impacts, adaptation, and sustainable mitigation measures. Environ Sci Pollut Res 29, 42539–42559 (2022). https://doi.org/10.1007/s11356-022-19718-6

[3] Yang, G., Yang, D., Liu, B., & Zhang, H. (2024). The role of short-and long-duration energy storage in reducing the cost of firm photovoltaic generation. Applied Energy, 374, 123914. https://doi.org/10.1016/j.apenergy.2024.123914

[4] Bin Abu Sofian, A. D. A., Lim, H. R., Siti Halimatul Munawaroh, H., Ma, Z., Chew, K. W., & Show, P. L. (2024). Machine learning and the renewable energy revolution: Exploring solar and wind energy solutions for a sustainable future including innovations in energy storage. Sustainable Development, 32(4), 3953–3978. https://doi.org/10.1002/sd.2885

[5] Dambhare, M. V., Butey, B., & Moharil, S. V. (2021, May). Solar photovoltaic technology: A review of different types of solar cells and its future trends. In Journal of Physics: Conference Series (Vol. 1913, No. 1, p. 012053). IOP Publishing. https://doi.org /10.1088/1742-6596/1913/1/012053

[6] Al-Shahri, O.A., Ismail, F.B., Hannan, M., Lipu, M.H., Al-Shetwi, A.Q., Begum, R., Al-Muhsen, N.F. and Soujeri, E. (2021) Solar Photovoltaic Energy Optimization Methods, Challenges and Issues: A Comprehensive Review. Journal of Cleaner Production, 284, Article ID: 125465. https://doi.org/10.1016/j.jclepro.2020.125465

[7] Abualigah, L.; Zitar, R.A.; Almotairi, K.H.; Hussein, A.M.; Abd Elaziz, M.; Nikoo, M.R.; Gandomi, A.H. Wind, Solar, and Photovoltaic Renewable Energy Systems with and without Energy Storage Optimization: A Survey of Advanced Machine Learning and Deep Learning Techniques. Energies 2022, 15, 578. https://doi.org/10.3390/en15020578

[8] Baouche, F.Z.; Abderezzak, B.; Ladmi, A.; Arbaoui, K.; Suciu, G.; Mihaltan, T.C.; Raboaca, M.S.; Hudișteanu, S.V.; Țurcanu, F.E. Design and Simulation of a Solar Tracking System for PV. Appl. Sci. 2022, 12, 9682. https://doi.org/10.3390/app12199682

[9] Malozyomov, B.V.; Martyushev, N.V.; Voitovich, E.V.; Kononenko, R.V.; Konyukhov, V.Y.; Tynchenko, V.; Kukartsev, V.A.; Tynchenko, Y.A. Designing the Optimal Configuration of a Small Power System for Autonomous Power Supply of Weather Station Equipment. Energies 2023, 16, 5046. https://doi.org/10.3390/en16135046

[10] A.Z. Hafez, A.M. Yousef, N.M. Harag, Solar tracking systems: Technologies and trackers drive types – A review, Renewable and Sustainable Energy Reviews, Volume 91, 2018, Pages 754-782, ISSN 1364-0321, https://doi.org/10.1016/j.rser.2018.03.094.

[11] Wibowo, Herdian & Bow, Yohandri & Sitompul, Carlos. (2021). Performance Comparison Analysis of Fixed and Solar-Tracker Installed Panel at PV System. IOP Conference Series: Earth and Environmental Science. 709. 012003. https://iopscience.iop.org/article/10.1088/1755-1315/709/1/012003

[12] M. S. Xavier et al., "Soft Pneumatic Actuators: A Review of Design, Fabrication, Modeling, Sensing, Control and Applications," in IEEE Access, vol. 10, pp. 59442-59485, 2022, https://doi.org/10.1109/ACCESS.2022.3179589.

[13] Xiuheng Wu, Liang Li, Xiangyu Wang, Xiang Chen, Shuo Cheng, Nonlinear controller design and testing for chatter suppression in an electric-pneumatic braking system with parametric variation, Mechanical Systems and Signal Processing, Volume 135, 2020, 106401, ISSN 0888-3270, https://doi.org/10.1016/j.ymssp.2019.106401.

[14] Deavers, C. J. (February 21, 2022). "Discussion: “Study of Pneumatic Processes in the Continuous Control of Motion With Compressed Air—I” (Shearer, J. L., 1956, Trans. ASME, 78, pp. 233–241)." ASME. Trans. ASME. February 1956; 78(2): 241–242. https://doi.org/10.1115/1.4013624.

[15] Amponsah-Abu, E. O., Nyarko, B. J. B., Edziah, R., Design and Construction of Pneumatic Transfer System Controller Unit for Ghana MNSR, Journal of Control Science and Engineering, 2019, 6450987, 15 pages, 2019. https://doi.org/10.1155/2019/6450987

[16] Hyeun-Seok Choi, Chang-Soo Han, Kye-young Lee, Sang-heon Lee, Development of hybrid robot for construction works with pneumatic actuator, Automation in Construction, Volume 14, Issue 4, 2005, Pages 452-459, ISSN 0926-5805, https://doi.org/10.1016/j.autcon.2004.09.008

[17] Morales, R., Badesa, F.J., García-Aracil, N. et al. Pneumatic robotic systems for upper limb rehabilitation. Med Biol Eng Comput 49, 1145–1156 (2011). https://doi.org/10.1007/s11517-011-0814-3

[18] Virgil Petrescu, R. V. (2019). Medical Service of Robots. Journal of Mechatronics and Robotics, 3(1), 60-81. https://doi.org/10.3844/jmrsp.2019.60.81

[19] H. Su et al., "State of the Art and Future Opportunities in MRI-Guided Robot-Assisted Surgery and Interventions," in Proceedings of the IEEE, vol. 110, no. 7, pp. 968-992, July 2022, https://doi.org/10.1109/JPROC.2022.3169146.

[20] Pustavrh, J., Hočevar, M., Podržaj, P. et al. Comparison of hydraulic, pneumatic and electric linear actuation systems. Sci Rep 13, 20938 (2023). https://doi.org/10.1038/s41598-023-47602-x

[21] Falcão Carneiro J, Bravo Pinto J, Gomes de Almeida F. Accurate Motion Control of a Pneumatic Linear Peristaltic Actuator. Actuators. 2020; 9(3):63. https://doi.org/10.3390/act9030063

[22] Chen Y, Yang Y, Li M, Chen E, Mu W, Fisher R, Yin R. Wearable Actuators: An Overview. Textiles. 2021; 1(2):283-321. https://doi.org/10.3390/textiles1020015

[23] Luo, Yiyue & wu, Kui & Spielberg, Andrew & Foshey, Michael & Rus, Daniela & Palacios, Tom?s & Matusik, Wojciech. (2022). Digital Fabrication of Pneumatic Actuators with Integrated Sensing by Machine Knitting. https://doi.org/10.1145/3491102.3517577

[24] Sun, G., Li, S., Yu, Q., & Zhang, J. (2024). Enhancing position control in pneumatic systems using ANFIS and high-speed on-off valves with compound PWM. International Journal of Hydromechatronics, 7(4), 347-367. https://doi.org/10.1504/ijhm.2024.10064700

[25] Jiménez, M., Kurmyshev, E. & Castañeda, C. Experimental Study of Double-Acting Pneumatic Cylinder. Exp Tech 44, 355–367 (2020). https://doi.org/10.1007/s40799-020-00359-8

[26] Satalagaon, A. K., Guha, A., & Srivastava, D. K. (2024). Development and Design Optimization of a Single-Acting Electro-Pneumatic Variable Valve Actuator for a Camless Engine Using Experiments, Mathematical Theory and Genetic Algorithm. Energy, 134186. https://doi.org/10.1016/j.energy.2024.134186

[27] A. -A. Năstase, I. -A. Sgârciu, A. Nedelcu, B. Nedelcu and V. Sgârciu, "Alternative Solutions for Making Impulse Ordered Proportional Valves,"

2021 13th International Conference on Electronics, Computers and Artificial Intelligence (ECAI), Pitesti, Romania, 2021, pp. 1-5, https://doi.org/10.1109/ECAI52376.2021.9515177.

[28] Bhowmik PK, Sabharwall P. Sizing and Selection of Pressure Relief Valves for High-Pressure Thermal–Hydraulic Systems. Processes. 2024; 12(1):21. https://doi.org/10.3390/pr12010021

[29] Zhang, B.; Jiang, A.; Jiang, J.; Qi, Y.; Xue, L.; Wang, Y. A New Positioning Strategy Based on Parameter Tuning and Optimal Control Technique for Pneumatic Control Valve. Actuators 2022, 11, 279. https://doi.org/10.3390/act11100279

[30] Ibemezie, N. P.-D., Obinna, N., Arua, J. E., Dare, B. A., Alexander, A. A., Akpan, B. K., & Uduma, I. L. (2024). Hybrid Neuro-Fuzzy Based Improved Control Design of Electro-Pneumatic Clutch Actuation Control System for Heavy Duty Vehicles. Journal of Engineering Research and Reports, 26(10), 199–216. https://doi.org/10.9734/jerr/2024/v26i101299

[31] Tudorache, T., Oancea, C. D., & Kreindler, L. (2012). Performance evaluation of a solar tracking PV panel. University" Politehnica" of Bucharest Scientific Bulletin, Series C: Electrical Engineering, 74(1), 3-10.

[32] Rengasamy, Dr. Dhanabal & Bharathi, Venuturla & Ranjitha, R. & Ponni, A. & Deepthi, S. & Mageshkannan, P.. (2013). Comparison of efficiencies of solar tracker system with static panel single-axis tracking system and dual-axis tracking system with fixed mount. Intern. J. Eng. Technol.. 5. 1925-1933.

[33] EL Hammoumi A, Motahhir S, EL Ghzizal A, Chalh A, Derouich A. A simple and low-cost active dual-axis solar tracker. Energy Sci Eng. 2018; 6: 607–620. https://doi.org/10.1002/ese3.236

[34] Mohanapriya, V., Manimegalai, V., Praveenkumar, V., & Sakthivel, P. (2021, March). Implementation of dual axis solar tracking system. In IOP Conference

Series: Materials Science and Engineering (Vol. 1084, No. 1, p. 012073). IOP Publishing. https://doi.org/10.1088/1757-899x/1084/1/012073

[35] Khan, M. T. A., Tanzil, S. M. S., Rahman, R., & Alam, S. M. S. (2010). Design and construction of an automatic solar tracking system. In ICECE 2010 - 6th International Conference on Electrical and Computer Engineering (pp. 326-329). Article 5700694 (ICECE 2010 - 6th International Conference on Electrical and Computer Engineering). https://doi.org/10.1109/ICELCE.2010.5700694

[36] Shang, H.; Shen, W. Design and Implementation of a Dual-Axis Solar Tracking System. Energies 2023, 16, 6330. https://doi.org/10.3390/en16176330

[37] Toylan, H., & Hüner, E. (2017). Solar Tracking System based on Adaptive Neuro-Fuzzy Inference System (ANFIS). Afyon Kocatepe University Journal of Sciences and Engineering, 17, 546-554. https://doi.org/10.5578/fmbd.60776

[38] Baisrum, Baisrum & Setiadi, Budi & Sudrajat, Sudrajat & Wijayakusuma, Varian & Ulhaq, Hilmi & Hikmawati, Rina & Qamaruddin, Naufal & Hardiansyah, Sandi. (2021). Implementation of Adaptive Neuro-Fuzzy Inference System Control on Pneumatic Solar Tracker. https://doi.org/10.2991/aer.k.211106.067

[39] Sarr, M. P., Thiam, A., & Dieng, B. (2023). ANFIS and ANN models to predict heliostat tracking errors. Heliyon, 9(1). https://doi.org/10.1016/j.heliyon.2023.e12804

[40] Zulkornain, M. S. I., Noor, S. Z., Rahman, N. H., & Musa, S. (2023). The Analysis of Dual Axis Solar Tracking System Controllers Based on Adaptive Neural Fuzzy Inference System (ANFIS). Journal of Mechanical Engineering (1823-5514), 20(2). https://ir.uitm.edu.my/id/eprint/76335

[41] Aldair, A. A., Obed, A. A., & Halihal, A. F. (2016). Design and Implementation of Neuro-Fuzzy Controller Using FPGA for Sun Tracking System. Iraqi Journal for Electrical & Electronic Engineering, 12(2). https://uobasrah.edu.iq/

[42] Zadeh, L.A. (2015) Fuzzy Logic—A Personal Perspective. Fuzzy Sets and Systems, 281, 4-20. https://doi.org/10.1016/j.fss.2015.05.009

[43] Rosyadah, M., Kusumanto, R., & Dewi, T. (2022). Smart optimization of PV panel output using Fuzzy Logic Controller based solar tracker. Sinergi, 26(1), 73-80. http://dx.doi.org/10.22441/sinergi.2022.1.010

[44] Abadi, I., Musyafa, A. and Soeprijanto, A. (2014) 'Design of single axis solar tracking system at photovoltaic panel using fuzzy logic controller,' The Institution of Engineering and Technology, p. 2.04 (6). https://doi.org/10.1049/cp.2014.1086

[45] Kiyak, E., Gol, G. A comparison of fuzzy logic and PID controller for a single-axis solar tracking system. Renewables 3, 7 (2016). https://doi.org/10.1186/s40807-016-0023-7

[46] Yang Z, Xiao Z. A Review of the Sustainable Development of Solar Photovoltaic Tracking System Technology. Energies. 2023; 16(23):7768. https://doi.org/10.3390/en16237768

[47] Aliyari-Shoorehdeli, Mahdi & Najafi, Farid & Jafari, Sahar. (2013). Position Control of a Pulse Width Modulated Pneumatic Systems: An Experimental Comparison. International Journal of Robotics Theory and Applications. 3. 57-66. https://ijr.kntu.ac.ir/article_12519.html

[48] Alboteanu, Laurentiuand .A, Bulucea and Degeratu, Sonia. (2015). Estimating Solar Irradiation Absorbed by Photovoltaic Panels with Low Concentration Located in Craiova, Romania. Sustainability. 2015. 2644-2661. https://doi.org/10.3390/su7032644

[49] Sebastian Bader, Xinyu Ma, Bengt Oelmann, One-diode photovoltaic model parameters at indoor illumination levels – A comparison, Solar Energy, Volume 180, 2019, Pages 707-716, ISSN 0038-092X, https://doi.org/10.1016/j.solener.2019.01.048.

[50] Abdul-Lateef, Wisam & Alexeevich, Glebov & Farhood, Naseer & Khdir, Ahmed & Shaker, Dina. (2020). Modelling and Controlling of position for electro-pneumatic system using Pulse-Width-Modulation (PWM) techniques and Fuzzy Logic controller. IOP Conference Series: Materials Science and Engineering. 765. 012020. https://doi.org/10.1088/1757-899X/765/1/012020

[51] Benjelloun, S. (2021). Thermodynamic identities and thermodynamic consistency of Equation of States. arXiv preprint arXiv:2105.04845. https://doi.org/10.48550/arXiv.2105.04845

[52] M. S. Xavier, A. J. Fleming and Y. K. Yong, "Modelling and Simulation of Pneumatic Sources for Soft Robotic Applications," 2020 IEEE/ASME International Conference on Advanced Intelligent Mechatronics (AIM), Boston, MA, USA, 2020, pp. 916-921, http://doi.org/10.1109/AIM43001.2020.9158802.

[53] Soleymani, F., Rezaei, S. M., Zareinejad, M., Baghestan, K., & Rahimi, A. (2017). Position control of a servo-pneumatic actuator with mismatched uncertainty using multiple-surface sliding mode controller and high-gain observer. Transactions of the Institute of Measurement and Control, 39(10), 1497-1508. https://doi.org/10.1177/0142331216640870

[54] E. Richer, Y. Hurmuzlu, A high performance pneumatic force actuator system: Part I—Nonlinear mathematical model, J. dyn. sys., meas., Cont., 122 (3) (2000) 416–425. https://doi.org/10.1115/1.1286336

[55] Yaïci, W., & Entchev, E. (2016). Adaptive Neuro-Fuzzy Inference System modelling for performance prediction of solar thermal energy system. Renewable Energy, 86, 302-315. https://doi.org/10.1016/j.renene.2015.08.028

[56] Garud, K. S., Jayaraj, S., & Lee, M. Y. (2021). A review on modeling of solar photovoltaic systems using artificial neural networks, fuzzy logic, genetic algorithm and hybrid models. International Journal of Energy Research, 45(1), 6-35. https://doi.org/10.1002/er.5608

[57] Lughofer, E. (2016). Evolving fuzzy systems—fundamentals, reliability, interpretability, useability, applications. In Handbook on computational intelligence: volume 1: fuzzy logic, systems, artificial neural networks, and learning systems (pp. 67-135). https://doi.org/10.1142/9789814675017_0003

[58] Khashan, Karam & Al-Qrimli, Fadhil. (2020). Improving Photovoltaic Panel (PV) Efficiency via Two Axis Sun Tracking System. Journal of Engineering. 26. 123-140. https://doi.org/10.31026/j.eng.2020.04.09

Appendices

1. NREL website

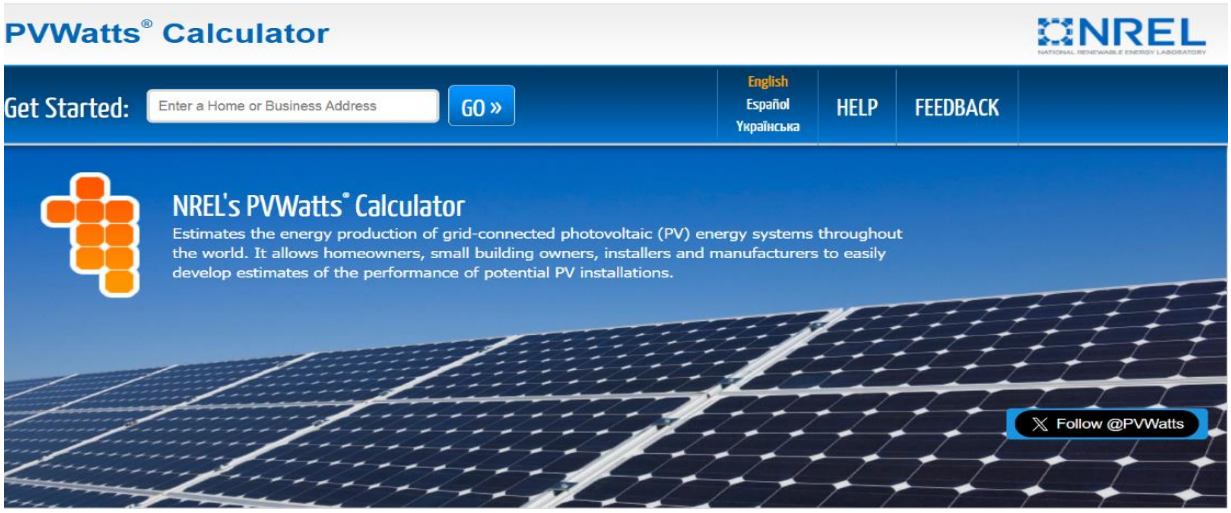

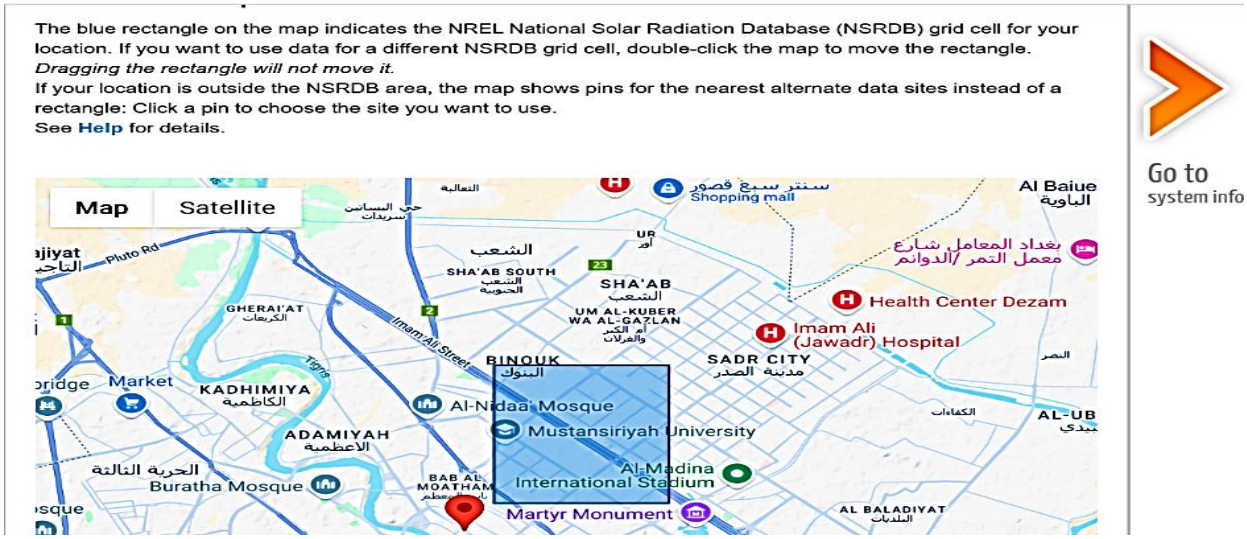

NREL solar irradiance database

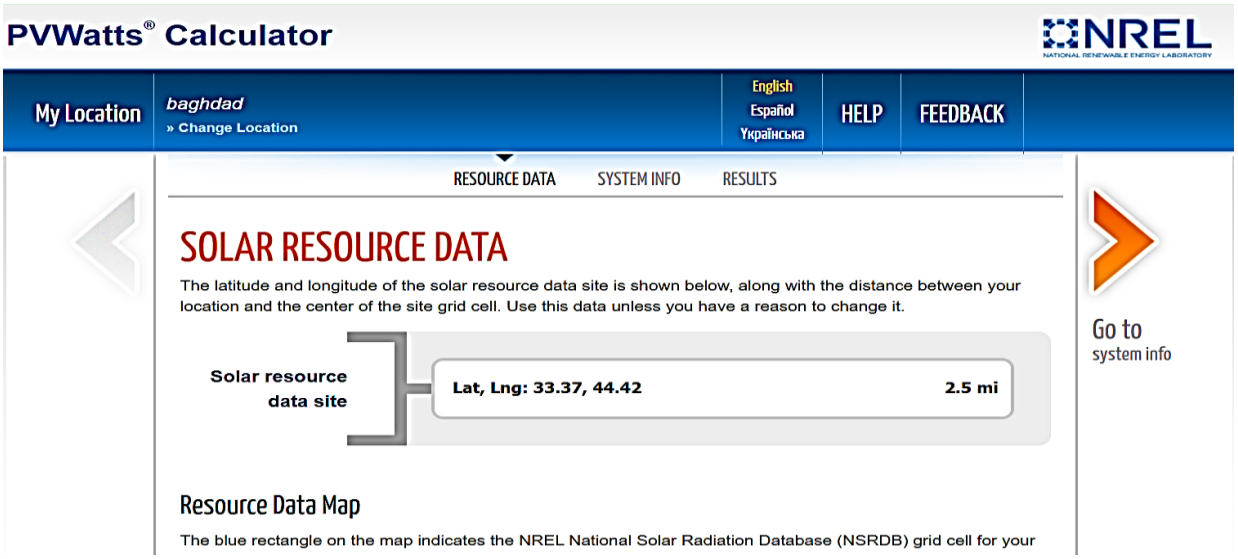

Latitude and longitude of the proposed system (Baghdad)

2. C++ Code for compare method

```
void setup()
{
  Serial.begin(4500);                              //serial connection setup  //opens  serial port, sets data rate
  Serial.println("CLEARDATA");                     //clear  all data that's been place in already
  Serial.println("LABEL,t,voltage,current,power,Mode");   //define the column headings (PLX-DAQ command)

  pinMode(12, INPUT);              //Mode  switch Button
  pinMode(11, INPUT);              //Axis switch
  pinMode(A4,  INPUT);//Potentiometer for right-left movement and for up-down movement
  pinMode(7, OUTPUT);    //azi right
  pinMode(8, OUTPUT);    //azi left
  pinMode(9, OUTPUT);    //ele right
  pinMode(10, OUTPUT);   //ele left

  servo_updown.attach(5);             //Servo motor up-down movement
  servo_rightleft.attach(6);          //Servo motor right-left movement
}

void loop()
{
//  pv_power();
char  Mode;
   float volt = analogRead(A5)*5.0/1023;
   float voltage = 2*volt;               //  Volt=(R1/R1+R2)*Voltage / R1=R2=10Ohms  => voltage=2*volt)
```

```
  float current = voltage/20;            //  I=voltage/(R1+R2)
  float power  = voltage*current;
  //Serial.print("DATA,TIME,"); // PLX-DAQ command
  //Serial.print(voltage);    //send the voltage to serial port
  //Serial.print(",");
  //Serial.print(current);    //send the current to serial port
  //Serial.print(",");
  //Serial.print(power);  //send the power to serial port
  //Serial.print(",");

//    Serial.println(Mode);
 buttonState1 = digitalRead(12);
 if (buttonState1 != prevButtonState1)  {
   if (buttonState1 == HIGH) {
     //Change mode and ligh up the correct  indicator
     if (mode == 1) {
       mode = 0;
     } else {
       mode = 1;
     }
   }
 }
 prevButtonState1 = buttonState1;
 delay(50); // Wait for 50 millisecond(s)
 if (mode == 0) {
   Mode='M';
   Serial.println(Mode);   //send Mode "Manual" to serial port
   //manualsolartracker();
 } else
  { // mode automatic
   Mode = 'A';
   Serial.println(Mode);
   automaticsolartracker(); //send Mode "Automatic" to serial port
   }
}
void  automaticsolartracker()
   {
    top= analogRead(ldrtop);          //capturing analog value of top right LDR
    bot= analogRead(ldrbot);          //capturing analog value of top left LDR
    right= analogRead(ldrright);          //capturing analog value of bot right LDR
    left= analogRead(ldrleft);          //capturing analog value of bot left LDR
    Serial.println(top);
    delay (100);
    Serial.println(bot);
    delay (100);
```

```
    Serial.println(left);
    delay (100);

  // calculating average
    //int avgtop = (topr + topl) / 2;     //average  of top LDRs
    //int avgbot = (botr + botl) / 2;     //average of bottom LDRs
    //int avgleft = (topl + botl) / 2;    //average of left LDRs
    //int avgright  = (topr + botr) / 2;   //average of right LDRs

  //Get the different
    int diffelev = top - bot;      //Get the different average betwen  LDRs top and LDRs bot
    int diffazi = right - left;    //Get the different  average betwen LDRs right and LDRs left

  //left-right movement of  solar tracker

     if (abs(diffazi) >= threshold_value)
     {        //Change  position only if light difference is bigger then the threshold_value
       if  (diffazi > 0)
       {
        digitalWrite (7,HIGH);
        digitalWrite (8,LOW);
       }
       else
       {
       digitalWrite (8,HIGH);
       digitalWrite (7,LOW);
       }
     }
     else
       {
        digitalWrite (7,LOW);
        digitalWrite (8,LOW);
       }
     if (abs(diffelev) >= threshold_value)
     {    //Change position only if light  difference is bigger then thethreshold_value
       if (diffelev > 0)
       {
        digitalWrite (9,HIGH);
        digitalWrite (10,LOW);
       }
      else
      {
       digitalWrite (10,HIGH);
       digitalWrite (9,LOW);
      }
       }
     }
    else
       {
         digitalWrite (9,LOW);
         digitalWrite (10,LOW);
       }
  }
```

REPUBLIC OF IRAQ
Ministry of Industry &Minerals
Corporation of Research and Industrial Development

جمهورية العراق
وزارة الصناعة والمعادن
هيأة البحث والتطوير الصناعي
قسم التنسيق البحثي والعلمي -

رقم الشهادة ١/٢٠٢٢/٤٠

العـــدد/٠٣/ ٥٠٧٠
التاريـــخ/ ٧/ ١١/ ٢٠٢٤

الى/ جامعة كربلاء /كلية الهندسة –الشؤون العلمية

م/ بيان استفادة دراسة علمية

تحية طيبة ....

اشارة الى كتابكم المرقم ١٣٩٦ في ٢٠٢٤/١٠/٢٣ المتضمن بيان الرأي حول الاستفادة من الدراسة العلمية الموسومة(تأثير استخدام المحركات الهوائية في تحسين كفاءة أنتاج الطاقة الكهربائية من الالواح الشمسية في العراق). نود اعلامكم بان الدراسة العلمية تبين جدوى استخدام المحركات الهوائية في انظمة تتبع الطاقة الشمسية، حيث تستخدم الطاقة الهوائية المضغوطة لتحريك الالواح الشمسية بزاويتين لتحقيق اقصى تعرض لاشعة الشمس، اذ ان هذه المحركات توفر تحكما دقيقا ذات موثوقية عالية وصيانة قليلة والقابلية الجيدة في العمل حتى في الظروف المناخية الصعبة. اما من الناحية الاقتصادية فان تكلفتها الاولية مرتفعة نسبيا لكنها تعوض بتكاليف تشغيل منخفضة مما يجعلها حلا مستداما وصديقة للبيئة مع زيادة انتاج الطاقة بحوالي ٢٩،٤٧% مقارنة بالالواح الثابتة وبالتالي فأنه بالامكان الاستفادة من الدراسة اعلاه في المجالين العلمي والعملي لمركز بحوث الطاقة العائد الى هيأتنا.

مع التقدير...

المهندس
عبدالرزاق داود جاسم
المكلف بتسيير اعمال هيأة البحث والتطوير الصناعي
٢٠٢٤/١٠/٣١

جمهورية العراق
وزارة الصناعة والمعادن
هيأة البحث والتطوير الصناعي

نسخة منه الى :
- مكتب المدير العام / للتفضل بالاطلاع ... مع التقدير .
- مركز بحوث الطاقة المتجددة والبيئة مذكرتكم بالعدد ٩٤٦ في ٢٠٢٤/١٠/٢٩/ للتفضل بالعلم ..مع التقدير.
- قسم التنسيق البحثي والعلمي /شعبة تدريب الطلبة وبحوث الدراسات العليا /مع الاوليات.

Email: crid.comm@industry.gov.iq
Website: crid.industry.gov.iq

العراق – بغداد – مجمع الجادرية العلمي

List of Publications:

1. A paper entitled " Comparison of Fuzzy Logic and Adaptive Neuro-Fuzzy Inference System Techniques in Controlling Pneumatic Solar Tracker" has been accepted for publication in the 5th International Conference on Electromechanical Engineering and its Applications (ICEMEA-2024), September 2024.
2. EVERGREEN Joint Journal of Novel Carbon Resource Sciences & Green Asia Strategy, Vol. 11, Issue 03, pp1848-1855, September 2024 “ Simulation of Pneumatic Actuators under Fuzzy Logic Control for Driving Solar Tracking System”.
3. A paper entitled “A Comprehensive Review of Solar Tracking Technologies” has been accepted for publication in the Kerbala Journal for Engineering Science.
4. A Patent has been submitted to the Central Organization for Standardization and Quality Control – Industrial Property Department - Iraq entitled " Using Artificial Intelligence with Pneumatic System for Solar Tracking Systems" by Ali Altahir, Hussain M. Khalaf, and Jamal Mohammed Abdul Kareem, 2024.

1) First Paper

ICEMEA-2024

ACCEPTANCE LETTER

Dear, [Hussain M. Khalaf, Jamal A.-K. Mohammed and Ali Abdul Razzaq Altahir]

We are pleased to inform you that your manuscript entitled (Comparison of Fuzzy Logic and Adaptive Neuro-Fuzzy Inference System Techniques in Controlling Pneumatic Solar Tracker) has been accepted for oral presentation at the 5th International Conference on Electromechanical Engineering and its Applications (ICEMEA-2024) to be held on September 24th – 25th, 2024 at the University of Technology, Baghdad, Iraq. Decision was made upon double-blind review process. The exact date, time and place of your presentation will be posted at the conference website.

On behalf of the organizing committee of ICEMEA 2024, we are looking forward to seeing you at the University of Technology, Baghdad, Iraq. If you have any further questions, please do not hesitate to contact us.

Sincerely,

The Chairman of ICEMEA-2024
Asst. Prof. Dr. Ghassan A. Bilal

+964-7736-833726
eme.icemea@uotechnology.edu.iq
https://eme.uotechnology.edu.iq/icemea

Certificate of Participation & Attendance

This certificate is proudly awarded to

Hussain M. Khalafa, Jamal A.-K. Mohammedb and Ali Abdul Razzaq Altahi

for participating and attendance in event type on **"Comparison of Fuzzy Logic and Adaptive Neuro-Fuzzy Inference System Methods in Controlling Pneumatic Solar Tracker"** in the 5Th International Conference on Electromechanical Engineering & its Applications (ICEMEA) held in Kocaeli Üniversitesi, Kocaeli, Türkiye on September 24-25, 2024.

Asst. Prof. Dr. Ghassan Abdul Hussein Bilal

Dean of College of Electromechanical Engineering

SCAN FOR MORE

2) Second Paper

EVERGREEN Joint Journal of Novel Carbon Resource Sciences & Green Asia Strategy, Vol. 11, Issue 03, pp1848-1855, September, 2024

Simulation of Pneumatic Actuators under Fuzzy Logic Control for Driving Solar Tracking System

Hussain M. Khalaf[1,*], Jamal A.-K. Mohammed[2], Ali Abdul Razzaq Altahir[1]
[1]Department of Electrical and Electronics Engineering, University of Kerbala, Karbala, Iraq.
[2]University of Technology, Electromechanical Engineering Department

*Author to whom correspondence should be addressed:
E-mail: hussain.khalaf@s.uokerbala.edu.iq

(Received April 1, 2024: Revised July 1, 2024: Accepted July 6, 2024).

Abstract: Photovoltaic (PV) systems need solar trackers to function as efficiently as possible. These trackers may be driven by a variety of actuators; hydraulic, electric, or pneumatic. Initial expenditures, leakage potential, high power consumption, high maintenance, complex design, and slower movement are some drawbacks of hydraulic actuators. Also, electric actuators are distinguished by elevated operational expenses, high maintenance prerequisites, and complexity of design and control. Pneumatic actuators have been proposed as an alternative to solve most of these problems due to their advantages over other actuators, including lower initial costs, longer operating life, less maintenance, relative simplicity of operation, and less prone to failure. Since the response of pneumatic actuators is rather poor, fuzzy logic techniques must be used to efficiently control the actuators. This paper aims to build a Matlab/Simulink model of a dual-axis solar tracker driven by pneumatic actuators, controlled by fuzzy logic. The azimuth and tilt angles of the PV panel are controlled by two double-acting cylinders to rectify the position of the tracker at the maximum irradiance position. Air pressure source, valve's input signal frequency, and solenoid valves' orifice diameter are the main factors influencing the cylinders' rod position response. The simulation shows that after changing the orifice diameter from 10 to 2.5 mm and the input pressure source from 0.7 to 0.1 MPa, the smoothest response of the rod position occurred at a pressure of 0.5 MPa and a diameter of 2.5 mm. Also, it was found that at a signal frequency of 1 Hz, the piston rod speed will be 0.5 steps/sec, while using 10 Hz gives 10 steps/sec, resulting in a more accurate rod position. There is a 12.35% improvement with fuzzy logic in rod position accuracy and better handling of sudden changes in input signals compared to no fuzzy logic use.

Keywords: Solar tracking system; pneumatic actuator; double-acting cylinder; fuzzy logic; LDR; PV panel

1. Introduction

Renewable energy methods including solar, wind, geothermal, biomass, and hydroelectric power are common sources of green energy. A variety of uses for solar energy exist, such as water air/water heating systems[1,2], crop drying systems[3–5], generating electric energy[6,7], etc. Solar energy collection technology through photovoltaic (PV) panels is one of the important and popular methods of generating electricity. To optimize the solar energy collected throughout the day, the PV panels need to be positioned in a way that maximizes their efficiency by making them perpendicular to the sun's rays. Actuators are responsible for the task of solar tracking.

Pneumatic actuators are among the common devices that have several unique features that make them very suitable for many applications. They have numerous uses in a variety of industries and applications, such as medical devices[8,9], tracking systems[7,10], lifting systems[11,12], and the automotive industry[13,14], etc.

In the past two decades, solar tracking has gained significant attention due to its role in enhancing solar collector efficiency and the accessibility of tracking-enabling equipment[15]. Solar panels with a dual-axis sun tracker can capture up to 40% more energy than those that are stationary[10]. Many studies in the literature have investigated different approaches to how to control the actuators that drive the solar tracker. Some of them focused on intelligent controllers in the optical sensor-based sun tracker[16,17].

Aldair et al.[18] developed a one-axis sun tracker powered by a stepper motor and a Sugeno fuzzy logic controller (FLC) to boost the energy generation efficiency of solar cells. The FLCs' input memberships, input gain, and output gain have all been optimized using a genetic algorithm (GA). Using the Matlab/Simulink program, the

3) Third Paper

Kerbala Journal for Engineering Science

https://kjes.uokerbala.edu.iq

A Comprehensive Review of Solar Tracking Technologies: A Survey with Future Directions

Hussain M. Khalaf*, Ali Abdul Razzaq Altahir**, Jamal A.-K. Mohammed***

*Department of Electrical and Electronics Engineering, Collage of Engineering, University of Kerbala, Iraq.
E-mail: hussain.khalaf@s.uokerbala.edu.iq

**Department of Electrical and Electronics Engineering, Collage of Engineering, University of Kerbala, Iraq.
E-mail: ali.altahir@uokerbala.edu.iq

*** Department of Electromechanical Engineering, University of Technology, Baghdad, Iraq

E-mail: 50128@uotechnology.edu.iq

Received: 17 September 2024; Revised: 13 October 2024; Accepted: 24 December 2024

Abstract

Solar tracking systems offer significant benefits in solar energy applications, including increased power and efficiency compared to fixed systems. They are classified according to their components and drivers, into include active, passive, semi-passive, manual, and chronological system. Active trackers are the most efficient among other categories, as they contribute to boosting harnessed solar energy by 28.8-43.6 %, depending on the season. Single-axis tracking improves efficiency by 13% while, passive trackers can improve efficiency by 25%. Manual trackers improve efficiency by 15%, and chronological tracking systems provide the same efficiency as active trackers under similar climatic conditions. This paper presents a literature survey on solar tracking systems. It summarizes multiple comprehensive reviews that studied different literature on solar tracking technologies aiming to provide guide to researchers and practitioners relate their work to existing research. The review concludes with a summary of future recommendations and insights on designing and building effective and reliable solar tracking system.

Keywords: Solar tracking system; Time-based tracker; Semi-passive tracker; Passive tracker; Manual tracker; Future directions.

عدم الممانعة الخاصة لبراءة الاختراع

Republic of Iraq
Ministry of Higher Education and
Scientific Research
University of Kerbala
Department of Scientific Affairs
Division of scientific products

جمهورية العراق
وزارة التعليم العالي والبحث العلمي
جامعة كربلاء
قسم الشؤون العلمية
شعبة تسويق النتاجات العلمية

Issue No : العدد : ع/ش.ع/ ٥٨٤٣
Date : التاريخ : ٢٠٢٤/١٢/٨

الى/ الجهاز المركزي للتقييس والسيطرة النوعية / مديرية براءات الاختراع والنماذج الصناعية

م / تسجيل براءة اختراع (عدم ممانعة)

تحية طيبة ...

بناءاً على الطلب المقدم من قبل الذوات المدرجة اسماؤهم ادناه التدريسيين في كلية الهندسة بجامعتنا واللذين يرومون فيه تسجيل براءة الاختراع الموسومة **(استخدام الذكاء الاصطناعي مع المحركات الهوائية في أنظمة تتبع الاشعاع الشمس).**

(Using artificial intelligence with Pneumatic System for solar radiation tracking systems) .

- نود اعلامكم لامانع لدينا بقدر تعلق الامر بنا.

للتفضل بالاطلاع .. مع التقدير

الاسماء///
١- أ.د علي عبد الرزاق عباس .
٢- حسين مصعب خلف .

أ.م.د. حيدر محمد عمران
مساعد رئيس الجامعة للشؤون العلمية
٢٠٢٤/١٢/٨

المرافقات///
- موجز البراءة

نسخة منه الى///
- مكتب السيد رئيس الجامعة .. تفضلكم بالاطلاع وابلاغ الموما اليهم .. مع التقدير.
- عمادة كلية الهندسة / للتفضل بالاطلاع وابلاغ الموما اليهم...مع التقدير.
- قسم الشؤون العلمية / شعبة تسويق النتاجات العلمية / اولويات .
- الصادر

رسل ١٢/٣ م.ش./ تسويق النتاجات العلمية .. م.د.ثامر سلمان جبر

العراق- كربلاء المقدسة – جامعة كربلاء - مجمع فريحة ص.ب ١١٢٥ - الشؤون العلمية
ايميل قسم الشؤون العلمية scientific.affairs@uokerbala.edu.iq

موقع ندوق الاشارات الالكترونية

الورش التي تمت المشاركة بها لتطوير مهارات السنة البحثية:

وزارة التعليم العالي و البحث العلمي
جامعة كربلاء

شهادة مشاركة

نؤيد مشاركة الطالب

حسين مصعب خلف شهاب الدين

في الورشة الموسومة **(التفكير النقدي في البحث العلمي والأطاريح الجامعية)** من برنامج تطوير المهارات الاكاديمية لطلبة الدراسات العليا للعام الدراسي 2023-2024

ا.د. نجم عبد الحسين نجم
مساعد رئيس الجامعة للشؤون العلمية

12/12/24, 1:07 PM ASDPS

وزارة التعليم العالي و البحث العلمي
جامعة كربلاء

شهادة استيفاء

نؤيد استيفاء الطالب

حسين مصعب خلف شهاب الدين

الوحدات الدراسية المطلوبة في نظام تطوير المهارات الاكاديمية لطلبة الدراسات العليا للعام الدراسي 2024-2025

أ.م.د. حيدر محمد عمران
مساعد رئيس الجامعة للشؤون العلمية

الخلاصة

الشمس هي أحد أهم مصادر الطاقة النظيفة التي لا غنى عنها على كوكبنا. تعد الطاقة الكهروضوئية (PV) في الوقت الحاضر أكثر أنواع الطاقة الشمسية قابلية للتطبيق وقبولاً. تتضمن الطاقة الكهروضوئية الشمسية تحويل طاقة الشمس إلى طاقة كهربائية. إحدى الطرق لتعزيز كفاءة نظام الطاقة الشمسية الكهروضوئية هي زيادة الوقت الشمسي، مما يعني تسخير المزيد من ضوء الشمس على الألواح الشمسية. يتم تحقيق ذلك باستخدام متتبعات الشمس، والتي تحافظ على توجيه الألواح الشمسية الكهروضوئية دائمًا نحو أشعة الشمس بالزاوية المثلى. تهدف هذه الأطروحة إلى تصميم وبناء نموذج أولي لنظام تتبع شمسي ثنائي المحور مدفوع بمحركين هوائيين على نطاق أصغر، والذي يمكنه محاكاة نظام الحياة الواقعية بحمل فعلي. تم إجراء مجموعة من الاختبارات على نظام التتبع في يوم 16 سبتمبر 2024 في مدينة بغداد على خط عرض (33.367 درجة شمالا). أيضًا، مقارنة بين لوحة شمسية ثابتة وأخرى مدفوعة بمحركات هوائية لإظهار مقدار الطاقة التي يمكن إنتاجها لحمل محلي معين. أولاً، سيتم نمذجة مكونات نظام التتبع، والذي يحتوي بشكل أساسي على اللوحة الكهروضوئية ونظام المحرك الهوائي ونظام التحكم. تم استخدام ثلاث طرق تحكم عند محاكاة نظام التتبع بواسطة Matlab/Simulink نظام الاستدلال الضبابي العصبي التكيفي(ANFIS) ، والمنطق الضبابي (FL)، وطريقة المقارنة للتحكم في المحركات الهوائية. أظهرت المحاكاة أن طريقة ANFIS زادت من كفاءة النظام الشمسي بنحو 44.6٪ مقارنة بنظام اللوحة الثابتة، بينما أظهرت طريقة FL زيادة بنسبة 30.6٪ في حصاد الطاقة الشمسية مقارنة بنظام اللوحة الثابتة. طريقة المقارنة هي عملية بسيطة لمقارنة قراءات مستشعرين متطابقين وقد حققت كفاءة أكبر بنسبة 38.15٪ من اللوحة الثابتة.

عند مقارنة أداء إعداد متتبع الشمس في العمل التجريبي تحت نظام ANFIS بالنتائج المحاكاة المقابلة، أظهرت نتائج الطاقة العملية انخفاضًا بنسبة 6.51٪ عن نتائج المحاكاة. كما أن النتائج التجريبية للنظام تحت سيطرة FL وطريقة المقارنة أعطت حوالي 7.6% و7.25% أقل من نتائج المحاكاة.

جمهورية العراق
وزارة التعليم العالي والبحث العلمي
جامعة كربلاء
كلية الهندسة
قسم الهندسة الكهربائية والالكترونية

التحكم في متتبع الطاقة الشمسية الهوائي باستخدام نظام الاستدلال العصبي الضبابي التكيفي

رسالة مقدمة الى مجلس كلية الهندسة / جامعة كربلاء وهي جزء من متطلبات نيل درجة الماجستير في علوم الهندسة الكهربائية

من قبل:

حسين مصعب خلف

باشراف

أ.د جمال عبد الكريم محمد

أ.د علي عبد الرزاق عباس الطاهر

شوال 1446 نيسان 2025